MECHANICAL AND THERMO-ELECTRICAL PROPERTIES EVALUATION OF HELICAL MULTIWALL CARBON NANOTUBE ENHANCED CARBON COMPOSITE

ALI NAEM S ALAMRY

FACULTY OF ENGINEERING
UNIVERSITY OF MALAYA
KUALA LUMPUR

2022

MECHANICAL AND THERMO-ELECTRICAL PROPERTIES EVALUATION OF HELICAL MULTIWALL CARBON NANOTUBE ENHANCED CARBON COMPOSITE

ALI NAEM S ALAMRY

THESIS SUBMITTED IN FULFILMENT OF THE REQUIREMENTS FOR THE DEGREE OF DOCTOR OF PHILOSOPHY

FACULTY OF ENGINEERING
UNIVERSITY OF MALAYA
KUALA LUMPUR

2022

UNIVERSITY OF MALAYA

ORIGINAL LITERARY WORK DECLARATION

Name of Candidate: **ALI NAEM S ALAMRY**

Matric No: **KVA180033 & 17198594/1**

Name of Degree: **DOCTOR OF PHILOSOPHY**

Title of Project Paper/Research Report/Dissertation/Thesis ("this Work"): **MECHANICAL AND THERMO-ELECTRICAL PROPERTIES EVALUATION OF HELICAL MULTIWALL CARBON NANOTUBE ENHANCED CARBON COMPOSITE**

Field of Study: **MATERIALS ENGINEERING**

I do solemnly and sincerely declare that:

(1) I am the sole author/writer of this Work;
(2) This Work is original;
(3) Any use of any work in which copyright exists was done by way of fair dealing and for permitted purposes and any excerpt or extract from, or reference to or reproduction of any copyright work has been disclosed expressly and sufficiently and the title of the Work and its authorship have been acknowledged in this Work;
(4) I do not have any actual knowledge nor do I ought reasonably to know that the making of this work constitutes an infringement of any copyright work;
(5) I hereby assign all and every rights in the copyright to this Work to the University of Malaya ("UM"), who henceforth shall be owner of the copyright in this Work and that any reproduction or use in any form or by any means whatsoever is prohibited without the written consent of UM having been first had and obtained;
(6) I am fully aware that if in the course of making this Work I have infringed any copyright whether intentionally or otherwise, I may be subject to legal action or any other action as may be determined by UM.

Candidate's Signature Date: 01 May 2022

Subscribed and solemnly declared before,

Witness's Signature Date: 11 May 2022

Name:

Designation:

MECHANICAL AND THERMO-ELECTRICAL PROPERTIES EVALUATION OF HELICAL MULTIWALL CARBON NANOTUBE ENHANCED CARBON COMPOSITE

ABSTRACT

The introduction of carbon nanotubes (CNTs) inside a polymer matrix is preferred as a reinforcing medium to enhance the mechanical, physical, and electrical properties of composite materials. It was therefore the purpose of this study to experimentally investigate the role of helical multi-walled carbon nanotubes (HMWCNTs) on the fracture behavior of polymer composites and understand the underlying failure mechanisms under monotonic and impact loading conditions. Nanocomposite laminates were manufactured and subjected to various mechanical, thermal, and electrical tests to evaluate their properties. This was followed by a detailed examination of the fracture surface with the help of a field emission scanning electron microscope (FESEM) and ultrasonic C-scanning to investigate the underlying fracture and damage mechanisms. It was found that there was an increase in the mechanical strength of the nanocomposite laminates with the addition of HMWCNTs in comparison with the control sample. From the morphology analysis of fractured surfaces by FESEM, it was also found that upon increasing the number of HMWCNTs in the composite laminate, a higher bridging effect was achieved, which enhanced the strength of the composite laminates. Evidence that fewer HMWCNTs aggregated over the fracture surface was also found in this work.

Keywords: Helical Multiwalled Carbon Nanotubes, Composite Laminate, Interfacial Bond, Fracture Toughness, Dispersion Technique.

PENILAIAN SIFAT-SIFAT MEKANIKAL DAN TERMO-ELEKTRIK KOMPOSIT KARBON DIPERTINGKAT KARBON BERBILANG DINDING HELIKAL

ABSTRAK

Pengenalan tiub nano karbon (CNT) di dalam matriks polimer diutamakan sebagai medium pengukuhan untuk meningkatkan sifat mekanikal, fizikal dan elektrik bahan komposit. Oleh itu, adalah tujuan kajian ini untuk menyiasat secara eksperimen peranan berdinding heliks (HMWCNTs) pada tingkah laku patah komposit polimer dan memahami mekanisme kegagalan yang mendasari di bawah keadaan pemuatan monoton dan impak. Laminat nanokomposit telah dihasilkan dan tertakluk kepada pelbagai ujian mekanikal, haba dan elektrik untuk menilai sifatnya. Ini diikuti dengan pemeriksaan terperinci permukaan patah dengan bantuan mikroskop elektron pengimbasan pelepasan medan (FESEM) dan pengimbasan C ultrasonik untuk menyiasat mekanisme patah dan kerosakan yang mendasari. Didapati terdapat peningkatan dalam kekuatan mekanikal laminat nanokomposit dengan penambahan HMWCNTs berbanding dengan sampel kawalan. Daripada analisis morfologi permukaan patah oleh FESEM, didapati juga bahawa apabila meningkatkan bilangan HMWCNT dalam lamina komposit, kesan penyambungan yang lebih tinggi telah dicapai, yang meningkatkan kekuatan lamina komposit. Bukti bahawa lebih sedikit HMWCNT yang diagregatkan di atas permukaan patah juga ditemui dalam kerja ini.

Kata kunci: Tiub Nano Karbon Dinding Berlapis Helik, Laminat Komposit, Ikatan Antara Muka, Keliatan Patah, Teknik Serakan.

ACKNOWLEDGEMENTS

It was end of 2018 when I decided to pursue my study and I could not describe my feeling when it finally comes to an end now. I could not have done this without the support from my family and friends. First and foremost, I would like to express my sincere gratitude to my supervisor, Assoc. Prof. Dr. Andri Andriyana for his patient in continuing guiding me whenever I am lost. He is not only just being a mentor in my academic, but I appreciate his advice to me in life and my future undertaking. Also, I would like to thank my co-supervisor, Assoc. Prof. Ir. Dr. Ang Bee Chin for providing me guidance throughout the years. Next, my thesis will never be completed without the help from the external co-supervisor from Universiti Teknologi Malaysia. I would like to thank Assoc. Prof. Dr. Shukur Bin Abu Hassan for his guidance and support. Last but not least, I would like to dedicate this to my beloved parent and family for their endless support on my decision.

TABLE OF CONTENTS

MECHANICAL AND THERMO-ELECTRICAL PROPERTIES EVALUATION OF HELICAL MULTIWALL CARBON NANOTUBE ENHANCED CARBON COMPOSITE Abstract iii

PENILAIAN SIFAT-SIFAT MEKANIKAL DAN TERMO-ELEKTRIK KOMPOSIT KARBON DIPERTINGKAT KARBON BERBILANG DINDING HELIKAL Abstrak iv

Acknowledgements v

Table of Contents vi

List of Figures x

List of Tables xiv

List of Symbols and Abbreviations xv

List of Appendices xvii

CHAPTER 1: INTRODUCTION 1

1.1 Research Background 1

1.2 Research Problem 3

1.3 Research Objectives 4

1.4 Research Significance 5

1.5 Research Scope 6

1.6 Thesis Layout 7

CHAPTER 2: LITERATURE REVIEW 9

2.1 Introduction 9

2.2 Polymer Composite Materials 10

2.2.1 Types of Polymer Matrix Composite 17

2.2.2 Types of Matrix and Fibres 19
2.2.3 Other types of Laminated Composites 20
2.2.4 Mechanical Behaviour of Polymer Composite 22
2.3 Applications of Polymer Composite Materials 10
2.4 Fibre Reinforced Composites 24
2.5 Carbon Nanotubes (CNTs) 27
2.5.1 Different Kinds of CNTs 28
2.5.1.1 Single-Walled Carbon Nanotubes (SWCNTs) 28
2.5.1.2 Multi-Walled Carbon Nanotubes (MWCNTs) 29
2.5.1.3 Helical Multi-Walled Carbon Nanotubes (HMWCNTs) 30
2.5.1.4 Other Kinds of CNTs 31
2.5.2 Mechanical Properties of CNTs 32
2.5.3 Thermal and Electrical properties of CNT-based composites 37
2.5.4 CNTs in Composites 39
2.5.5 Dispersion Techniques for CNTs in Polymeric Matrix 40
2.5.5.1 Ultrasonic Dispersion 41
2.5.5.2 Magnetic Stirring 45
2.5.5.3 Mechanical Mixer 46
2.5.6 Fabrication Techniques for CNTs-Based Composites 47
2.5.6.1 Solution Mixing 48
2.5.6.2 Melt Processing and Melt Blending 48
2.5.6.3 In Situ Polymerization 49
2.5.6.4 Layer-By-Layer (LBL) Technique 50
2.5.6.5 Swelling Technique 51
2.6 Limitations of CNTs-Based Composites 51
2.6.1 Failures of CNTs-Based Composites 53

2.6.2 CNTs Breakages and Bridging 53
2.6.3 CNTs Pull Out Failures 54
2.6.4 Matrix Material Cracking 55
2.6.5 Delamination and De-Bonding 55
2.6.6 Modes of Fracture Toughness 57
2.6.7 Impact Damages 62
2.6.8 Compression After Impact (CAI) 63
2.7 CNTs-Based Epoxy Composite 65
2.8 Challenges Faced During Applications of CNTs-Based Composites. 66

CHAPTER 3: METHODOLOGY 71
3.1 Research Methodology 71
3.2 Research Materials 72
3.2.1 Materials 73
3.2.2 Fabrication of Composite Panel 73
3.2.2.1 Mixture Preparation 73
3.2.2.2 Fabrication of Composite Laminate for DCB and ENF Test 75
3.2.2.3 Fabrication of Composite Laminate for LVI and CAI Tests 77
3.2.3 Dimension of Test Specimens 79
3.2.4 Characterization of Samples 79
3.2.4.1 Destructive Testing 80
3.2.4.2 Non-Destructive Characterization 87

CHAPTER 4: RESULTS AND DISCUSSION 90
4.1 Double Cantilever Beam (DCB) Test Results 90
4.2 End Notched Flexure (ENF) Test Results 99
4.3 Low-Velocity Impact (LVI) Test Results 103

4.4 Compression After Impact (CAI) Test 110
4.5 Electrical Conductivity 114
4.6 Thermal Stability 115
4.6.1 Thermogravimetric Analysis (TGA) 115
4.6.2 Differential Scanning Calorimetry (DSC) 117
4.7 FESEM Characterization of HMWCNTs and Polymer Composite 119
4.8 Ultrasonic C-Scan 122
4.9 Analytical Modeling of Mechanical Properties 125
4.10 Results Summary 130
4.11 Reference Material Comparison 132

CHAPTER 5: CONCLUSION AND FUTURE RECOMMENDATIONS 134

5.1 Conclusions 134
5.2 Research limitations 137
5.3 Future Recommendations 138
REFERENCES 139
LIST OF PUBLICATIONS AND PAPERS PRESENTED 163
APPENDICES 165

LIST OF FIGURES

Figure 2.1: Different Components of Aircrafts Made from Composite Materials (Kumar et al., 2014) 11

Figure 2.2: Laminated Composite Materials (Koide et al., 2013) 21

Figure 2.3: Structure of a Single-Walled Carbon Nanotube (Ribeiro et al., 2017) 28

Figure 2.4: Structure of Multi-Walled Carbon Nanotube (Ribeiro et al., 2017) 29

Figure 2.5: Structure of a Helical Multi-Walled Carbon Nanotube (Saether et al., 2003) 31

Figure 2.6: Formation of Single-Wall Carbon Nanotubes by Rolling of a Graphene Sheet along Lattice Vectors (Dresslhaus, 2004; Terrons, 2003; Zhang & Li, 2009) 32

Figure 2.7: Three Types of Carbon Nanotubes: Armchair, Zigzag and Chiral Tubes respectively (Dresslhaus, 2004; Terrons, 2003; Zhang & Li, 2009) 32

Figure 2.8: Effect of Sonication Time on the Length of MWCNTs: (a) Effect of 1 Hour and (b) 10 Hours (Huang & Terentjev, 2012) 41

Figure 2.9: Effect of Sonication Time on Alumina Particle Size (Afzal et al., 2019) 42

Figure 2.10: Effect of Sonication Time on Cluster Particle Size (Afzal et al., 2019) 43

Figure 2.11: Images of MWCNTs Aqueous Suspensions after Ultra-Sonication and Standing for Different Times (Ultra-Sonication Time: A. 0 min; B. 20 min; C. 1 hr; and D. 2 hr) (Afzal et al., 2019) 44

Figure 2.12: (A) Scheme of the LBL film-deposition (B) Two adsorption routes, depicting LBLdeposition for polymers and polymers with NPs (Srivastava & Kotov, 2008) 51

Figure 2.13: Different Damage Types in Composite Laminates (Eggers et al., 1994) .. 57

Figure 2.14: Schematic of Different Fracture Modes (Nasuha et al., 2017) 59

Figure 2.15: Generic Plots between Load and Displacement of the Nano-Reinforced Specimens (Khaled et al., 2014) 61

Figure 2.16: (a) Effective Compressive Modulus (b) Compression After Impact Strength on Neat and 0.5 wt. % MWCNTs Reinforced Epoxy (Kostopoulos et al., 2010) 65

Figure 3.1: Research Flow Chart 72

Figure 3.2: (a) Magnetic Stirrer Mixing of HMWCNTs with Solvent and (b) Mechanical Stirring 74

Figure 3.3: Ultrasonic Bath 74

Figure 3.4: Coating of Composite Laminates 75

Figure 3.5: (a) Oven and (b) Fan Drying of Carbon Fibre-Epoxy Laminates (c) Hot Air Curing Oven 76

Figure 3.6: (a) Vacuum Debulking and (b) Prepared Composite Panel 76

Figure 3.7: Hot Press Machine for Curing 77

Figure 3.8: Schematic Representation of the Work Flow 78

Figure 3.9: (a) Prepared Specimens for DCB Test, (b) Prepared Specimens for LVI and CAI Test and (c) Prepared Specimens for ENF Test 79

Figure 3.10: (a) Universal Testing Machine and (b) DCB Specimen Under Testing 81

Figure 3.11: (a) Universal Testing Machine and (b) ENF Specimen under Load 82

Figure 3.12: Drop Weight Impact Machine 83

Figure 3.13: Composite Laminates after LVI Testing 84

Figure 3.14: (a) CAI Test Machine and (b) Specimen Under Loading 86

Figure 3.15: Volume Resistivity Testing 87

Figure 3.16: (a) Field Emission Scanning Electron Microscope and (b) Analysis of Fractured Surfaces 88

Figure 3.17: Ultrasonic Raster Scanning to Prepare a C-scan of a Specimen Containing an Internal Flaw 89

Figure 4.1: Force versus Displacement Graphs Obtained during DCB Tests on Different Samples: (a) Control, (b) 0.2 wt. % HMWCNTs-epoxy, and (c) 0.4 wt. % HMWCNTs-epoxy Composite 91

Figure 4.2: Interlaminar Fracture Toughness G_{IC} (kJ/m^2) for Propagation 94

Figure 4.3: Interlaminar Fracture Toughness G_{IC} (kJ/m^2) for Initiation 94

Figure 4.4: R Curves for DCB Samples for Control 96

Figure 4.5: R Curves for DCB Samples for 0.2 wt. % HMWCNTs-epoxy Composite . 96

Figure 4.6: R Curves for DCB Sample for 0.4 wt. % HMWCNTs-epoxy Composite... 97

Figure 4.7: Force versus Displacement Graphs Obtained during ENF Tests of Different Samples: (a) Control, (b) 0.2 wt. % HMWCNTs-epoxy, and (c) 0.4 wt. % HMWCNTs-epoxy Composite 100

Figure 4.8: Average Values of Interlaminar Fracture Toughness 102

Figure 4.9: Force versus Time Curves from LVI Tests: (a-c) At 15 J (Control, 0.2 % HMWCNTs-epoxy and 0.4 % HMWCNTs-epoxy, respectively) and (d-f) at 25 J (Control, 0.2 % HMWCNTs-epoxy and 0.4 % HMWCNTs-epoxy, respectively)..... 104

Figure 4.10: Displacement versus Time Curves from LVI Tests: (a-c) At 15 J (Control, 0.2 % HMWCNTs-epoxy and 0.4 % HMWCNTs-epoxy, respectively) and (d-f) at 25 J (Control, 0.2 % HMWCNTs-epoxy and 0.4 % HMWCNTs-epoxy, respectively)..... 105

Figure 4.11: Energy versus Time Curves from LVI Tests: (a-c) At 15 J (Control, 0.2 % HMWCNTs-epoxy and 0.4 % HMWCNTs-epoxy, respectively) and (d-f) at 25 J (Control, 0.2 % HMWCNTs-epoxy and 0.4 % HMWCNTs-epoxy, respectively)..... 106

Figure 4.12: Incipient Energy Measured for Different HMWCNTs Content of Composite: (a) 15 J and (b) 25 J 107

Figure 4.13: Absorbed Energy versus Impact Energies..... 107

Figure 4.14: Compression Load versus Displacement Behaviour at: (a) 0 J, (b) 15 J and (c) 25 J..... 112

Figure 4.15: Volume Resistivity of Samples..... 114

Figure 4.16: Thermogravimetric Analysis of (a) Control, (b) 0.2 wt. % HMWCNTs-epoxy, (c) 0.4 wt. % HMWCNTs-epoxy Samples and (d) Comparison of all Graphs. 115

Figure 4.17: Derivative Curves Calculated from the Thermal Gravimetric Analysis Profiles of (a) Control, (b) 0.2 wt. % HMWCNTs-epoxy, (c) 0.4 wt. % HMWCNTs-epoxy Samples and (d) Comparison of all Graphs 117

Figure 4.18: Differential Scanning Calorimetric Analysis of (a) Control, (b) 0.2 wt. % HMWCNTs-epoxy, (c) 0.4 wt. % HMWCNTs-epoxy Composite and (d) Comparison of all Graphs 118

Figure 4.19: Micrographs of HMWCNTs from Powder..... 119

Figure 4.20: FESEM Images of Fracture Surface for Control Sample..... 120

Figure 4.21: (a-b) Elongated HMWCNTs, (c-e) Good Dispersion of HMWCNTs in Epoxy, (f) Single Strand of HMWCNTs Visible in Image after DCB Tests 120

Figure 4.22: (a-c) Good Dispersion of HMWCNTs, (d) Dispersed Epoxy Over CF, (e-f) Agglomerated HMWCNTs after ENF Tests 120

Figure 4.23: (a-b, d) Image of CF-E Matrix with HMWCNTs Dispersed in Epoxy, (c) CF-E Matrix, (e-f) Two Overlapping HMWCNTs after Compression Tests 121

Figure 4.24: C-scan Images of all the Samples Impacted at Energy level of 15 J and 25 J; Blue-White Section Represents Damage Area Hit by a Projectile, the White Area Exhibits Delamination of the Laminates, Blue Area Represents Splitting and Delamination of the Back-Face 123

Figure 4.25: Damaged Area from Specimens Tested with Impact Energies 15 J and 25 J 124

Figure 4.26: Fitting of Interlaminar Fracture Toughness G_{IC} (kJ/m^2) for Propagation with Respect to HMWCNTs Content for (OBT, MBT, CCM & MCC) 126

Figure 4.27: Fitting of Interlaminar Fracture Toughness G_{IC} (kJ/m^2) for Initiation with Respect to HMWCNTs Content for (OBT, MBT, CCM & MCC) 127

Figure 4.28: Fitting of Interlaminar Fracture Toughness G_{IIC} (kJ/m^2) with Respect to HMWCNTs Content 128

Figure 4.29: Fitting of Incipient Energy with Respect to HMWCNTs Content 129

LIST OF TABLES

Table 2.1: Elastic Properties of Samples versus CNTs Fractions 23

Table 2.2: Cohesive Zone Model..... 23

Table 2.3: Failure Load and Critical Strain of Multiple Orientations of CNT Bundles . 34

Table 2.4: Elastic Properties of SWCNTs (Individual and Bundles) 35

Table 2.5: Elastic Properties of MWCNTs (Individual and Bundles)..... 36

Table 2.6: Tensile Strength of SWCNTs (Individual and Bundles)..... 36

Table 2.7: Tensile Strength of MWCNTs (Individual and Bundles)..... 36

Table 2.8: Mechanical Properties of Nanoparticle Reinforced Composite..... 37

Table 4.1: Interlaminar Fracture Toughness (GIC) of Control Samples 92

TTable 4.2: Interlaminar Fracture Toughness (GIC) of 0.2 wt. % HMWCNTs-epoxy Samples 93

Table 4.3: Interlaminar Fracture Toughness (G_{IC}) of 0.4 wt. % HMWCNTs-epoxy Samples 93

Table 4.4: Increment Percentage of Interlaminar Fracture Toughness G_{IC} for all Compositions..... 95

Table 4.5: Interlaminar Fracture Toughness (G_{IIC}) of Control Sample 100

Table 4.6: Interlaminar Fracture Toughness (G_{IIC}) of 0.2 wt. % HMWCNTs-epoxy Samples 101

Table 4.7: Interlaminar Fracture Toughness (G_{IIC}) of 0.4 wt. % HMWCNTs-epoxy Samples 101

Table 4.8: CAI Experimental Force and Compressive Strength Values for all Specimens 111

Table 4.9: Impacted Area of the Samples as Evaluated by C-Scan and the % Decrement Compared to Control Sample for 15 J 124

Table 4.10: Impacted Area of the Samples as Evaluated by C-Scan and the % Decrement Compared to Control Sample for 25 J 124

LIST OF SYMBOLS AND ABBREVIATIONS

AFRP	:	Aramid Fibre Reinforced Polymer
ASTM	:	American Society for Testing and Materials
CAI	:	Compression-After-Impact
CCM	:	Compliance Calibration Method
CFRP	:	Carbon Fibre Reinforced Polymer
CNTs	:	Carbon Nano Tubes
CSIPAP	:	Composite Structure Impact Performance Assessment Program
DBSA	:	Dodecylbenzene Sulfonic Acid
DCB	:	Double Cantilever Beam
DSC	:	Differential Scanning Calorimetry
DWCNT	:	Double Wall Carbon Nanotube
ENF	:	End Notched Flexure
EV	:	Electric Vehicle
FEA	:	Finite Element Analysis
FESEM	:	Field Emission Scanning Electron Microscope
FRP	:	Fibre Reinforced Polymer
G_{IC}	:	Interlaminar Fracture Toughness
GFRP	:	Glass Fibre Reinforced Polymer
GPa	:	Giga Pascal
HMWCNT	:	Helical Multi-Wall Carbon Nanotube
J	:	Joule
J/m^2	:	Joule per Square Meter
LBL	:	Layer-By-Layer technique
LDPE	:	Low Density Polyethene

LVI	:	Low-Velocity Impact
MBT	:	Modified Beam Theory
MCC	:	Modified Compliance Calibration
MMT	:	Montmorillonite
MPa	:	Mega Pascal
MWCNTs	:	Multi-Walled Carbon Nanotubes
nm	:	Nano Meter
N	:	Newton
OBT	:	Original Beam Theory
PAH	:	Poly-Allylamine Hydrochloride
PMC	:	Polymer Based Matrix
PU	:	Polyurethane
PVC	:	Polyvinyl Chloride
PVDF	:	Poly (Vinylidene fluoride)
SDBS	:	Sodium Dodecylbenzene Sulfonate
SDS	:	Sodium Dodecyl Sulphate
SEM	:	Scanning Electron Microscope
SWCNTs	:	Single-Walled Carbon Nanotubes
TEM	:	Transmission Electron Microscopy
TGA	:	Thermo-Gravimetric Analysis
THF	:	Tetrahydrofuran

LIST OF APPENDICES

Appendix A: Samples Dimensions for DCB Test …… 158

Appendix B: Samples Dimensions for ENF Test……... 159

Appendix C: Samples Dimensions for Low Velocity Impact…… 160

Appendix D: Systematic Method Used in Collecting Data ……. 161

Appendix E: Materials Data Sheet…… ……. 166

This page left blank

CHAPTER 1: INTRODUCTION

1.1 Research Background

Carbon nanotubes (CNTs) are well-known as one of the most promising advanced carbon materials in the 21st century. The discovery of salient carbon nanoforms has paved the way for researchers to investigate the usage of CNTs in various scientific applications. CNTs are allotropes of carbon with a nanostructure in a cylinder shape. The length-to-diameter ratio of nanotubes is up to 132 million times, significantly larger than any other material. These cylindrical nanotubes have properties valuable in nanotechnology, electronics, optics, and other materials science and technology (Goel et al., 2020; Xiong et al., 2021). Formally derived from the graphene sheet, they exhibit exceptional mechanical properties, such as high toughness and elastic moduli. Nanotubes are categorized as single-walled and multiple-walled nanotubes. The properties and characteristics of CNTs are still being researched, and scientists are still researching to tap the potential new applications.

Current industrial and commercial applications demand lightweight composite materials with improved chemical and mechanical properties such as compressive strength tensile strength, tensile modulus, and strong thermodynamic stability. This combination of properties is difficult to obtain with traditional filler reinforced composite materials. The recent developments in fabrication of various composite materials reinforced with CNTs has advanced significantly and helped to overcome many limitations industries have faced over time and brought a new revolution in the materials innovation world (Goel et al.,2020; Leone et al., 2022; Ogwana, Mormune-Moriya and Nakamura, 2022; Xiong et al., 2021).

The usage of CNTs as an advanced reinforcement in polymer composites has begun since it was discovered in 1991 by Iijima (1991). The use of CNTs in the field of polymer composites is especially interesting. The smaller size of nanotubes has beneficial effects.

For instance, CNTs have large surface areas compared to traditional fibers, offering enhanced interaction between CNTs and the surrounding polymer matrix. Moreover, due to the one-dimensional structure of CNTs, oriented CNTs/polymer composite fibers have also generated great interest as such oriented systems can result in high reinforcing efficiency and excellent uniaxial conductivity. In the case of fiber-polymer composite materials, a good polymer matrix material is the one that can infiltrate between fibers and form a strong intermolecular bond and interaction among various components in the matrix. Depending on the type of matrix material, the composites can be divided into three main categories: (i) ceramic/inorganic matrix composites, (ii) metal matrix composites, and (iii) polymer matrix composites (Toozandehjani et al., 2018).

Generally, CNTs are called single-walled carbon nanotubes (SWCNTs) and multi-walled carbon nanotubes (MWCNTs). SWCNTs have a diameter of <1 nm, while several concentrically interlinked nanotubes with diameters >100 nm are known as MWCNTs. Microscopically, CNTs forms strong intermolecular bonds and interact with various matrix material through sp^2 electron clouds. However, achieving a desired mechanical property of the composite while balancing other properties and the finished material's optimum surface quality depends on the degree of dispersion reached by the CNTs within the polymer matrix material. Therefore, selecting the most suitable composite processing and fabrication method would be vital for every targeted commercial and industrial products development in order to achieve the intendend material quality and properties of the composites (Cha et al., 2016). To demonstrate this with an example, a fabricated composite may break in places where a higher percentage of CNTs are present because of ununiform fiber concentration in the polymer matrix (Shtein et al., 2013). In such circumstances, fiber breakage areas are the weakest point in the composite structure (Ivan'kova et al., 2020). Therefore, particular attention must be given when a composite

is being fabricated and cured while mixing is carried out. This will avoid the formation of localized defects in the composites.

1.2 Research Problem

Existing literature has greatly reported the development of various advanced polymer composite materials reinforced with CNTs. It has shown that various CNTs improve the yield strength, tensile modulus of rigidity, and the fracture strength of a polymer matrix through various mechanisms. In all cases, CNTs and polymer matrix interface play a significant part in determining advanced composites' accomplishment. For example, different loading modes (tensile and compressive) dictate respective mechanisms of damage in unidirectional (UD) composites in respect of fiber direction in the composite (Cheng, 2010). If the UD composites are exposed to axial loading to that of fiber direction, then micro-damage in the form of breakage of fiber or matrix develops during service life. This failure can account for 80 % of all service failures due to fracture (Christensen, 2006).

Previous studies conducted to analyze the failure mechanisms of CNT show that carbon nanotubes fail mainly based on fracture and pull out (Goony et al, 2005; Tang et al, 2011). The N-T polymer interfacial adhension and NT length have been dictating the failure mechanisms. The NT tends to be fractured during crack propagation in systems with strong filler matrix interfacial adhesion; otherwise they are pulled out of the matrix. In most cases, the determination of the failure mechanisms on imaging of fracture surface by scanning electron microscopy (SEM) (Zohar, et al, 2011; Guadagno et al, 2009) or transmission electronic microscopy (TEM) (Fiedler et al, 2006; Qian, 2006). Moreover, most of the studies conducted, have not tried to find a solution to this failure mechanisms.

However, this research study has methodically conducted a deep analysis of various failure mechanisms (shear failure, panel micro buckling, matrix yielding, and filament

micro buckling) that are linked with various composite processing and fabrication methods and parameters (Sun et al., 2018) and has identified various means by which the failures can be overcome to improve various mechanical performances of the polymer composites. Consequently, there is a need to understand better various mechanical and physical properties and the failure modes associated with the various composite structures, including tensile strength, impact resistance, impact damages, fracture toughness. However, this research study has primarily focused on the failure mechanisms which are likely to occur in the composite structures and materials. Thus, to overcome the limitation of SWCNTs and MWCNTs on polymer composite, helical multi-walled carbon nanotubes (HMWCNTs) as a reinforcing medium of polymer composite were explored in the present research. Hence, in this study, a selection of most used industrial carbon-fiber epoxy polymers was employed as matrix materials, and HMWCNTs were used as reinforcement.

1.3 Research Objectives

This research aimed to improve the fracture behavior of the carbon fiber reinforced polymer (CFRP) matrix and to understand the underlying failure mechanisms due to the addition of different content of HMWCNTs. In order to reach these objectives, calculated loading of 0, 0.2, and 0.4 wt. % HMWCNTs were dispersed in an epoxy polymer resin matrix to fabricate the nanocomposites. This was achieved through experimental analysis by focusing on the following research objectives (ROs):

RO1: To investigate the effect of adding HMWCNTs of different concentrations on the fabricated nanocomposite laminates (inter and intra-laminar failure).

RO2: To investigate the deformation and damage characteristics involved in the fabricated nanocomposite laminates' impact and after an impacted event.

RO3: To evaluate the fabricated nanocomposite laminates' thermal and electrical properties.

RO4: To characterize the fracture surface and the damaged area of the nanocomposite laminates under monotonic and impact loading conditions and correlate it with the underlying failure mechanism.

1.4 Research Significance

The significance of this research was two-fold. The first step was the fabrication of the nanocomposite laminates with different concentrations (0, 0.2 & 0.4) wt. % of HMWCNTs. A series of development studies was carried out through a systematic procedure to understand the various amounts of carbon nanotube loading on composite laminates. A series of composite laminate fabrication was prepared, developed, tested, and analyzed to understand the changes in their mechanical, thermal, and electrical properties. After analyzing the fabrication parameters, the suitable compositions of carbon nanotube on composite laminate were selected. Various efficient mechanical mixers and a suitable coating process were employed for this composite fabrication process.

The second step of this research study was to understand various interlaminar fracture mechanisms of the fabricated composite laminates via a series of analytical experiments. First, to evaluate various fracture mechanisms, low-velocity impact (LVI) and compression after impact (CAI) testing were conducted, followed by an ultrasonic C-scan for damage area analysis. Next, double cantilever beam (DCB) and end notched flexure (ENF) tests were carried out for fracture toughness investigation, followed by field emission scanning electron microscopy (FESEM) investigation. Furthermore, high-temperature thermal of the fabricated composite laminates was carried out using thermo-gravimetric (TGA) and differential scanning calorimetry (DSC) analysis and electrical conductivity.

Novelty exists in this study in the following areas: The use of HMWCNTs as a reinforcing element on polymer matrix composite; the dispersion of HMWCNTs in epoxy

was developed by using multi-dispersion technique; and application of the HMWCNTs/resin mixture by spraying in prepreg surface in contrast of direct mixing. In addition, the unique role of HMWCNTs on fracture toughness and impact loading was also reported in this study. This research study provides insight into a unique and new carbon nanotube and polymer composite laminate fabrication and development technique.

1.5 Research Scope

This research study primarily focused on improving the fracture behavior of CFRP matrix a carbon nanotube composite laminate and to identify its failure mechanisms under various modes of external loading.

This study will make use of procedures and equipment that differ slightly from other methods used in ealier studies. For instance; in the study conducted by Shukla et al., (2016) to analyze the alteration in flexural performance of epoxy composites, they used 0.1, 0.3 and 0.5 wt. % MWCNT. Also, the modulus and flexural tests were done using 3-point bend test. In another study conducted by Yang et a.l, (2018) to investigate fatigue failure and electrical resistance behavior of CNTs based composite at cryogenic temperature, tension -tension fatigue tests were conducted using a servo-hydraulic testing machine. Moreover, in most studies, the determination of the failure mechanisms on imaging of fracture surface was done either by SEM imaging (Zohar, et al, 2011; Guadagno et al, 2009) or TEM imaging (Fiedler et al, 2006; Qian, 2006).

However, for this study experiments were carried, 0.2 wt. % HMWCNTs-epoxy and 0.4 % HMWCNTs-epoxy composite were incorporated. In addition, the failure mechanism analysis was achieved using DCB, ENF, LVI, and CAI tests. Also, fractures surface morphological characterization was carried out using FESEM. The composite laminate's thermal stability and intermolecular bonding were analyzed using TGA and

DSC. Electrical conductivity analysis was also conducted to understand the effects on various physical properties. This research provides an in-depth understanding of various carbon nanotube-polymer composite laminate failure modes and failure mechanisms with the help of an ultrasonic C-scan. However, the scope of the present research is limited concerning the fracture and impact loading of the polymer composite and the electrical and thermal characteristics of the polymer composites.

1.6 Thesis Layout

The entire thesis is organized and presented in a systematic and orderly manner. The research study presented in this thesis will guide the readers to understand and recognize various strategic steps taken to complete the study. All the sections and sub-sections presented in this thesis are well explained with examples, scientific facts, and experimental evidence.

Following the standard thesis structure protocols, it began with abstracting the entire research work followed by introduction, literature overview, methodology, results and discussion, conclusion and future recommendations, and finally references. Various subsections were introduced under the introduction section, such as background study, research objective, research significance, and scope of work. Similarly, under the literature overview, topics such as composite materials and their applications, various damage sources in composite laminates, physical and mechanical behavior of various composite structures were discussed. Other subsection topics include an overview of CNTs and their properties, carbon nanotube-based composites, mechanical and other properties of carbon nanotube-based composites, various composite fabrication issues, and challenges. These discussions were also associated with various failure mechanisms in CNT composites and analyzed.

Under the methodology section, subsection topics such as materials used to fabricate composite laminate and fabrication process, analytical and mechanical performance

testing, and analysis. Then, under the chapter of results and discussion, various composite laminate fracture toughness modes were discussed alongside experimental evidence and analysis. Furthermore, various low-velocity impacts, composite laminate's electrical conductivity, and thermal stability were also discussed. Then finally, conclusions and future recommendations were drawn based on the provided results, discussion, and data analysis followed by references.

CHAPTER 2: LITERATURE REVIEW

2.1 Introduction

Composite materials or 'Composites' are materials made from two or more physically and chemically distinct and combined so that their constituent elements remain distinct (Nurazzi et al., 2017). Nurazzi et al. (2017) further indicate that composite materials have properties different from the constituent materials. Additionally, they state that composites find their place as an integral part of modern engineering applications ranging from defense to biological ones because they are biodegradable especially the polymeric composites. Moreover, Nurazzi et al. (2017) comment that the uniqueness of composites is their distinct mechanical and chemical properties. The ability to tailor these properties opens a wide range of applications and offers key advantages against conventional materials, making their use popular in many industries. Composites can be manufactured into different shapes, allowing design flexibility. This, coupled with the ability to tailor properties, offers optimum composites in industries (Nurazzi et al., 2017). A few examples of composites' ground-breaking advantages in particular industries are described hereafter.

Advanced composites offer a combination of being lightweight and having high strength, making their use very desirable in the aerospace and transportation industries. The use of composites in the manufacturing of aircraft and vehicle bodies has led to improved aerodynamic performances and a weight reduction of up to 20-30%, resulting in improved fuel economy (Mallick, 2007). Furthermore, greater dynamic properties such as fatigue resistance, creep resistance and good damping characteristics make composites the ideal materials to be used in airframe repair applications (Hu, 2012; Mallick, 2007). Furthermore, composites offer higher corrosion resistance and low maintenance costs with enhanced chemical properties. This has led to the transportation industry developing vehicles and components with longer services lives together with lower maintenance

costs. A similar revolutionary impact has been observed in the shipping and marine industry, resulting in cargo ships with better fuel efficiency, larger cargo-carrying capacity, and longer life cycles (Mallick, 2007). These developments include the domain of material and chemical science and the manufacturing regime. The improvement of manufacturing techniques and new techniques have further favored composites. Besides these industries, composites find effective uses in sports, process, energy, and construction industries (Ravishankar et al., 2019).

All the above applications are partly due to the enhancement of composite materials' mechanical and chemical properties. The major outcomes of these enhanced properties are weight reduction, increase in strength, dimensional stability, increased corrosion resistance, durability, and earthly life, higher impact strength, high electrical conductivity, improved surface properties, and ease of manufacturing (Yasa & Ersoy, 2018).

2.2 Applications of Polymer Composite Materials

In the twentieth century, composites were first developed and appeared as the spectacular alternative for several materials due to their best properties, mostly metal. The world deliberated the composites for aerospace applications, automotive, and power generation industries considering the environmental effects. Over the past years, the use of composite materials has increased considerably due to their extraordinary physical and chemical properties (Prabhakar et al., 2018). In today's life, composite materials play an essential role in improving our living standards and ultimate safety. Composite materials have many advantages over traditional materials, such as lightweight improved mechanical, physical, and chemical properties. In the 4th industrial revolution, various composite materials became extremely popular in multiple advanced application fields due to their superior nature over conventional materials. This increased use of composite materials is attributed to the fact that different materials with different physical and

chemical properties can be combined to fabricate and develop a composite material of individual-specific property and its specific application (Mahato et al., 2014). There are thousands of prominent applications of various composite materials in various fields. Some of the most common and well-known high-end applications of composite materials are aircraft, vehicles, bicycles, boats, sports accessories, sporting goods, fishing, shoes, tennis racquet (Hagezi, 2011).

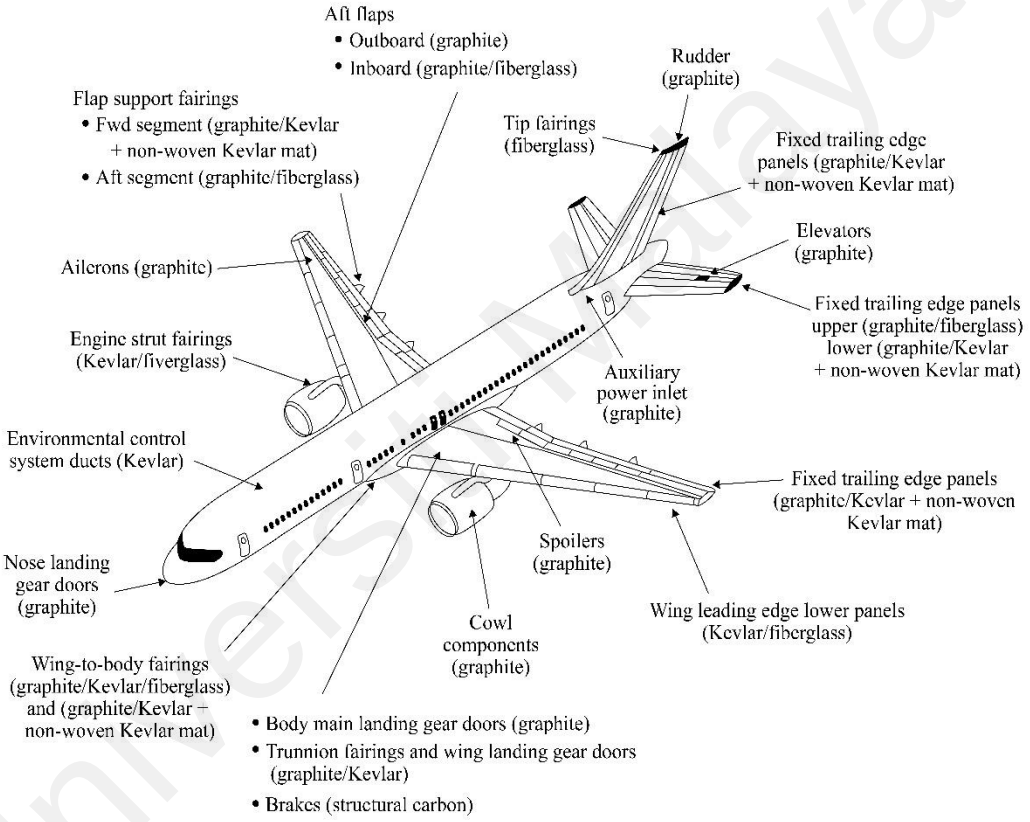

Figure 2.1: Different Components of Aircrafts Made from Composite Materials (Kumar et al., 2014)

Fiber-reinforced composites have numerous applications due to their exceptional mechanical, thermal, and physical properties. Major applications of these composite materials include aerospace, aircraft, furniture, electronics, oil and gas, medical, sports, textile, construction, and automobiles; Aircraft and aerospace industries are major users of composites (Mahato et al., 2014). Polymeric composites have a higher weight to strength ratio, better mechanical properties, and ease of processing. Furthermore,

polymeric composite materials can form various complex geometries and shapes. As a result, composites are used in cabins, flooring, ceilings, seats, food trays, and structural applications (Hagezi, 2011). In addition, composites are used to fabricate stabilizers, fins, rudders, tail boxes, fuselage, ailerons, and landing gear parts of aircraft (Mallick, 2007), as illustrated in Figure 2.1.

For instance, two major commercial aircraft manufacturers, Airbus and Boeing, have been using composites for various loading and non-loading application in aircraft. Carbon fiber composite is extensively used in these aircraft. Various military and commercial helicopters use composite materials to reduce overall weight and enhance performance (Mallick, 2007). Rotter blades, tail rotors, vertical fins, doors, are made from composite materials. When compared to their metallic counterparts, these composite components are significantly lighter (Yadav et al., 2020). Composites' physical and mechanical properties can be reformed by changing the type of fibers, matrix material, fiber concentration, fiber orientation, and dispersion (Mallick, 2007). Reduction in weight in the aviation industry leads to fuel and cost-saving. Some of the limitations of fiber-reinforced composites in the aircraft and aviation industry are manufacturing costs, lower impact resistance, and damages through lightening (Soutis, 2005). It is worth mentioning that over 70 % of the structural parts and components are made from composite materials in today's aircraft and spaceships. As a result, fuel efficiency increased by at least 30 %.

Moreover, composites in the aerospace industry reduce carbon footprint (greenhouse gas emissions) significantly, protecting from global warming. As the composites present a high strength to mass ratio, that’s the reason the composites are being used in propellers, superstructures, and bulkheads. Using these composites in a particular application decreases the weight and improves the processing or fabrication assembly (Soni et al., 2020). Furthermore, composite materials also have shown significant benefits in the construction industry. There is a substantial increase in the usage of composite products

in residential and various commercial construction projects. Over the years, stainless steel has been replaced by similar and better properties composite structures. Composite structures provide a significant advantage over similar sizes and dimensions of stainless and other alloy structures. Compared, composite structures are lightweight and give much better physical and mechanical strength, reducing total building and housing weight and providing better safety (Soni et al., 2020). Recently, most buildings have been done through plastic-laminated beams and trusses. It is possible to prevent termite invasion of rotting using plastic-laminated beams, which increases the structure's lifespan. In addition, these composite products are commonly used to build outdoor decks and porches (Sanjay et al., 2016). Thus, the homeowners can cut the costs to repair their roofs by using composites like fiber-reinforced cement shingles.

The increased resemblance of composites with wood plays an essential role in improving homes' aesthetic value. Similarly, doors and floors made using various composite materials often look like wood and are cost-friendly for most homeowners (Gupta et al., 2016). Composite-based construction materials can also make the kitchen and bathroom walls durable and waterproof by using selective composite construction materials. It is quite easy to clean such composite material surfaces (Gupta et al., 2016). Furthermore, composite materials are also being used to improve the fire safety of residential and commercial complexes. Various composite materials are developing multiple fire-retardants (resistant) parts and components. Using various composite materials in various construction applications also reduces the total carbon footprint and significantly protects from greenhouse gas emissions (Gupta et al., 2016).

Polymeric composites are used in the main body, non-load-bearing components, and engine parts in automobiles. Exterior components such as hoods, bumpers, side mirror casing, door handles, mud guards, are made from composite materials (Muhammad et al., 2021). Glass fiber-based composite materials are used to fabricate exterior parts. Glass

fiber is preferred over carbon fibers due to lower cost. Interior automobiles use composite materials in cup holders, dashboard, seats, floor linings, door panels, glove compartments, and roof panels. Roof, floor, and door panels manufactured through composite are much lighter in weight and have increased thickness for better strength and mechanical properties (Ravishankar et al., 2019). Composite materials have become the most important parts of sports cars. Due to the reduced weight, these composite materials actively enhance the performance and efficiency of sports and formula F1 cars. Major body parts of formula F1 cars, such as chassis, interior parts, and suspension parts, are carbon fiber-based composites (Ozkan et al., 2020).

In sports, composites make rackets, bicycles, fishing rods, hockey sticks, helmets, gym equipment, surf and snow boards, cricket bats, baseball bats, and shoes. The use of composite materials offers advantages such as weight reduction, reductions in vibration, cost reduction, and flexibility in designing. For example, bicycle frames are mostly carbon fiber-based composites (Karbhari, 2007). Similarly, fiber-enforced composites are extensively employed in various marine applications to manufacturing boats and different components (Su, 2014). In construction industries, composites are used in doors, window panels, roof tiles, wall partitions, beams, and trusses (Karbhari, 2007). Composites are also employed in medical, textile, and packaging industries owing to their physical and mechanical properties (Park et al., 2017).

The CNTs are being used in composite laminates for various applications, including automotive, aeronautical, wind energy, and boating sector. The popularity of these materials has demanded proper research and development to improve particular properties (Mouritz et al., 2001). Applications of CNTs primarily related to composite laminates are always considered and preferred because of the attainment and enhancement of the required multifunctional properties, including mechanical properties, strain, and crack propagation (Islam et al., 2015). According to the research by Mouritz

et al. (2001), the mechanical properties, including shear, flexural and elastic modulus, of the same composite were compared. But the actual comparison was between the fabrication methods of this composite having glass fiber and vinyl-based polyester epoxy fiber-based as reinforcement. The fabrication method involves a hand layup and a vacuum-infused approach. This study concluded that the hand layup method increased the composite's porosity, exhibiting lower mechanical properties of overall structural composite based on glass reinforced fiber. This study was also about the development of the composite for the application of submarine and naval ships.

In a sort of statistical research by Islam et al., fiber-reinforced polymers are widely used for the applications of the marine sector. During this research, carbon fiber reinforced composite modification was done with the 2 % and 0.3 % addition of montmorillonite (MMT) nano-clay and (MWCNTs) respectively by mass. The results revealed that the modification has drastically increased the mechanical and thermo-mechanical properties of the carbon-based polymer composite (Islam et al., 2015). A study was made possible to discover and analyze the characteristics of aramid fiber-reinforced composite and the glass fiber reinforced composite, especially for marine applications. The corrosion resistance and the strength to weight ratio were the main properties considered the most in this research (Selvaraju & Ilaiyavel, 2011). A similar trend goes for automobile industries as well. As more new and innovative composite materials are commercially available, automobile companies replace traditional materials.

As more composite materials are being used in an automobile structure, it saves manufacturers in production costs and, at the same time, improves fuel efficiency and ultimate safety. Moreover, it is worth mentioning that EV automobiles are hitting the more and more composites are being consumed (Selvaraju & Ilaiyavel, 2011). Recently carbon nanotube reinforced polymer composites have shown great potential and interest in all the above-demonstrated applications and usage. In some instances, CNTs showed

better performance improvement. However, further research and development are needed to optimize various performance aspects and improve usability. Over hundreds of research findings were reported in the literature regarding possible carbon nanotubes usage in various high-end applications, those cited in multiple references in this research report. This research study also demonstrated the possible carbon nanotube usage as reinforcement material in composite laminate in various composite structures. The future of composites is very bright and will be improved further. The researchers have a great chance to explore more about composites' properties. This research and development will also explore more fabrication, design, and analysis methods for composites.

2.3 Polymer Composite Materials

Composites can be categorized as natural and synthetic composites. Natural composites have been in use and available in nature for millennia. One of the examples of a natural composite is wood, which consists of long cellulosic fibers and lignin (Faruk et al., 2012). The human body's bones are another example of a natural composite made of a brittle and stiff substance called hydroxyapatite and a comparatively softer material called collagen (Hu, 2012). In modern engineering applications, several artificial composites are being developed and used. Bricks used in the construction industry are a typical example of a composite made of mud and straws. Concrete is another synthetic composite that combines sand and cement. This combination improves the overall compressive and tensile strength and tensile modulus (Gurunathan et al., 2015). Steel bars are added to concrete blocks to increase strength, and such further concrete blocks are referred to as reinforced concrete (Hollaway, 2010).

Composites can be further classified into a broad range of categories based on the nature of the materials used to formulate them. For example, the materials used to fabricate a composite are often termed a ‘Resin.’ If the resin material is polymeric and infused with fibers, this results in a class of composites known as fiber reinforced polymer

(FRP) composites. FRP composites can be classified into bio-FRP, synthetic FRP, and hybrid FRP composites based on the constituent matrix material and fibers (Hollaway, 2010; Satyanarayana et al., 2009).

2.3.1 Types of Polymer Matrix Composite

To introduce the new aspects of polymer matrix composite on modern technology, the composites made their way from the 1940s as a significant material for engineering applications. Furthermore, polymers as a matrix in the composite field made these materials very attractive for industrial applications. These applications enabled polymer-based composites as an alternative to metals such as steel and aluminum (Ravishankar et al., 2019). Typically, composites are fabricated of two or more components of similar or dissimilar physical, chemical, and structural properties. When these different component materials combine using various fabrication methods, new physical and chemical properties are formed. Examples of such composite materials are concrete, mortar, wood, reinforced plastics (e.g., fiber/filler-reinforced polymers), ceramic composites, metallic alloys. In all these composites, various component materials are combined methodically using suitable fabrication methods depending on each component's nature (Ravishankar et al., 2019).

All the available composite materials can be considered into two types, namely-natural and human-made (artificial) composites. Natural composites can be found in nature and have been around for thousands of years (Ram et al., 2020). One such example of a natural composite is wood, made of long cellulose fibers and lignin (Geerinck et al., 2016; Smith et al., 2019). The bones in the human body are another example of a natural composite, developed with a brittle and stiff substance called hydroxyapatite and a much softer material called collagen (Polovina, 2018). All these natural composites are formed naturally and without any outside interference. However, millions of artificial composites are also being produced for various applications and usage. Concrete is considered as a

synthetic composite, which combines small stones, sand, and cement. This combination gives them excellent compressive strength, tensile strength, and tensile modulus. In addition, there are currently various metal rods and wires that are also added to concrete in such blocks to increase strength and are referred to as reinforced concrete (Shinagawa et al., 2018). These artificial composites are being produced using suitable fabrication methods depending on individual components' nature and properties.

Another popular artificial polymer composite is fiberglass used in various industry sectors such as automobile, sports, construction. Furthermore, it has recently been shown that using multiple fibers in composite material increases fracture resistance, which is one of the most desired properties (Scotti et al., 2016). Nowadays, some of the most complex composite structures are made from carbon fibers, stronger than fiberglass. However, such materials tend to be lighter with enhanced mechanical and physical performances, so their production process is somewhat more expensive than others (Ram et al., 2020).

In recent days one of the most significant milestones achieved in the invention of modern composites is that they are both light-weight and robust, and affordable. It is very important to properly choose the right matrix and reinforcement material recipe to ensure that the final composite material exhibits the desired property for a specific application (Shinagawa et al., 2018). The benefits offered by various forms of composites are remarkable and sometimes surprising. Some of the most important benefits are resistance towards corrosion and erosion, thermal and chemical durability, mechanical and physical flexibility, extremely lightweight, and higher physical strength. They can also be used as ultra-strong building materials for various construction and architecture projects, high-strength aerospace and automobile parts in many industries, and replacing materials such as aluminum, steel, granite, marbles (Stankovich et al., 2006). Composite materials' popularity is increasing faster than one imagined years ago, as it offers a versatile choice for designers and manufacturers from various applications fields.

2.3.2 Types of Matrix and Fibres

Despite the fact that many matrix materials are accessible and employed for a variety of commercial and industrial purposes, the current study will focus solely on polymer matrix materials. As a result, the discussion will be limited to the polymer matrix system, which has the potential to build a variety of polymer-based composites. Thermosetting and thermoplastic resins are the two types of matrix systems. A thermoplastic resin consists of a number of thermoplastic polymers that combine to form a variety of composites. Fabric composites are commonly made from polyamides and polypropylene (Shinagawa et al., 2018). The thermoplastic polymer's recyclability and high scale production allow the composite industries to adjust for economic factors. Although the mechanical qualities of thermoplastic materials are less than those of thermosetting materials, many mechanically stable thermoplastics are presently being developed for composite applications. However, the thermosetting polymer matrix system includes thermosetting polymers well known for their curability. When the structure of these materials is cured fully, they can't be reshaped or remolded again even upon heating. Generally, epoxy and polyesters (unsaturated) are used as thermosetting in composite fabrications (Stankovich et al., 2006).

The polymers may be further classified according to their morphological properties. The morphology of the polymers can be crystalline, amorphous, or semi-crystalline (Scotti et al., 2016). In crystalline structure, the molecules are aligned in a regular pattern, while in an amorphous structure, the random arrangement of molecules is observed. Furthermore, semi-crystalline structures represent both regular and irregular structural arrangements. Many of the properties of polymers are dependent on their structure. Due to an organized structure, crystalline materials possess a solid phase. When heated up to their sharp melting point, they transform into the liquid form and the solid phase representing a melting transition. On the other hand, due to its irregular pattern, the

amorphous structure shows a sliding trend with a range of temperatures on which they remain soft, that is, a temperature transition. While in the case of semi-crystalline structures, both melting and transition temperatures are observed due to crystalline and amorphous regions (Scotti et al., 2016).

Fibers are generally being used as a positive reinforcement additive. Various fibers are being used to improve mechanical, physical, chemical, electrical, thermal, corrosion resistance, and fire-retardant properties (Geerinck et al., 2016; Smith et al., 2019). Currently, there are a wide variety of advanced fibers available for various applications. Examples of such fibers are carbon fiber, Kevlar, carbon nanotube, cellulose, lignin. The polymer-based matrix with the enforcement of the fibers forms a polymer-based matrix usually called polymer matrix composite (PMC) (Geerinck et al., 2016; Smith et al., 2019). Fibers are added to the composite to bear the load from the polymer matrix. The main reasons for the PMCs' popularity are their light weight, high modulus, and high strength in specialized fiber directions. They are also very attractive materials because of their low cost and simple fabrication with better abrasion and corrosion resistance characteristics (Geerinck et al., 2016; Smith et al., 2019).

2.3.3 Other types of Laminated Composites

A composite laminate in material sciences combines layers of various composite material fibers. This combination is necessary because it collectively provides strength, stiffness, and thermal coefficient to the layers' final developed assembly. The layers present in the assembly may be of polymer, metal, or ceramic fibers with the required strength, modulus, and other properties (Geerinck et al., 2016). The commonly used fibers are silicon carbide, glass, boron, graphite, and cellulose, while the typically used matrix are aluminum, epoxy. (Smith et al., 2019). The main component of laminates is ply, and in the ply, all the fibers follow the same direction, as shown in Figure 2.2. The fibers must be stronger and stiffer, so the ply is used because of its modulus and anisotropically

oriented flexibility. A laminate can have more than plies for an assembly. Not all the plies' directions can be kept in the same direction as for unidirectional fiber orientation, and lateral contraction causes weak load-bearing ability in the direction transverse to the fibers. The laminate's direction or assembly is demonstrated in ply directions (Koide et al., 2013).

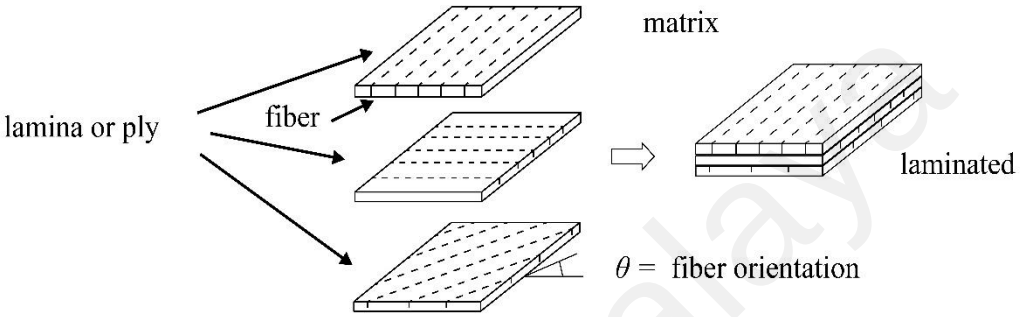

Figure 2.2: Laminated Composite Materials (Koide et al., 2013)

Different layers can form a hybrid and very strong structure for the laminate. The direction of the layers in laminates is significant. Generally, the layers are oriented as orthotopically or transverse isotopically, presenting the directions as orthotropic, anisotropic, and quasi-isotropic (Koide et al., 2013). The quasi-isotropic laminates mostly show the response of in-plane isotropic nature but are not confined to show bending or out of plane response. The layers' gambling sequence may also exhibit the coupling of the responses in or out the plane. The direction of the outer ply is mostly kept as a reference, while the medium layers of plies are kept thick twice of the outer layer and are kept in the direction of the reference layer. This anisotropic nature has developed a chance to design and optimize the laminate properties by controlling core material properties, which are not observed in metals (Koide et al., 2013).

2.3.4 Mechanical Behaviour of Polymer Composite

The polymer composites consist of polymer matrix fillers of various shapes, sizes, and forms. These fillers are dispersed or suspended in the polymer matrix. The composites' properties are desirably exhibiting the best modulus, stiffness, impact, and low weight characteristics (Lee & Chung, 2003).

In a study conducted by Lee & Chung (2003), the addition of nanoparticles in the composites, even in a minimal ratio 2-3 %, can enhance many other properties such as toughness and wear resistance. In this study, several nanoparticles were incorporated in the polymer composites, especially silver and carbon nanoparticles, to attain the required properties for the textile, glass, and carbon-related industries. The authors explained that incorporating carbon nanotubes is vital because of its dramatic effect on the betterment of the polymer composites' mechanical characteristics; a small volume of 2-5 % can generate excellent results. In the same study, the mechanical properties of a composite based on polyester fiber and glass reinforcement were analyzed. The mechanical properties, including the tensile modulus, impact strength, and bending strength, were inspected using multiple fibers. As a result of this research, a numerical model was also developed to study the laminated composites mechanical characteristics considering incorporating one and multiple fibers. It was also concluded that the strength of glass fiber reinforced composites drops gradually after the elastic deformation of the composite.

Vallbo (2005) studied the mechanical properties with vinyl epoxy and polyvinyl chloride (PVC) based matrix with carbon-based fiber reinforcement. The composite showed better mechanical, electrical, and environmental properties, reducing weight, fuel consumption, and environmental effects. In another study to determine various mechanical and structural properties of MWCNTs reinforced polymer composites using instrumental indention testing, Tarfaoui et al. (2018) developed a finite element analysis model using ABAQUS software to simulate a micro-indentation test and then conducted

experimental tests. Table 2.1 shows the elastic properties of samples versus CNTs fractions while Table 2.2 shows the cohesive zone model. Numerous testing and analysis revealed that the polymer-based composites' mechanical characteristics were enhanced using MWCNTs as a possible reinforcement additive. In a similar study conducted by Tam & Wu (2017); (Torabi et al., 2013). An evaluation of the microstructure of the crater created by indentation was conducted using an SEM and compared with the microstructure of numerical models. The authors concluded that adding a small number of CNTs to polymer composites improved interfacial fracture rigidity and can significantly stop the growth and propagation of micro-cracks along with other mechanical properties. This research study primarily indicates that carbon nanotubes can be used as a positive reinforcement additive to improve interfacial fracture rigidity. In addition, the research was made to reduce the fabrication cost and improve stiffness. This study fabricates the composites with various resins, including polyester, epoxy, and various reinforcement such as carbon and aramid-based fibers.

Table 2.1: Elastic Properties of Samples versus CNTs Fractions

	0%	0.5%	1%	2%	4%
E_{11} (GPa)	59.11	59.138	59.16	59.219	59.33
E_{22} (GPa)	59	59	59	59	58.55
E_{33} (GPa)	7.6	7.623	7.6	7.67	7.81
v_{12}	0.089	0.089	0.0892	0.0892	0.0892
v_{13}	0.27	0.27	0.27	0.274	0.275
v_{23}	0.28	0.28	0.277	0.279	0.28
G_{12} (GPa)	8.250	8.257	8.270	8.285	8.316
G_{23} (GPa)	3.97	3.99	4.017	4.04	4.105
G_{13} (GPa)	0.27	0.27	0.27	0.274	0.275

(Source: Tarfaoui et al., 2018)

Table 2.2: Cohesive Zone Model

	0%	0.5%	1%	2%	4%
G_{Ic} (KJ/m²)	0.943	1.175	1.132	1.1	1.1
G_{IIc} (KJ/m²)	0.1	0.1	0.1	0.1	0.1
G_{IIIc} (KJ/m²)	0.1	0.1	0.1	0.1	0.1

Similarly, Prabhakar et al. (2018) fabricated several composites with various combinations of resins and reinforcement to study the composites' mechanical properties. The variation of volume percentage for a particular fiber or resin was also considered in

this study. It was observed that, in a combination of nano-clay and polyester, an increase in the amount of nano-clay caused an increase in impact the strength. Still, at the same time, it affects the ultimate tensile strength of the composite to lower down. Another research was made by Kimpara et al. (1991) to analyze the various composites for the application of marine construction. Rathore et al. (2016) assessed the durability of glass fiber/epoxy composite for high-temperature applications to provide further evidence. The study used MWCNTs under loading conditions subjected to a temperature range of 20 to 200 degrees. Upon various testing and analysis, the researchers found that the addition of 0.1 wt. % MWCNT to the composite yielded a 32.8 % increase in tensile strength and 11.5 % increase in tensile modulus over the glass fiber/epoxy composite for flexural testing of glass fiber/epoxy and MWCNTs composite at room temperature. The results also concluded that nano-fillers may not always help gain higher mechanical properties. It also depends on the in-service environmental temperature and relevant parameters. Many similar research reports are being published in the literature demonstrating potential carbon nanotubes usage as a positive reinforcement additive (Rathore et al., 2016).

2.4 Fibre Reinforced Composites

The composite materials based on polymers as matrices appeared in the mid of previous century because of the demanding properties like high-strength and light materials in various branches of technology, primarily in the aircraft and space ones. At present, a wide variety of structural composites based on strong reinforcing fibers (glass (GFRP), carbon (CFRP), graphite, boron, aramid (AFRP), basalt), and polymeric binders, both thermosetting (epoxies, polyesters, vinyl esters, phenolics, polyimides), and thermoplastic (nylon, polyethylene, polypropylenes, polycarbonates) have been developed (Lubin, 2013). In the middle of the past century, the demand for such structural materials was so high that these structural composites' large-scale production started in

just 15-20 years. Previously, industries took 25 years to produce or develop a product on an industrial scale (Lubin, 2013). Shortly, many fiber-reinforced polymer composites were developed with suitable optimization, research, and approach. Several techniques were discovered to fabricate various types of composites in a very short time, including lamination techniques (manual or automated), various types of filament winding, protrusion, textile preforming (braiding, weaving, knitting), vacuum-assisted resin transfer, and resin infusion molding (Lubin, 2013).

In generally, composites have two main levels of heterogeneity: the microscale level (for instance, the heterogeneity of a monolayer composed of reinforcing fibers and a matrix) and the macroscale one (e.g., the heterogeneity of a laminated structure composed of monolayers with an arbitrary layup across the thickness of a laminate (Lubin, 2013). It should be noted that an interface layer between the reinforcing fibers and matrix is also introduced to describe composites' mechanical behavior better. The development of modern composites has materialized the idea of manufacturing materials with prescribed or controlled properties. Unique in its simplicity, the idea of fiber reinforcement was laid at the basis of composites. Dissimilar materials, as regards their properties, were joint as a yielding matrix and useful reinforcing elements (Lubin, 2013). This idea was replicated from nature − the leaves and stalks of plants and human and animal bones are anisotropic materials reinforced by fibers, for instance, composites (Raju & Shanmugaraja, 2020). The fibers are mainly responsible for the high modulus properties of structural composites in the reinforcing directions. In contrast, the polymeric resin matrix operates as a medium to transfer stresses between adjoining fibers through adhesion and protects them from mechanical damage and environmental actions. Their morphology fiber-reinforced composites are markedly heterogeneous anisotropic materials; for instance, their mechanical and physical properties vary from point to point in the body and are different in different directions (Raju & Shanmugaraja, 2020).

FRP composites are formulated using a polymer matrix reinforced with fibers as a dispersed phase. Materials such as glass have greater mechanical properties (e.g., hardness), which is not apparent in their traditional solid form since external loading induces failures due to flaws such as surface cracks and cause brittleness (Raju & Shanmugaraja, 2020). However, when produced in fibrous form, such materials can display these higher mechanical properties in an optimized form as the failures will be restricted in relatively smaller fibrous areas. Hence, a combination of polymeric matrix and fiber materials in the form of FRP composites yields exceptional properties. The composite material will combine the polymeric matrix's properties and reinforcements (Raju & Shanmugaraja, 2020). The matrix spreads out the load applied in the composite among each of the individual fibers and defends the fibers from mutilation caused by abrasion and impact. This is commonly known as glass fiber reinforced composite. Furthermore, using multiple reinforcement fibers in a composite material increases fracture resistance by many folds, which is one of the most desired properties (Raju & Shanmugaraja, 2020).

The polymer matrix used in the composites is usually of two types: (i) Thermosets (e. g., epoxies, phenolics) and (ii) Thermoplastics (e.g., low-density polyethylene (LDPE), high-density polyethylene (HDPE), polypropylene, nylon, acrylics). The reinforcement fibers are either synthetic (e.g., glass fiber, CNTs) or natural fibers (e.g., cellulosic fibers, wool (Prashanth et al., 2017)). The reinforcing fibers can be arranged in the matrix in different forms: (i) as unidirectional arrangement of fibers, (ii) roving - a long narrow bundle of fiber arrangements, (iii) veil mat – a thin pile of randomly orientated, (iv) looped continuous fibers, (v) chopped strands and even as (vi) woven fabric (Gurunathan et al., 2015; Kmetty et al., 2010; Prashanth et al., 2017). Polymeric matrices in composites are a cost-effective choice for industrial applications. These applications push FRP

composites to alternative metallic materials such as steel and aluminum in different fields (Chung, 2010).

One of the most popular FRP composites is glass fibers and is being excessively used in sports, automobile, aerospace, and construction industries (Sathishkumar et al., 2014). The properties of FRP composites are determined by mechanical and chemical properties of the matrix and reinforcing fibers, the orientation and geometry of reinforcement fibers, fiber content, fiber-matrix interface, and type of dispersion technique during the fabrication process (Chung, 2010). Usually, reinforcement fibers have greater mechanical properties along certain lengths resulting in anisotropic properties of composites. As the mechanical properties of the reinforcement fibers are greater than the polymeric matrix, higher fiber content usually offers greater mechanical properties of the resultant FRP composite to some extent (Prashanth et al., 2017). The use of carbon fibers in the composites as reinforcement medium is well-establish as evident in the literature. In light of that, the use of CNTs is also promising as a reinforcing medium due to their unique properties, and in the present work, this aspect was explored in detail. Towards that, the background information regarding CNTs is presented in short hereafter.

2.5 Carbon Nanotubes (CNTs)

CNTs are often known as bucky tubes, and their structure consists of hexagonal geometry. They possess unique electrical and mechanical properties and have extraordinary strength (Soni et al., 2020). The term CNTs first came up in front of the research community when Kroto et al. (1985) discovered it in 1985 and placed them under the fullerene family. Both bucky-balls and CNTs are members of the fullerenes family and possess different structures. CNTs are cylindrical, while bucky-balls are spherical fullerenes. Thostenson & Chou (2002) concluded that the morphology of CNTs strongly depends on the magnitude and orientation of the chiral vector.

2.5.1 Different Kinds of CNTs

The atomic arrangement of CNTs plays a vital role in defining nature as either metallic or semi-conductive. In 1991, (MWCNTs) were synthesized by Iijima (1991) by using the arc-evaporation technique. CNTs are divided into the following categories based on the number of tubes present in their structure.

2.5.1.1 Single-Walled Carbon Nanotubes (SWCNTs)

Single-walled carbon nanotubes are one-dimensional material and consist of one sheet of graphene rolled upon itself whose length varies and depends on the preparation technique used. The tube diameter generally varies from 1 to 2 nm (Moradi et al., 2012), and the representative structure is demonstrated in Figure 2.3. SWCNTs are anisotropic and have directional mechanical, electrical, and thermal properties.

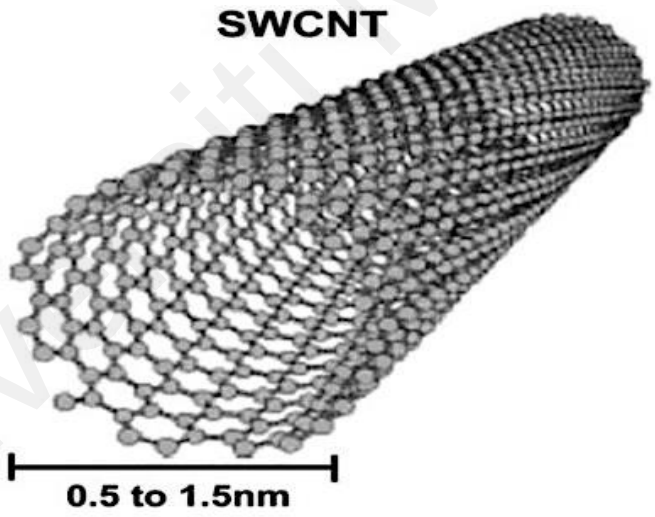

Figure 2.3: Structure of a Single-Walled Carbon Nanotube (Ribeiro et al., 2017)

Saether et al. (2003) observed that the thermal conductivity of CNTs was nine times more than copper in the direction of the tube length, while it was reduced 250 times in their radial direction. Defects in CNTs cause the reduction of mechanical, electrical, and thermal properties. Scattering occurs when low-frequency photons interact with these defects, causing a reduction in the thermal conductivity. SWCNTs can be produced using different methods such as the electric arc technique and laser ablation (De Volder et al.,

2013). The electric arc technique generates multi-walled and single-walled carbon nanotubes and yields a much smaller number of fullerenes. On the other hand, Journet et al. (1997) produced a high yield (70 - 90%) of SWCNT using laser ablation technology. Advanced research towards the synthesis of low-cost production of CNTs is making it possible to use them in a wide range of applications (Ibrahim, 2013).

2.5.1.2 Multi-Walled Carbon Nanotubes (MWCNTs)

MWCNTs have more complex structures than SWCNTs. MWCNTs consist of multiple SWCNTs nested in each other, and the diameter of the MWCNTs generally ranges from 2 to 50 nm. The inter-layer distance between these tubes is approximately 0.34 nm (Moradi et al., 2012), as in Figure 2.4.

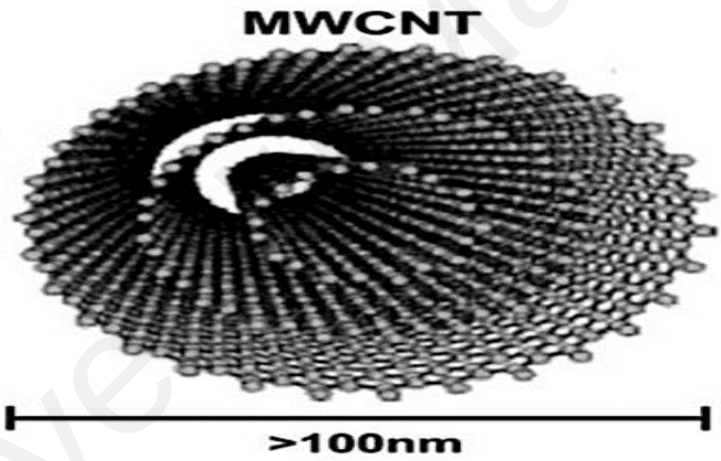

Figure 2.4: Structure of Multi-Walled Carbon Nanotube (Ribeiro et al., 2017)

MWCNTs have a 3-dimensional structure due to the positioning of the carbon atoms. Different structural types are present in the tubes and sheets, which are orientated at an angle to the tube axis. This angle is generally affected by synthesis condition, presence of a catalyst, and composition (Arunkumar et al., 2020). MWCNTs can be formed by using different synthesis techniques. Chemical vapor deposition has been proven the most promising technique for the production of MWCNTs (Brukh & Mitra, 2006). Andrews et al. (2002) had developed a cheaper CVD method for continuous production of MWCNTs and highlighted the important factors such as reaction temperature, partial pressure,

purity, size, and reactor temperature. It has been reported that CNTs at higher concentration are toxic and needs a detailed analysis before using them for medical application such as drug delivery (Francis & Devasena, 2018). MWCNTs are widely used in food packaging, electrical appliances, and applications where high strength is required (Ibrahim, 2013). They are extensively used in electron-emitting applications due to their superior electrical properties, high thermal conductivity, and higher length to diameter ratio (Soni et al., 2020).

2.5.1.3 Helical Multi-Walled Carbon Nanotubes (HMWCNTs)

Helical MWCNTs are also known as coiled MWCNTs, whose diameter ranges from 20 to 30 nm. They are synthesized when many MWCNTs are assembled and twisted around each other. Similar to textile fabric, Helical MWCNTs provide enhanced load transfer between fillers and matrix material, and their mechanical strength largely depends on the helical structure (Zhang et al., 2010). Helical MWCNTs are synthesized using catalytic chemical vapor deposition technique where the source of carbon is graphite and catalyst is FeMo/MgO (Somanathan & Pandurangan, 2010). A typical structure of the HMWCNTs is illustrated in Figure 2.5, which is 20 to 30 nm diameter.

Helical MWCNTs are known for unique properties with a vast range of applications. Extensive research, development, and innovations pave the path for using these promising materials in the industrial sector. Helical MWCNTs promise filler materials due to their physical, mechanical, thermal, electrical, chemical, and corrosion resistance properties (M.-Q. Zhao et al., 2014). In addition, nanometric size, diameter, aspect ratio, and cylindrical geometry make this material ideal for thermal and electric conductivity applications (Vijayan et al., 2019).

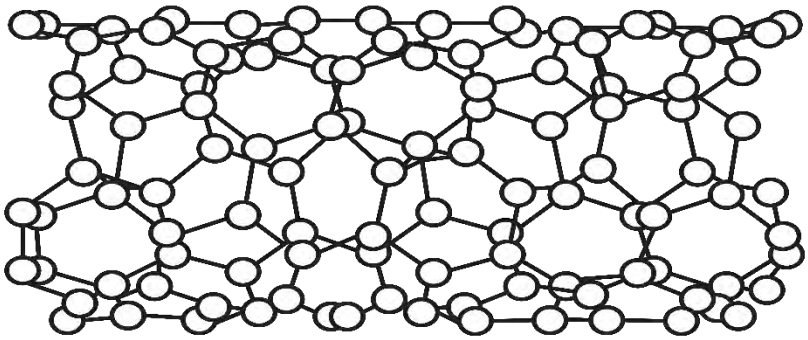

Figure 2.5: Structure of a Helical Multi-Walled Carbon Nanotube (Saether et al., 2003)

In this study, helical MWCNTs (HMWCNTs) was selected as reinforcing element in the polymer matrix composite for the following reasons:

- HMWCNTs can physically intertwine better over traditional microfiber reinforcements in a polymer matrix and thus are foreseen to enhance the composite's mechanical, thermal, and electrical properties.
- HMWCNTs are foreseen to enhance cohesion/inter-facial bonding better than straight CNTs due to the 3D helical interlocking mechanism.
- HMWCNTs are highly desirable due to their unique geometrical elegance and inherent physical properties.
- HMWCNTs in the polymer matrix can absorb more impact loads and possess higher resilience and flexibility in composites upon external loading.

2.5.1.4 Other Kinds of CNTs

Apart from the two basic structures of CNTs (MWCNTs and SWCNTs) there are three more possible types of CNTs; this is; chiral carbon nanotubes (CCNTs), zig-zag carbon nanotubes (ZZCNTs), and armchair carbon nanotubes (ACNTs). The three CNTs are shown in Figure 2.7. These three CNTs differ based on the " rolling up" of the graphite sheets along lattice vectors during the creation process of the graphite. A pair of indices m and n is used to represent chiral vectors. These two vectors correspond to the number of unit vectors along with the two directions in graphene's honey comb crystal lattice. The

nanotube is called armchair when m= n. The nanotube is called zigzag when m= 0. The chiral vector .The chiral vector mechanism is shown in Figure 2.6. All other forms of configurations are designated as chiral (Dresslhaus, 2004; Terrons, 2003; Zhang & Li, 2009)

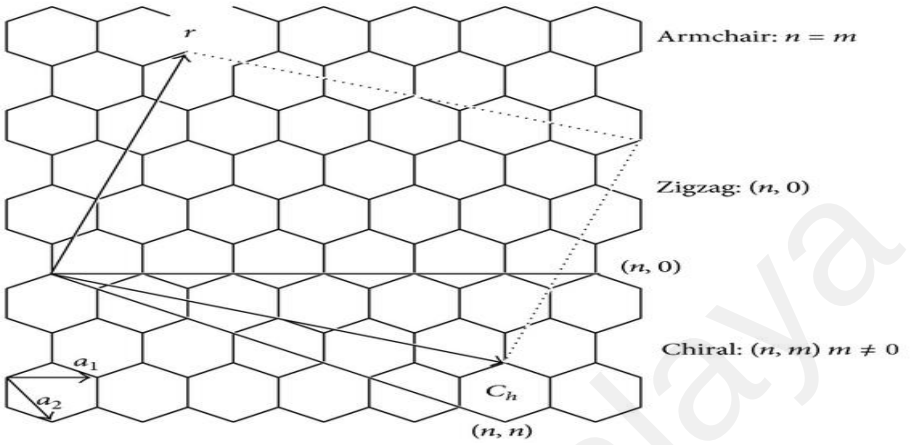

Figure 2.6: Formation of Single-Wall Carbon Nanotubes by Rolling of a Graphene Sheet along Lattice Vectors (Dresslhaus, 2004; Terrons, 2003; Zhang & Li, 2009)

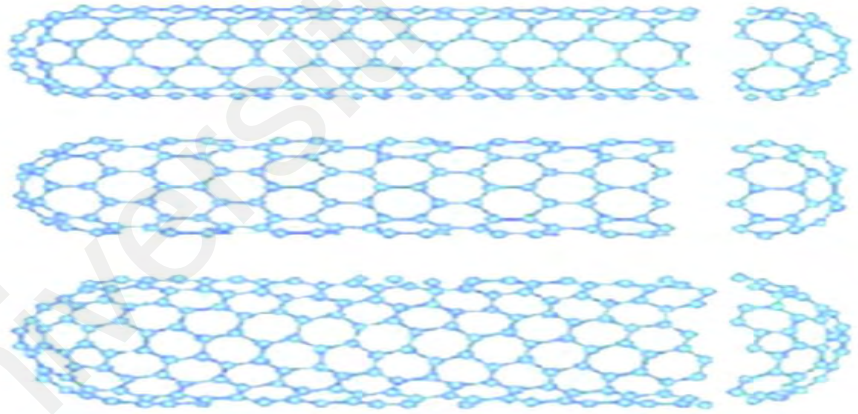

Figure 2.7: Three Types of Carbon Nanotubes: Armchair, Zigzag and Chiral Tubes respectively (Dresslhaus, 2004; Terrons, 2003; Zhang & Li, 2009)

2.5.2 Mechanical Properties of CNTs

Carbon nanotubes are anisotropic and ideally have a few defects. Due to the high aspect ratio, CNTs exhibit excellent mechanical properties. The excellent strength of CNTs is due to the carbon-carbon sp^2 bonding among the carbon atoms (Shokrieh & Rafiee, 2010). Synthesis of CNTs, the study of their behavior, and the effect of synthesis conditions on mechanical, thermal, and electrical properties are still under investigation.

Salvetat-Delmotte et al. (Salvetat-Delmotte & Rubio, 2002) explained the mechanical properties of CNTs and described the effect of reinforcement for composite materials. The strength of composite material is a multi-dimensional field and requires microscopic as well as macroscopic modeling. The modeling explains various properties except for the failure mechanisms. Failure mechanisms require the complete analysis of the anisotropic phenomenon, which explains bond formation and breakages.

For a proper understanding at the atomic level, classical dynamic modeling was utilized to bridge the gap between microscopic and mesoscopic modeling, explaining the processes occurring at the smaller level (Malikan et al., 2019). When these models explain the material phenomenon at different levels and are bridged together, the material behavior can be predicted accurately (Zhigilei et al., 2005). It is possible to apply different macroscopic and microscopic models in CNTs to predict the mechanical response (Tserpes & Papanikos, 2005). The mechanical strength of CNTs depends on the interatomic bonds, which are covalent. In a molecular structural model of CNTs, stiffness is directly proportional to atomic bonding. At the same time, Young's modulus (E) is represented by K/ro, where K is constant spring andro is the interatomic layer distance (Xiao et al., 2005). Inter atomic layer distances almost remain the same for different bonds, but K varies significantly for carbon-carbon, metallic and ionic bonds. Salvetat-Delmotte and Rubio (Salvetat-Delmotte & Rubio 2002) worked on the mathematical model of CNTs to explain their deformation under stress. Their work reported that CNTs could elongate up to 0.05 % of their original length before buckling. The recent experiment reported that experimental results were aligned with the molecular dynamic calculation, and CNTs of thin structures failure will occur at 100 to 150 GPa pressure.

A new mechanism was introduced to find the compressive strain of CNTs using strain energy phenomena (Liew et al., 2006). Immediately graphite bonding bridges the void when straining energy is released from fractured parts as can be seen in Table 2.3.

Table 2.3: Failure Load and Critical Strain of Multiple Orientations of CNT Bundles

	Failure load P_n(nN)	Average failure load P_n^{ave} of each SWCNT (nN)	Critical strain ε_{cr}
CNT bundle of three (5,5) SWCNTs	233.5	77.8	0.269
CNT bundle of three (7,7) SWCNTs	313.0	104.3	0.269
CNT bundle of three (10,10) SWCNTs	441.2	147.1	0.266
CNT bundle of three (12,12) SWCNTs	532.7	177.6	0.256
CNT bundle of seven (5,5) SWCNTs	551.6	78.8	0.266
CNT bundle of seven (7,7) SWCNTs	741.3	105.9	0.266
CNT bundle of seven (10,10) SWCNTs	103.7	148.1	0.266
CNT bundle of seven (12,12) SWCNTs	123.6	176.6	0.243

(Source Liew et al., 2006)

Experimental results proved the validity of the new theory and calculated the critical stress values for CNTs (Wegner, 2002). As a result, these CNTs show the highest strength of any other fiber known to us. In all mathematical modeling and experiments, it has been proven that when CNTs are deformed and reshaped, it causes a sudden release of a large amount of strain energy (Srivansa & Reddy, 2013; Pantano et al., 2003; Meher & Panda, 2018). However, this deformation process is reversible for a very large bending angle due to the presence of a carbon-carbon sp^2 covalent bond (Pantano et al., 2004). Generally, the calculation of release of strain energy in each model developed to understand CNTs is to find the ultimate tensile strength of CNTs under uniaxial loading (Natsuki et al., 2004).

CNTs with diameters up to 12 nm have been studied and investigated using classical molecular dynamics simulations with physical assumptions (Jang et al., 2004). However, these simulations have failed to investigate the CNTs having a larger diameter. It has been proven that the defects and behavior of the hexagonal structures have a diameter less than 12 nm depending on the applied tension and temperature. All CNTs exhibit brittle behavior when strain is high and the temperature is low. The behavior of larger CNTs (ductile or brittle) depends on the symmetry of the hexagonal structure (Fernández-Toribio et al., 2018). Treacy et al. (1996) tried to find Young's modulus of the CNTs by using an experimental technique by correlating the amplitude of free vibration as a function of temperature without any success. However, this was rectified using an atomic

force microscope (AFM) and a feedback control interface. In a recent development, MWCNTs were tied with SWCNTs and calculated ultimate tensile strength ranges from 11 to 63 GPa and independent of outer diameter (Li et al., 2000). This technique suffers from main drawbacks: the adhesion between CNTs did not allow load transfer towards the inner part of the structure. The radial compressibility of the CNTs was investigated by using AFM (Yang & Li, 2011). The modulus was about 10 GPa, similar to graphite when applied pressure was low. Still, in the case of higher pressure, the modulus was significantly high due to the attraction between the deformed sides. Soni et al. (2020) have investigated mechanical properties for CNTs in their work. A numerical model was developed to study the various mechanical properties such as tensile modulus and impact strength. Table 2.4 and 2.5 show the elastic properties of SWCNTs and MWCNTs, respectively, while Table 2.6 and 2.7 show the tensile strength of SWCNTs and MWCNTs. These features made CNTs crucial in different applications (Breuer & Sundararaj, 2004; Rathore et al., 2016). A comparison of mechanical properties of different nanoparticle reinforced epoxy composite is tabulated in Table 2.8.

Table 2.4: Elastic Properties of SWCNTs (Individual and Bundles)

Manufacturing Methods	Radius (nm)	Elastic Modulus (TPa)
Arc Discharge (AD)	0.5-3.3 (ID) 2.8-12.4 (OD)	0.3-4
Laser Ablation (LA)	0.5-0.75	0.78-1.5
Laser Ablation (LA)	0.70	2.5-3.4
Arc Discharge (LA)	1.5-10	1
Laser Ablation (LA)	4.5-20.5	0.25-1.2
Chemical Vapour Deposition (CVD)	1.5±0.1	1.1

(Source: Soni et al., 2020; Tebeta et al., 2020).

Table 2.5: Elastic Properties of MWCNTs (Individual and Bundles)

Manufacturing Methods	Radius (nm)	Elastic Modulus (TPa)
Arc Discharge (AD)	5-10	1.6-2.5
Arc Discharge (AD)	5-10	1.6-2.5
Arc Discharge (AD)	5-10	1.6-2.5
Arc Discharge (AD)	5-10	1.6-2.5
Chemical Vapour Deposition (CVD)	15 (OR) 6 (IR)	0.42
Arc Discharge (AD)	6.25	0.8
Chemical Vapour Deposition (CVD)	5	0.29

(Source: Soni et al., 2020; Tebeta et al., 2020).

Table 2.6: Tensile Strength of SWCNTs (Individual and Bundles)

Manufacturing Methods	Radius (nm)	Tensile Strength (GPa)	Strain (ε_{max})
Laser Ablation (LA)	10-20	13-52 (mean 30)	1-5
Arc Discharge (AD)	1.6-2.25 (ID) 4.2-6 (OD)	55	-
Chemical Vapour Deposition (CVD)	-	3.6-22	-

(Source: Soni et al., 2020; Tebeta et al., 2020).

Table 2.7: Tensile Strength of MWCNTs (Individual and Bundles)

Manufacturing Methods	Radius (nm)	Tensile Strength (GPa)	Strain (ε_{max})
Arc Discharge (AD)	6-17 (OD)	6-32	11.69
Chemical Vapour Deposition (CVD)	5 µm	1.69	-
Arc Discharge (AD)	6.25 nm	1.49	-

Chemical Vapour Deposition (CVD)	5 nm	1.89	699

(Source: Soni et al., 2020; Tebeta et al., 2020).

Table 2.8: Mechanical Properties of Nanoparticle Reinforced Composite

Composite	Filler type/content (wt%)	Young's modulus (MPa)	Ultimate tensile strength (MPa)	Fracture toughness K_{Ic} (MPa $m^{1/2}$)
Epoxy	0.0	2599 (±81)	63.80 (±1.09)	0.65 (±0.062)
Epoxy/CB	0.1	2752 (±144)	63.28 (±0.85)	0.76 (±0.030)
	0.3	2796 (±34)	63.13 (±0.59)	0.86 (±0.063)
	0.5	2830 (±60)	65.34 (±0.82)	0.85 (±0.034)
Epoxy/SW CNT	0.05	2681 (±80)	65.84 (±0.64)	0.72 (±0.014)
	0.1	2691 (±31)	66.34 (±1.11)	0.80 (±0.041)
	0.3	2812 (±90)	67.28 (±0.63)	0.73 (±0.028)
Epoxy/DW CNT	0.1	2785 (±23)	62.43 (±1.08)	0.76 (±0.043)
	0.3	2885 (±88)	67.77 (±0.40)	0.85 (±0.031)
	0.5	2790 (±29)	67.66 (±0.50)	0.85 (±0.064)
Epoxy/DW CNT–NH_2	0.1	2610 (±104)	63.62 (±0.68)	0.77 (±0.024)
	0.3	2944 (±50)	67.02 (±0.19)	0.92 (±0.017)
	0.5	2978 (±24)	69.13 (±0.61)	0.93 (±0.030)
Epoxy/M WCNT	0.1	2780 (±40)	62.97 (±0.25)	0.79 (±0.048)
	0.3	2765 (±53)	63.17 (±0.13)	0.80 (±0.028)
	0.5	2609 (±13)	61.52 (0.19)	-
Epoxy/M WCNT–NH_2	0.1	2884 (±32)	64.67 (±0.13)	0.81 (±0.029)
	0.3	2819 (±45)	63.64 (0.21)	0.85 (±0.013)
	0.5	2820 (±15)	64.27 (±0.32)	0.84 (±0.028)

(Source: Gojny et al., 2005).

2.5.3 Thermal and Electrical properties of CNT-based composites

The thermal and electrical properties of CNTs may differ or change significantly based on the aspect ratio (Wu et al., 2010). Polymer composites have points of contact between CNTs. Note that CNTs are dispersed homogeneously in polymer composites. Electrical

paths that function as percolation networks are formed through the points of contact in CNTs (Li et al., 2018; Ha et al., 2019). In this case, the possibility of a percolation network to form depends on the aspect ratio of CNTs which also improves their thermal conductivity (Estelle et al., 2015; Sastry et al., 2008).

To explore thermal properties and present their thermal behavior, Park et al. (2010) came up with different polymer composites such as epoxy with CNT and carbon fiber and PDMS, which represent carbon fillers that are one dimensional. In another similar study, Guo et al. (2013) explained that when silica is coated on the outer wall of the MWCNT in multiple layers, the overall thermal conductivity of the polymer composite improves. In a study conducted by Xiao et al. (2018), it was found that, when studying the dispersion morphology of CNT inside CNT polymer complexes, the uniform dispersion of CNTs is of utmost importance for the enhancement of thermal and electrical properties. Moreover, Caradonna et al. (2019) outlined the advantageous properties of CNTs on conductive networks through discovering the thermal and electrical properties conduct of filler shapes by adding three types of carbon-based fillers with different shapes to a polymer matrix using graphene, graphite, and CNTs. Another study performed by Lee (2022) discovered that L-MWCNTs act as good conductors without phonon scattering and contact resistance than S-MWCNTs; also, S-MWCNTs require a large number of contact points and S-MWCNT to form a percolation network. It is not easy to characterize the electrical resistivity of a pure epoxy resin since it is very resistive even when high voltage is applied. In a pure epoxy matrix, the electrical conductivity is assumed to be 1.0 X 10^-10 S/m. Moreover, under loading conditions of a carbon nano type, the electrical conductivity of a nanostructured polymer becomes highly sensitive, i.e., under similar aspect ratio conditions, the electrical percolation threshold is reported to be less than 0.1 % (Junjie Chen et al., 2018). In CNTs, thermal energy transport can be related to a phonon conduction mechanism (Gonjy et al., 2006; Zhang et al., 2018). In an

experiment to determine the thermal and electrical conductivity based on aspect ratio, Junjie Chen et al. (2018) concludes that the physical properties of the nanostructured polymer composites can be interpreted in terms of CNT networks. Some studies have shown a decrease in decomposition temperature in epoxy composites with increasing HMWCNTs-to-resin ratio (Ciecierska et al., 2013; Loos et al., 2008; Zhou et al., 2007), is due to the better thermal conductivity of the composites, which is enhanced by adding HMWCNTs.

2.5.4 CNTs in Composites

The discovery of CNTs and subsequent composites has led researchers to fabricate advanced composites for various specific applications. Xue (2005) reports that studies are trying to exploit the mechanical, thermal, and electrical properties of CNTs in composites. CNTs have an advantage over traditional nanoparticle fillers due to the higher aspect ratios. In addition, CNTs are known to have high thermal conductivity and are used for thermal management optimization in composites. The thermal conductivity of CNTs is reported to be as high as twice that of diamond (Xue, 2005). Due to these extraordinary properties, CNTs are incorporated in metallic, ceramic, and polymeric matrix materials.

The fabrication cost of CNTs based polymeric composites can be significantly reduced by modifying traditional fabrication methods of polymers. Based on the applications, CNTs based polymeric composites are classified into functional and structural composites (Ibrahim, 2013). For structural application, properties of CNTs such as elastic modulus, tensile stress, tensile strain, twisting resistance, distortion and compression were examined (Moradi et al., 2012). Similarly, high electrical and thermal conductivity properties were used for functional composites. As a result, these functional composites have higher chemical, heat resistance, thermal, electrical conductivity, and energy storage capacity. Therefore, CNTs based composites are considered the most promising materials based on their properties and applications (De Volder et al., 2013).

CNTs have a higher aspect ratio than any other materials used as filler composites, along with better mechanical and physical properties. The use of CNTs to support the structure of matrix material increases the structural properties. This increase in properties can be utilized in various structural applications and open avenues for applying these composites in electronics, aerospace, bio-medical and field emitters. Some of the extraordinary properties of CNTs based composites include higher strength to weight ratio and higher aspect ratios (Liew et al., 2006). Epoxy-based CNTs composites have received a great deal of attention. CNTs in polymeric matrix materials have improved the mechanical properties significantly. Functionalized and modified CNTs improve the matrix material's tensile modulus (Trojanowicz, 2006). CNTs improve the stress transfer in the matrix material, and the stress transfer mechanism can be further improved through functionalization and modifications. High loading of CNTs in a composite leads to an increase in storage modulus (Ibrahim, 2013).

2.5.5 Dispersion Techniques for CNTs in Polymeric Matrix

Properties of CNTs based polymeric composites are strongly dependent on the orientation and dispersion of CNTs in the matrix material. Therefore, CNTs must be properly dispersed to avoid accumulation and impart useful mechanical properties in composites. To overcome the shortcomings and make the best use of CNTs in polymeric matrix materials, several techniques and methods were used to dispersion CNTs (Xie et al., 2005a). Mostly ultrasonication, magnetic stirring, and mechanical stirring are employed to overcome the issues of CNTs dispersion and aggregation in composites.

Furthermore, various modification and functionalization techniques were used to improve the dispersion of CNTs. Dispersion techniques generate localized stresses which disperse the aggregates of CNTs (Jogi et al., 2012). These techniques transfer the mechanical energy to overcome the binding of CNTs to disperse the agglomerations. To

effectively disperse the agglomerates of CNTs, the energy density provided by the dispersion techniques must be greater than the binding energies of CNTs.

2.5.5.1 Ultrasonic Dispersion

Ultrasonication techniques are used to break the accumulation and disperse CNTs uniformly throughout epoxy. However, during the ultra-sonication, CNTs are prone to structural damages. In addition, agglomeration of CNTs leads to poor stress transfer and ultimately decreases the overall performance of the composite (Vaisman, Marom, et al., 2006). Therefore, it must supply energy greater than the binding energy and less than the energy required to break CNTs. Figure 2.8 shows the effects of sonication time on the length of MWCNTs (Montazeri & Chitsazzadeh, 2014)

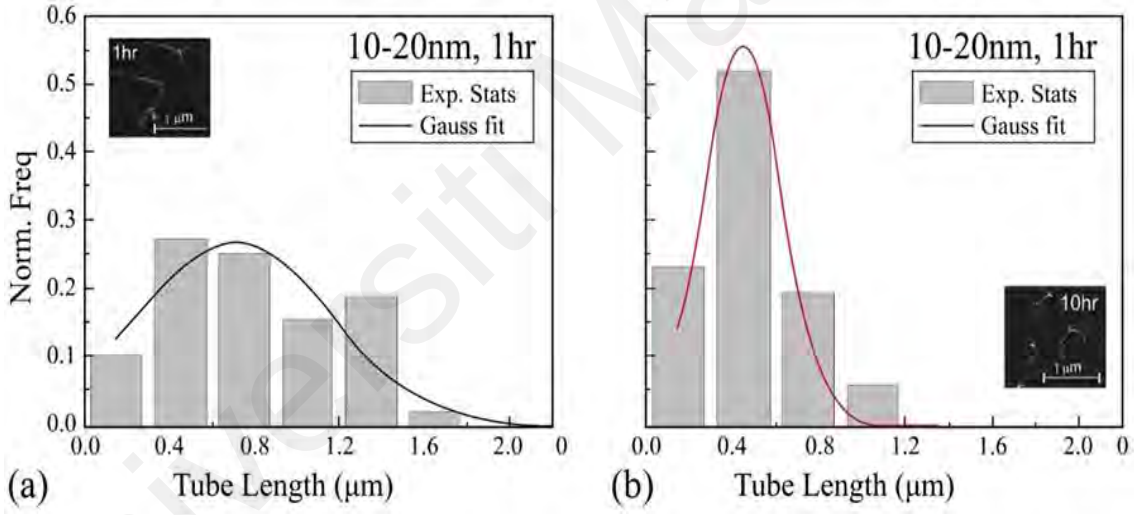

Figure 2.8: Effect of Sonication Time on the Length of MWCNTs: (a) Effect of 1 Hour and (b) 10 Hours (Huang & Terentjev, 2012)

CNTs are highly strong and elastic, but they possess cohesiveness—the uniform dispersion of CNTs in the liquids like water, resins, ethanol, and oil. The ultrasonic method has made its way for the efficient and effective dispersion of carbon nanotubes. Ultrasonication is a more prevalent method as it improves the dispersion of CNTs.

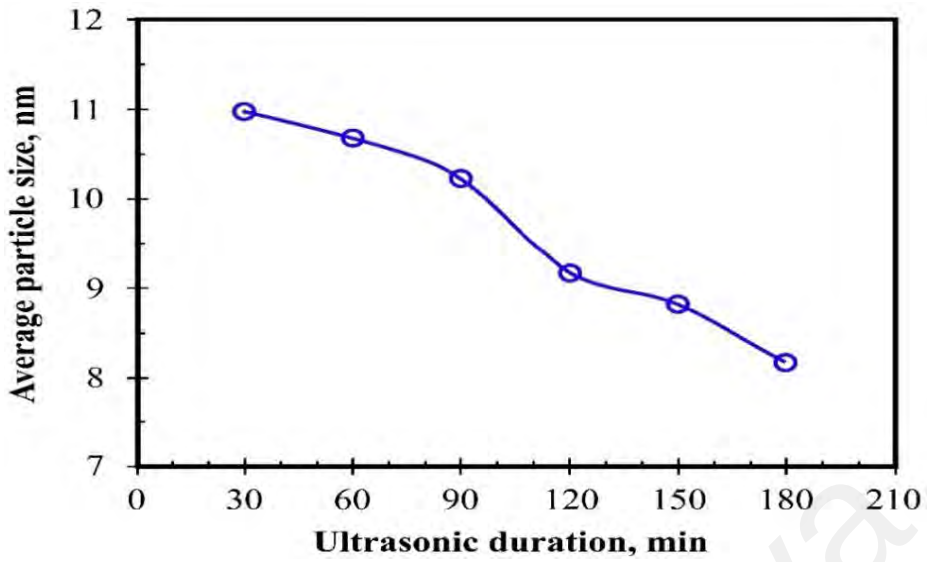

Figure 2.9: Effect of Sonication Time on Alumina Particle Size (Afzal et al., 2019)

Furthermore, sonication is a generic technique to improve aggregation dispersion, especially in solutions. But the ultra-sonication is not used without any treatment because the obtained results are not considered good (Afzal et al., 2019; Dai & Sun, 2016). Additionally, ultrasonication was forund to be inefficient in didpersion of cement matrices as it failed to produce a homogeneous distribution of CNTs within cement. On the other hand, Surfactants have been shown to cause steric repulsion between nanomaterials, resulting in uniform dispersion. Therefore, in research, the effect of sonication time was analyzed on the colloidal structure of alumina. This study recorded the effect for the cluster and fine particle by applying the ultra-sonication on alumina for a specific period (Afzal et al., 2019), as illustrated in Figure 2.9. Figure 2.10 illustrares the size of colloidal particles as they decrease with with increasing ultrasonication time for nanofluid.

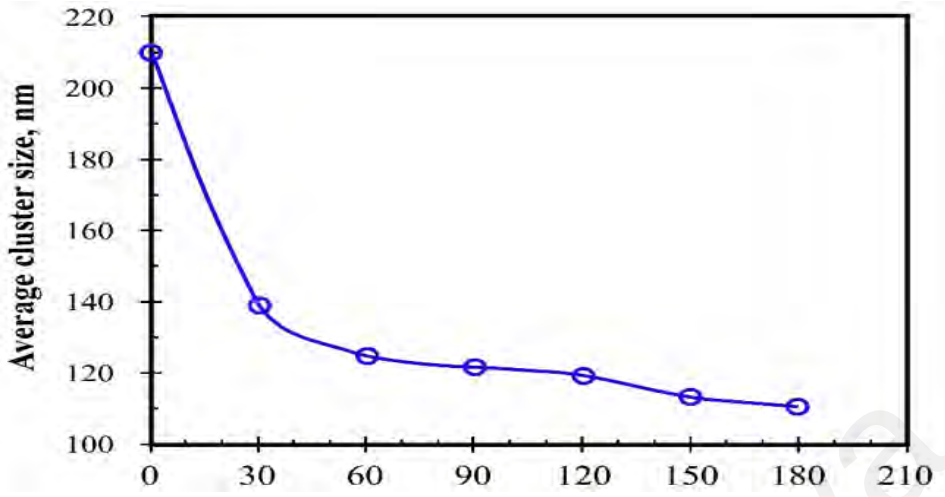

Figure 2.10: Effect of Sonication Time on Cluster Particle Size (Afzal et al., 2019)

After the sonication, many CNTs are combined to form aggregations in a very impulsive time (Dai & Sun, 2016). In a research study, the plotting of aqueous suspension is captured after multiple intervals to analyze the settling or agglomeration of MWCNTs, as in Figure 2.10. For the dispersion of carbon monoxide-type (or HiPco) type single-walled carbon nanotubes, which require high pressure, generally, the sonicator is run for approximately twelve to thirty-six hours considering the suitable solvent (Afzal et al., 2019).

The ultrasonic system's latest technology comprises a twin sonicator that requires only 10-30 minutes for a regular and effective dispersion through the standard wave and mobility formation throughout the fluid (Afzal et al., 2019). The main advantage of using the double sonicator, apart from providing less processing time, is that it reduces the probability of fiber fracture and provides the probe facility in the water bath, eliminating the dispersion of single-walled carbon nanotubes in the solution. The dispersion systems that allow this reduced dispersion time for the enforcements included the reactions and cleaning caused by the ultra-sonication. The effect of such sonication on the physical appearance of the solution is demonstrated in Figure 2.11.

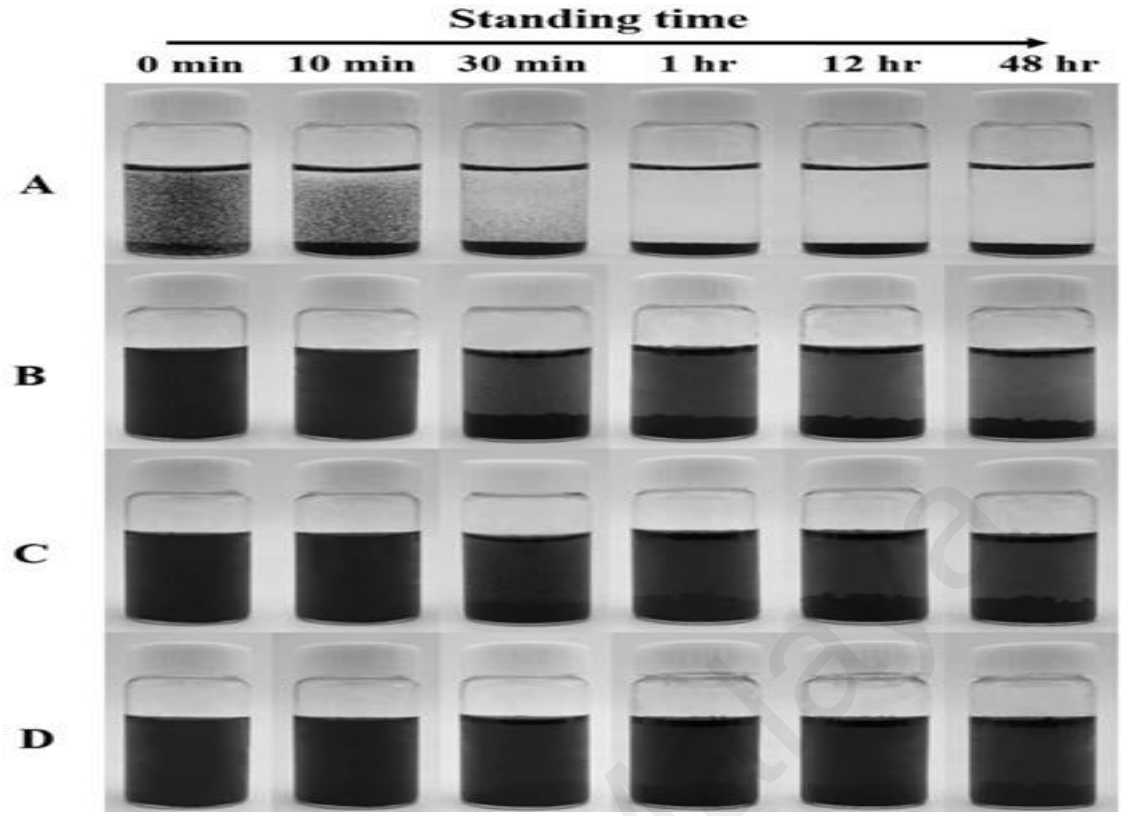

Figure 2.11: Images of MWCNTs Aqueous Suspensions after Ultra-Sonication and Standing for Different Times (Ultra-Sonication Time: A. 0 min; B. 20 min; C. 1 hr; and D. 2 hr) (Afzal et al., 2019)

Generally, the ultra-sonication of CNTs is typically combined with diverse kinds of surfactants to obtain improved dispersion efficiency. Ultra-sonication is used to disperse CNTs and enhance their effect using surfactants as stabilizers (Simões et al., 2017; Zhu et al., 2020). The most commonly used surfactants include sodium dodecyl sulfate (SDS) (Diouri & Baitoul, 2014), dodecylbenzene sulfonic acid (DBSA) (Mechrez et al., 2012), and sodium dodecylbenzene sulfonate (SDBS) (Karousis et al., 2010). In a typical ultra-sonication process, CNTs are mixed with surfactants, and after that, the mixture is sonicated. During this process, CNTs gradually exfoliated and untangled from their original aggregates. These untangled CNTs became stabilized by the effect of surfactants. Figure 2.9 shows images of aqueous solutions of MWCNTs where SDBS is a surfactant, at different settling times when the sonication is runoff. The addition of SDBS distinctly improves the degree of dispersion of MWCNTs, creates long-term stability, and increases thermal characteristics (Kim et al., 2018; Song et al., 2018).

In the ultra-sonication of carbon nanotubes, foaming is observed very commonly. This foaming typically reduces the efficiency of the dispersion of these CNTs. CNTs dispersions frequently create foam during ultra-sonication, which reduces the dispersion efficiency. The air bubbles and foaming may be overcome by adding anti-foaming agents typically composited of oligomers, including the compounds of polyether or polysiloxane, ultimately to reduce the layers of foams (Ko & Seo, 2020; Sato & Sano, 2008). Although used for dispersion, ultra-sonication was reported as early as 1996 to cause the destruction of CNTs in suspensions. In addition, it has been observed many times that sonication causes many morphological and structural changes in carbon linkages of CNTs like buckling, bending, or disarrangement of carbon bonds or linkages (Lu et al., 1996). Therefore, ultrasonication input and output parameters should be controlled to obtain the required properties.

2.5.5.2 Magnetic Stirring

Magnetic stirring is another technique used to disperse the agglomerates of CNTs in matrix materials. Generally, magnetic stirring is considered a more effective technique to disperse the agglomerates of CNTs by applying energy more than the binding energies of CNTs. Magnetic stirring imparts minimum damage to the morphology of CNTs in comparison with other dispersion techniques (Xu et al., 2014). Mechanical mixing is also used to effectively disperse the CNTs in the polymeric matrix. However, the mechanical dispersion technique can change the aspect ratio of CNTs and morphology due to excessive application of localized shear stresses and hence can change the aspect ratio of CNTs (Xie et al., 2005b). Magnetic stirring, consisting of a stationary electromagnet to create a rotating magnetic field and a permanent magnet, is widely used in laboratories. A coupled heating system is usually included in stirring magnetic systems to heat the liquid (Loos, 2014). The electric motor rotates the magnets in the current magnetic stirrers. Similar to mechanical agitators, magnetic stirrers provide closed stirring systems

without any need for isolation. Unlike the stirring rods, stir bars are easy to clean and sterilize because of their size. However, this system is used for volumes less than 4 liters because of the limited size of the stir bars.

In previous studies (Guo et al., 2018; Xu et al., 2014), it was shown that magnetic stirring plays an important role in preparing CNT/Ni-P composite coatings with homogenously embedded CNTs. The dispersions' coatings were observed through SEM and TEM after undergoing magnetic stirring to explain the surface morphology of deposited layers clearly. It was reported that there was a significant improvement in dispersion when proper process and treatment were followed to make a smooth surface of CNT/Ni-P through equal dispersion of CNTs throughout the matrix. This was achieved by improving the coating's interfacial bonding between Ni-P and CNTs. In addition, the nanotube distribution is significantly affected by aggregation. Ariu et al. (2016) stated that magnetic stirring's application offers satisfactory coating adhesion and uniform distribution of cobalt and nickel on the nanotubes and for cobalt-plated nanotubes at a lower extent.

2.5.5.3 Mechanical Mixer

The composites based on carbon nanotubes show various properties even with minor process parameters or methods changes. So, it’s essential to formulate the final composite's processing, fabrication, and composition to obtain the required properties. As many researchers have revealed their results and conclusion, explaining their achievement of required properties through controlled preparation, synthesis, or morphology, it becomes very hectic and challenging for a researcher to take responsibility to lead the research a further step up. This thought is very generic as the carbon nanotubes are often observed to form clusters or aggregations (Yan et al., 2019).

The most commonly used method to fabricate a composite is through direct mixing, in which the carbon nanotubes are added directly into the matrix of a polymer as a filler.

Here, the mechanical mixer is important in obtaining the final composite properties. The mixing controls the dispersion and aggregation of the carbon nanotubes, which ultimately act for composite structural properties. After adding fillers in a polymer matrix, they form a cluster. When it works, the mechanical mixer creates a shearing force on the filler clusters through the solvent or polymer melt conditionally (Yan et al., 2019). This external shearing force produces localized shearing stress to the particles, clusters, or fillers' aggregates. This localized shear stress controls the dispersion of filler in the matrix. This method is uncommon for dense and viscous liquids as the hydraulic pump because these solutions require mechanical stirring (Krishnan & Subramaniam, 2018; Yan et al., 2019). It is known that mechanical stirring creates a shearing force to facilitate dispersion via its stirrer's high-speed rotary motion. The process of mixing through a mechanical means is imparted to homogenize the phases of the solution by breaking down the clusters of fillers present in the blend. The factor that affects more to cease the mixing process is the interactions or linkages of filler, solvent, or matrix (Yan et al., 2019). It is very clear that the stronger interactions or linkages resist more and restrict the fillers' dispersion in the polymer matrix. While on the other hand, the weaker interactions will homogenize themselves very efficiently, causing a very useful dispersion of fillers (Yan et al., 2019).

2.5.6 Fabrication Techniques for CNTs-Based Composites

Several techniques have been reported in the literature to incorporate CNTs in polymeric composites. The primary aim was to fabricate CNTs composites with adequate dispersion of CNTs without aggregates. Fabrication of CNTs composites was a complex process due to various process parameters (Chou et al., 2010). Factors including mixing techniques, solvents, mixing speed, and process temperature are of utmost importance during the fabrication of CNTs based composites. These factors influence the dispersion of CNTs and the final properties of the composite. Therefore, the mechanical, electrical, and thermal properties of CNTs based composites strongly depend on the fabrication

methods (Li et al., 2020). The most common CNTs dispersion method in a polymer matrix is explained below.

2.5.6.1 Solution Mixing

Solution mixing consists of mixing CNTs and polymeric matrix in suitable solvents. It is commonly used to fabricate composites with low CNTs loading. After mixing, solvents are usually evaporated to obtain the final composite. Dispersion of CNTs is carried out through mechanical mixing, ultrasonication, and magnetic stirring. Solution mixing is one of the most used fabrication techniques due to the lower viscosity of the solution for the uniform dispersion of CNTs in a polymeric matrix (Ke et al., 2012). In addition, various methods such as heat treatment or surfactants for functionalization are used to obtain the required dispersion of CNTs. This fabrication technique has been widely reported in research studies to produce CNTs based composites. Commercially, solution mixing is used to incorporate CNTs into polyurethane (PU) with the use of tetrahydrofuran (THF) (Jung et al., 2001). Solution mixing and dispersion methods were used to obtain the required properties in the final composite (Coleman et al., 2006).

2.5.6.2 Melt Processing and Melt Blending

This method was used for the polymer matrices such as thermoplastics which are not soluble in most solvents. The polymeric matrix material was melted to intermix the CNTs. Melt spinning techniques were used for the formation of CNTs and polymer fibers. CNTs are mixed and dispersed in the polymeric matrix through mixing techniques such as sonication, mechanical, and magnetic mixing (Fornes et al., 2006). For the fabrication of CNTs based composites, conventional techniques such as single or twin-screw extrusion were used. This technique was useful to fabricate composites with higher loading of CNTs. Another technique used in melt processing was extrusion or compounding (Jung et al., 2001). Polymeric matrix materials and CNTs were added to running extruders.

Extruders disperse CNTs in a matrix material by applying shear stresses and forces. The generation of shear stresses and forces is strongly dependent on the melt and mixing techniques (Chen, Tao, et al., 2006). Masterbatch dilution technique was commonly used to fabricate the composites through melt processing. This method has high CNTs loading, which can be lowered with the addition of polymer for dilution of filler content in the composite. Processes with high shear stresses and forces produce composites with better mechanical properties than those with lower shear forces. The melt processing method was useful as it can fabricate CNTs based composites without any modifications in the processing method (Naz et al., 2016). Loading of CNTs can be adjusted per the requirements, and no modifications in the process were required to produce other polymeric composites. But the very high concentration of filler material was not advised in extrusion due to high torque values. MWCNTs are incorporated in matrix material using PU through melt processing using the same process parameters. Dispersion of CNTs in polymeric matrix material was highly dependent on the type of CNTs, fabrication method, matrix type, and dispersion technique (Rinaldi et al., 2017).

2.5.6.3 In Situ Polymerization

This technique consists of grafting the macromolecules directly on the CNTs walls. This method was usually employed for the insoluble polymer materials in most solvents and is not stable thermally. Polymerization was done directly on the surface of CNTs. Composites fabricated through in situ polymerization have better thermal resistance, electrical conductivity, and thermomechanical properties (Martin et al., 2005). This technique gives rise to strong bonding between polymer molecules and CNTs. Both low and high loading of CNTs can be achieved through this method. However, due to a lower degree of polymerization, this method was not desirable for all polymers. PU-based nanocomposites have been widely fabricated through in situ polymerizations (Naz et al., 2016).

2.5.6.4 Layer-By-Layer (LBL) Technique

LBL technique involves fabrication of layered composites structures through dipping the substrate into the CNTs dispersed poly-electrolyte solutions. Usually, cross-linking was integrated to improve the overall structural integrity. LBL techniques consist of a simple, low-cost, and versatile approach to fabricate composites' tailored structures and mechanical properties for various sensing and membrane material applications (Shim et al., 2007). This technique can easily control thickness, polymer-CNTs ratio, aspect ratios of CNTs, and CNTs loading. Due to these outstanding controlling parameters and exceptional mechanical properties of the final composite, the use of the LBL technique has been increased significantly in recent years (Feng et al., 2010). Figure 2.12 shows the LBL technique for the fabrication of modified MWCNTs and poly-allylamine hydrochloride (PAH) based composite (Srivastava & Kotov, 2008). The reaction was carried out on quartz substrate. Amine bonds were formed between MWCNTs and PAH to form a thermally stable thin composite film on the substrate. In the last decade, the LBL technique has produced high conductive and smart electronic yarns in the textile industry. These newly developed nanocomposites in textiles have exhibited higher mechanical strength, chemical durability, higher electrical conductivity, wearability, and wearability, along with better biosensing applications (M. Zhao et al., 2018).

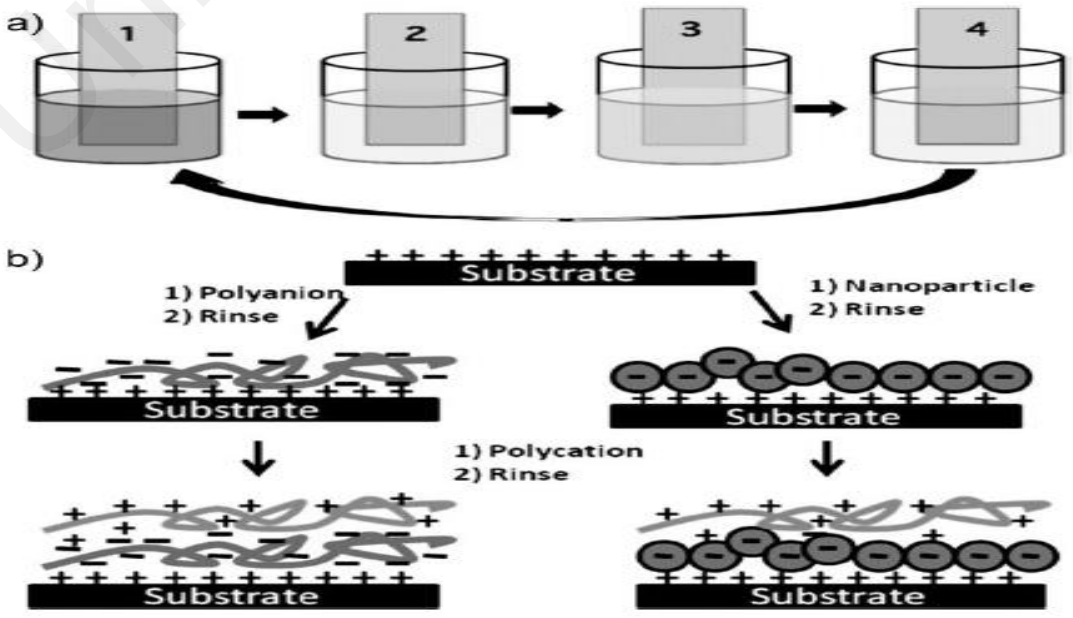

Figure 2.12: (A) Scheme of the LBL film-deposition (B) Two adsorption routes, depicting LBLdeposition for polymers and polymers with NPs (Srivastava & Kotov, 2008)

2.5.6.5 Swelling Technique

Swelling techniques were effectively employed to produce high strength and high toughness Kevlar-based CNTs composites. Kevlar-based composites were produced through the induction of Kevlar fibers in MWCNTs suspensions. Optimal dispersion occurs when the nanoparticles undergo ultrasonication for a period of approximately 150min. This implies that further ultrasonication would result in reagglomeration of nanofluids. These MWCNTs suspensions are prepared in N-methyl pyrrolidone (NMP) solution using ultrasonication (O'Connor, Hayden, et al., 2009). In this process, CNTs were diffused inside the fibers. As a result, even at the lower loading of CNTs, the toughness and strength of Kevlar fibers improved significantly.

Similarly, PE-based composites were prepared by the suspensions of MWCNTs in THF. This fabrication technique allowed the post-processing incorporation of CNTs into already fabricated polymers and was suitable for temperature-sensitive and insoluble polymers (O'Connor De et al., 2009). This technique enables incorporating CNTs of up to several hundred nanometres of polymers. However, only a small fraction of CNTs was enough to significantly alter surface electrical conductivity and mechanical properties (R. Zhang et al., 2019).

2.6 Limitations of CNTs-Based Composites

The high binding energy between CNTs leads to aggregation and aggregates. These agglomerations affect the dispersion and ultimately compromise the final properties of CNTs based composites. Some of the limitations during the processing of CNTs based composites were encountered to tailor the properties (Soni et al., 2020). Additionally, Soni et al. found that an atomically dispersed mixture was homogenous implying that it

contained mechanical, electrical, thermal and dielectric properties. Lack of homogenous dispersion limits the electrical, thermal, and mechanical properties of CNTs based composites. Moreover, dispersion is strongly dependent on the surface area, aspect ratio, loading ratio of CNTs, processing parameters, and type of fabrication technique (Shokrieh & Rafiee, 2010). Various fabrication techniques were employed in the mass-scale production of CNTs based composites. But the progress has been hindered by the issues like dimensional instability and fiber alignments. Uniform and homogenous dispersion and optimal dimensional control and aspect ratio were required to obtain desired results in composites (Shokrieh & Rafiee, 2010). It has been reported that CNTs were loading up to 6 wt. % were found to enhance properties of the composite while loading greater than six wt. % possibly decrease these properties. Higher loading of CNTs leads to aggregation, which hinders the increase in mechanical properties.

Furthermore, dispersion of CNTs was dependent on fiber loading and aspect ratio (Thostenson & Chou, 2002). Another important factor that governs the properties of CNTs based composite is interfacial fiber/matrix adhesion and bonding. Interfacial adhesion was responsible for effective stress/strain transfer throughout the composite and interfacial strength. A poor interface leads to uneven and non-uniform transfer of stress/strain in the composite, lowering its strength. Similarly, various fabrication defects and impurities in CNTs can lead to poor properties of composite materials (Khare & Bose, 2005).

Some processing methods such as Chemical vapor deposition (CVD) have been used in the fabrication of CNTs based composites. Still, the basic issues such as identifying optimal fabrication parameters, control in growth parameters of CNTs, and lack of control on structures of CNTs are to be addressed (Gulati et al., 2015). The lack of optimized fabrication parameters has been a challenge in choosing a fabrication method for the particular requirements and application (Andrews et al., 2002). Moreover, expensive

fabrication methods have limited the practical application of CNTs based composites. Therefore, cost-effective fabrication methods are needed for the progress of CNTs based composites (Yu et al., 2017).

2.6.1 Failures of CNTs-Based Composites

The failure of a composite reinforced with CNTs is highly dependent on interfacial properties, dispersion, orientation, and functionalization of CNTs in the matrix material. Therefore, atomic and sub-atomic level analysis is required to accurately determine the actual cause of failure in the composite (Khan & Kim, 2011b). Laminated composite materials were susceptible to various failure mechanisms due to the high probability of crack initiation. These cracks lead to failures and fractures of the composites. Based on the available information in literature, two arrangements were examined in the composite: (i) randomly dispersed CNTs and (ii) entangled agglomerates of CNTs (Khan & Kim, 2011b).

2.6.2 CNTs Breakages and Bridging

Fiber breakage causes severe damage to the composite. Fiber breakage occurs mainly due to impact loading and high shear stresses. These damages significantly reduce the mechanical properties of the composite (Sari et al., 2020). Failures in composites occur because of variable fiber strength and orientations. During loading, one or more fibers might experience breakage in the composites. Stress redistribution happens once a fiber breaks, and the debonding of fiber-matrix might happen as per-interface stress magnitude (Boroujeni & Al-Haik, 2019). Insights on stress redistribution rely on modeling efforts, while strength differences can be counted using single fiber tensile tests (St-Pierre et al., 2017). Fiber bridging damages have a significant role in understanding the improvement in mechanical properties of composites. To analyze the bridging effect and cracks in a matrix, continuum models of bridging were utilized. Considering these models, a relation

was developed among the crack bridging, displacement, and strain stresses to address crack propagation's causes and influencing factors (Opelt et al., 2018). Fiber bridging also occurs due to interfacial delamination. The delamination cracks cause a change in the physical appearance and geometry of the composite. Fiber bridging increases the fracture toughness of the composite several times, and the composite's characterization becomes challenging (Breuer & Sundararaj, 2004).

2.6.3 CNTs Pull Out Failures

Fibre pull-out failures and tests were considered among the most important testing mechanisms to evaluate the fiber/matrix interface bond strength. The increase in the interfacial shearing increases the rate of the energy released, consequently increasing the pull-out mechanisms and debonding initiation. The effect of compressive stresses was analyzed under fiber pull-out and debonding (Li & Chou, 2008). The effects of the interfacial bonding on elastic properties and fiber pull-out mechanism in composites have been studied to estimate mechanical and physical properties (Amraei et al., 2019; Gao et al., 2017). Chowdhury and Okabe (Chowdhury & Okabe 2007) calculated the interfacial shear strength between CNTs and the epoxy resin matrix using pull-out mechanisms from the simulation. The results indicated an effective stress transfer from the epoxy resin to the nanotubes. Gou et al. (Gou et al., 2004) analyzed the interfacial properties and fiber pull-out mechanisms of CNTs based polystyrene nanocomposites. The shear stress at fiber/matrix interface with CNTs outer diameter of 1.33 nm was around 160 MPa, higher than most polymer nanocomposites based on carbon fiber. In another study by Rafiee and Sharei (Rafiee & Sharaei, 2020), the influence of non-bonded and bonded interactions at the fiber/matrix interface was investigated through a pull-out mechanism via numerical simulations of functionalized and non-functionalized CNTs. The pull-out mechanism of CNTs from the matrix was simulated by performing multi-scale finite element modeling

based on semi-continuum modeling to help in analyzing the interfacial shear strength (Khare & Bose, 2005).

2.6.4 Matrix Material Cracking

The cracking in the matrix was usually caused by the nature of the matrix in the CNTs and the formation of agglomerates. Additionally, impurities and defects inside CNTs can contribute significantly to matrix material cracking. These impurities and defects concentrate and focus stress in matrix materials, causing cracking and ultimately failure (Fiedler et al., 2006; Sepasdar & Shakiba 2022; Li et al., 2018). Matrix cracking is mostly observed in fiber orientation and is also known as transverse cracking. Transverse cracking initiates additional damages in the composite material, ultimately damaging the composite and lowering the overall strength. Apart from decrement in mechanical properties, matrix cracking affects the composite structural stability cause agglomeration of fibers and fiber breakages (Katerelos et al., 2008; Yokozeki, Iwahori, & Ishiwata, 2007; Zhuang et al., 2018). Under fatigue stress, they were cracking stops the transformation or flexibility of the matrix. The cracking of the matrix in composite laminate results in loss of elastic properties and stress concentration (Katerelos et al., 2008).

2.6.5 Delamination and De-Bonding

Delamination severely affects and reduces the strength and stiffness of the composite. These failures can cause catastrophic failures to the composite structures. Delamination was initiated through external loading, tension or compression, high impact damage, and cyclic fatigue loading during fabrication or the use of the composite. Generally, the crack growth direction and the fracture mode explain the composite's delamination (Sridharan, 2008). Delamination in composite laminates is a common occurrence developed due to variation in the material structure caused by manufacturing defects, impurities, impacts,

and stress concentrations in weak areas. The delamination in composites due to drilling is classified into two modes. The first mode was the peel-up delamination mode, while the second was the push-down delamination mode (Panchagnula & Palaniyandi, 2018). Debonding and delamination are closely related. An in-plane fracture occurs in a composite with the release in energy response to the loading conditions (Davies et al., 2006). Interfacial debonding occurs due to fiber fracturing and delamination (Park et al., 2014).

In continuous fibers-based polymer composites, the damage is often caused by the cracking matrix in the transverse direction of the top load. This cracking can cause massive destruction of the composite structure following fiber fracture and plies delamination. These dominant damages have been recorded many times in the past researcher related to the composite laminates (Park et al., 2014). This impact fracture or damage is caused by the combination of localized indentation and the deformation of the whole structure. In the case of damages in laminates or laminated composites, the main damage properties are observed, including delamination, interfacial shearing, debonding, matrix cracking, and fiber breakage. Therefore, it's essential to understand composite laminates to understand the elastic or inelastic behavior of the material, access the service life and durability, and ensure the safe use of the product (Park et al., 2014). Mostly, the inelastic behavior of metals is dependent on plasticity and creep. In the case of polymer-based composites, this inelastic behavior causes damage on the micro-level, ultimately reducing the composite's efficiency due to the composite's lower load capacity. The schematic of further damages on composite laminates as a result of external loading is shown in Figure 2.13.

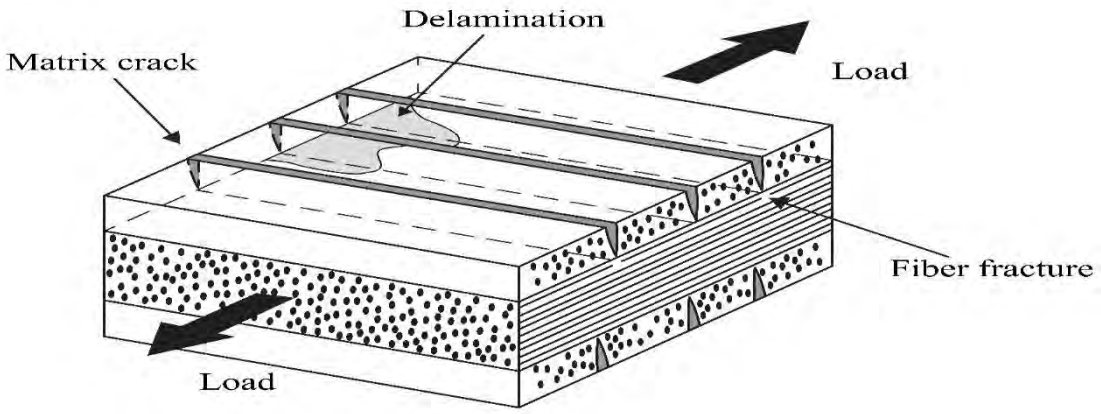

Figure 2.13: Different Damage Types in Composite Laminates (Eggers et al., 1994)

In recent studies, many researchers and industries have considered the damages of the composite laminates to analyze damage tolerances' possessions, especially for the damage caused by the impact, a principal and general damage source. Many types of research ensure that the damages caused by impact are widespread, and many types of research have been done to investigate their effects and characterization (Eggers et al., 1994). However, it is very challenging to keep material in operation with the hidden damage not highlighted by the designer in the designing phase. In the cases of major impact for the composite laminates, the impact energy is highly related to the damage instigation, its propagation in fibrous structure, and the energy level of the propagation with the consideration of stacking sequence (Malhotra et al., 2008) and thickness of laminates (De Morais et al., 2005). In many types of research, the characterization, modeling, and experimentation related to the impact damages near the edges have been recorded (Malhotra et al., 2008).

2.6.6 Modes of Fracture Toughness

Applications and structures of CNTs based composites depended on resistance to the crack and fracture propagation. One of the most important properties for CNTs based composites was withstanding and absorbing the impact. Various research studies focus on increasing the composite's overall fracture and impact toughness. The addition of

CNTs was known to enhance the interlaminar properties and interfacial adhesion (Falzon et al., 2013). Interlaminar properties were influenced by the factors such as processing parameters, processing technique, processing time, interfacial properties, and fiber/matrix material properties (Yokozeki et al., 2007). Studies focusing on Mode I and Mode II interlaminar fracture toughness showed enhanced properties with the incorporation of CNTs. Yokozeki et al. (Yokozeki et al., 2007) explained the increase in the Mode I and Mode II interlaminar fracture toughness with the addition of 5 wt. % loading of CNTs. Mode I fracture toughness increased by 98 %, while Mode II increased by 30 %. Karapappas et al. (Karapappas et al., 2009) explained the increase in fracture toughness of epoxy-based MWCNTs. With the addition of 1 wt. % of CNTs increased Mode I and Mode II toughness by 60 %, while a 75 % increase was observed by adding 0.5 wt. % of CNTs. CNTs bridging and fiber pull-out mechanism were responsible for increased fracture energy. Various techniques were introduced to enhance the fracture toughness at laminar interfaces. These techniques include applying powdered CNTs, using CNTs suspensions, using CNTs solvent paste and CNTs based bucky papers, and direct reinforcement of CNTs (Y. Li et al., 2009). Even the placement of vapor-grown carbon nanotubes directly into the laminar structure achieves a good increase in Mode I fracture resistance and toughness (Y. Li et al., 2009). Solvent pastes containing CNTs significantly impact Mode I and Mode II fracture toughness. Mode I roughly increases by 50 %, while up to 200 % for Mode II fracture toughness (Arai et al., 2008). The incorporation of CNTs in epoxy bucky papers into the laminar interfaces exhibited the increase of Mode II fracture toughness up to 104 % (Khan & Kim, 2011a). This fracture toughness increased due to the bridging of fibers and fiber pull-out mechanisms. Growing CNTs directly on the matrix materials offer better control over tensile properties, vibration properties, resistance to delamination, and fracture (Sharma & Lakkad, 2011). Veedu et al. (Veedu et al., 2006) increased Mode I fracture toughness up to 348 % by

directly growing CNTs on silicon carbide. Fracture toughness was enhanced with the increase in the mechanical interlocking of CNTs with the matrix material. Saboori and Ayatollahi (Saboori & Ayatollahi, 2017) studied the fracture toughness behavior of MWCNTs reinforced epoxy composites with 0.1 wt. %, 0.5 wt. % and 1 wt. % of CNTs loading in an epoxy composite. Due to the change in the loading conditions from Mode I to Mode III, the fracture toughness of the overall composite improved significantly. Mode III fracture toughness increased up to 20 % for 1 wt. % CNTs loading. The number of fabric layers is important for determining fracture toughness among the laminates.

Moreover, the number of fiber layers ultimately improves fiber's strength, increasing the fracture toughness of laminates. The delamination of the laminates becomes stable or propagate gradually with the increase in interlaminar toughness of fracture (Nasuha et al., 2017). Moreover, the toughness values are recorded higher than the values at the crack initiation. Therefore, it can be explored that the value of fracture toughness increases with the propagation of crack would be highest at the end of the propagated crack. The toughness value at an initial point is significant because, in double cantilever specimens, the delamination increases progressively due to fiber bridging. The schematic of Mode I, II, and III of fracture toughness are shown in Figure 2.14.

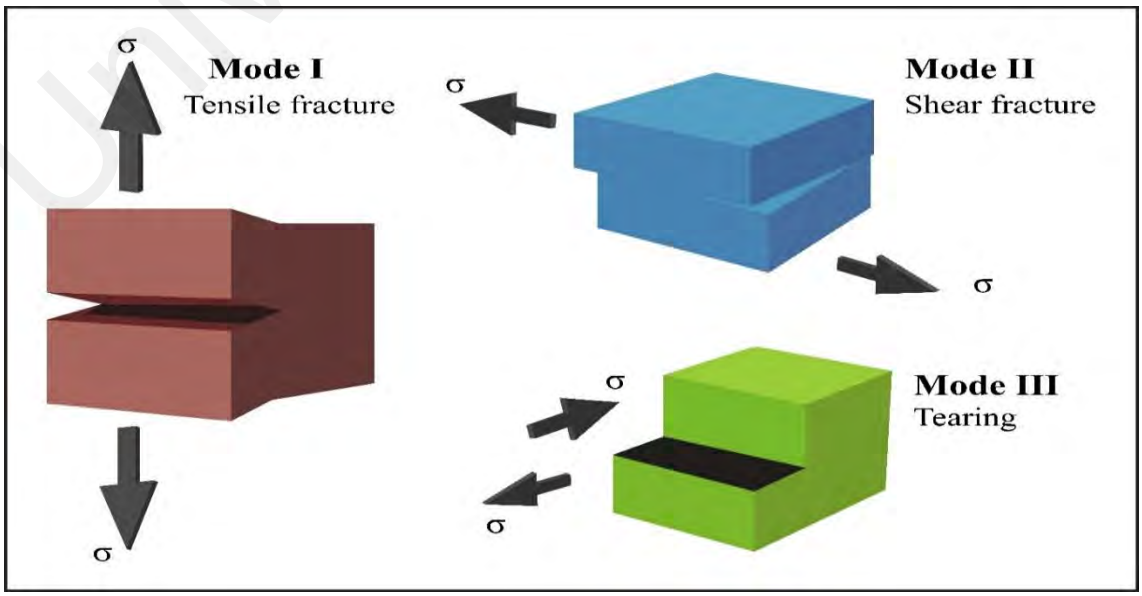

Figure 2.14: Schematic of Different Fracture Modes (Nasuha et al., 2017)

In research by Suppakul and Bandyopadhyay (2002), delamination initiation and propagation were determined to develop the strain energy release rate. The results showed that the twill weave has the highest released rate of energy strain. While on the other hand, the 8-harness satin weave provided the highest value of strain energy's initial release rate. This research also explored that the resistance to fracture is positively affected by the bridging of the fibers for the laminates of twill and eight harness satin weaves. However, the twill weaves have provided the highest values of fracture toughness. The most commonly used method in Mode II fracture toughness is the end notched flexure test, especially for determining critical release rate values of strain energies (Nasuha et al., 2017). Typically, it is observed that for Mode I, the propagation of crack occurs with brittleness with low consumption of energy, while in the case of Mode II, the energy consumption is recorded higher because of the frictional energy released between the fractured surfaces of a laminate composite. In addition, mode I involve utilizing uni-direction laminates, while in the case of Mode II, the multidirectional laminates are used for a wide range of applications. Many studies have been performed under Mode II to estimate fracture toughness, and the observed results are inconsistent. This is because of bending, twisting, and shearing in the layers of laminates that ultimately support the propagation. The inconsistent result may occur due to the coupling effect in fabric layers causing symmetrical changes in fibers' geometry. So, the specimens used should be free from displacements or any deformation (Khan et al., 2018).

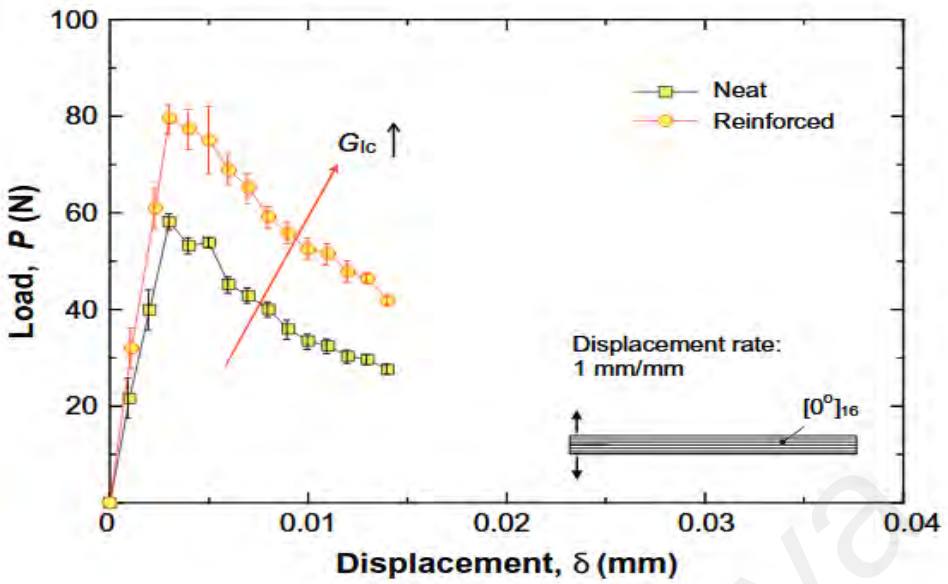

Figure 2.15: Generic Plots between Load and Displacement of the Nano-Reinforced Specimens (Khaled et al., 2014)

Interlaminar fracture toughness is one of the most observed phenomena in the laminates of composites, which is also known as interlaminar deformation or shearing. This fracture toughness is highly observed and a challenge for the polymer composites based on fiber reinforcement. Interlaminar strength is a significant consideration that affects the load-bearing capacity of composite materials in structural applications (Khan et al., 2018). Generic plots between load and displacement are acquired during the testing of double cantilever specimens, as shown in Figure 2.15. It's effortless to estimate the enhancement in the maximum loading value and the post-peak region by comparing the generic plots between load and displacement of the nano-reinforced specimens (Khan et al., 2018). The minor variance in the pre-peak portion of load versus displacement curves could be credited to slight differences in initial crack lengths. This difference was reported not to have any consequence on the results of the study's analysis. Moreover, there is an enhancement in the interlaminar fracture toughness in the presence of MWCNTs reinforced samples (Quan et al., 2018; Anderson et al., 2005).

The graphs or curves of resistance are used to determine the toughness of fracture for Mode I. The resistance behavior or curve describes the fracture toughness trend from the

initial point and each point at which the crack propagates or extends in a very gradual and steady-state (Wicks et al., 2014). The modified beam and modified compliance calibration theory were applied according to the ASTM D5528 to quantify G_{IC}. Since both of the techniques specifically gave comparable outcomes, thus associated modified beam theories were stated. This accounted for the root rotation effect at the crack's tip in the composite adherents. It occurs since the double cantilever specimen is not considered the default in the ASTM D5528 standard. The different mechanical properties in the post-peak region reveal the development in the toughness of interlaminar fracture. Interlaminar toughness in composites is generally highly dependent on the ply's relative orientation for Mode I (Ventura and Lubineau. 2013).

Khalid et al. (Khalid et al., 2014) obtained interlaminar fracture toughness of 340 ± 31 J/m^2 for neat prepreg specimens without reinforcement, while 400 ± 27 J/m^2 was obtained with nano-reinforcement. An improvement of about 17 % was found by comparing both values. Wei et al. (Wei et al., 2017) also carried out fracture examinations under the loading of Mode I to monitor attached composites joints of CFRP and the adhesive layers of polymers based on carbon nanotubes. The results indicated an increase in Mode I toughness around + 32 %.

2.6.7 Impact Damages

Damages caused by severe impacts, such as aerospace and military applications, are inevitable. Severe impacts are visible on the composite surface, but low energy impacts penetrate the composite structure and cause failures due to delamination (Kostopoulos et al., 2010). These low energy impacts are responsible for a rapid decrease in mechanical properties and have a severe impact on the stiffness and strength of the composite. Impact energies and loading cause complex failure mechanisms, including delamination and matrix failure through cracking and fiber breakages. Factors influencing these failures are loading conditions, geometric shape of the composite, matrix and fiber properties

(Kostopoulos et al., 2010). With the addition of CNTs in composites, the impact resistance can be significantly enhanced (Kostopoulos et al., 2010). Composite structures and laminates absorb the impact energies through plastic and elastic deformations.

CNTs based polymeric composites are generally brittle. Initially, these composite materials withstand impact energies through elastic deformation. As the elastic limit is reached, other damage mechanisms are kicked in to absorb the excessive impact energy. These factors are dictated by material properties and the environment and conditions around the composite. Yokozeki et al. (Yokozeki et al., 2007) explained the impact of CNTs loading on the impact resistance and damages. It was observed that CNTs loading did not enhance the impact resistance significantly. This was due to the thin geometries of the samples that underwent elastic deformations to absorb the impact energies. Inam et al. (Inam et al., 2010) explained the effect of low energy impact on functionalized CNTs reinforced epoxy composite. An increase of 6 % was observed in the impact resistance of the composite upon loading of 0.1 wt. % CNTs. High fiber loading of CNTs increases the impact resistance and enhances overall mechanical properties (Kostopoulos et al., 2010). Loading of CNTs exhibited much-enhanced results when high-impact energies were applied. Improved delamination and high impact resistance in CNTs composites are due to fiber bridging and pull out of CNTs fibers (Khan & Kim, 2011b).

2.6.8 Compression After Impact (CAI)

When loaded under compression, composite laminates face substantial reductions in strength because of local uncertainties rising from the widespread damage (Joshi et al., 2012). However, the compressive-after-impact strength of composite laminates has displayed an upsurge of around 8 % when 1.0 wt. % CNTs were used to modify the composite by Aqel et al. (Aqel et al., 2012). Xu et al. (Xu et al., 2014) achieved the dispersibility of MWCNTs in polyether ketone cardo (PEK-C)/dichloromethane. They found that CAI improved substantially for enclosed composite laminates compared to

standard composite laminates. Kostopoulos et al. (Kostopoulos et al., 2010) have reported an increase of effective compressive modulus and compression after impact strength of 0.5 wt. % MWCNTs epoxy composite compared to neat resin as shown in Figure 2.16. Similar results were also reported by Nikfar et al. (Nikfar et al., 2044), who examined the CAI performance of composite laminates reinforced with CNTs and found 30 % enhancement in CAI compared to non-reinforced composites. Residual CAI strength of the composites enhanced considerably for the reinforced sample, with the glass fiber composites displaying the maximum enhancement of 55 %. Erdogan and Bilisik (Erdogan et al., 2018) have investigated the CAI properties of the multi-stitched composite. The CAI strength of the multi-stitched composite was high compared to the unstitched composites. Ismail et al. (Ismail et al., 2019) examined LVI and CAI response of carbon fiber-epoxy composites reinforced with carboxylic functionalized MWCNTs (COOH-MWCNTs) and reported an enhanced impact property by 15.55 % and compressive strength of composites by 10.75 %.

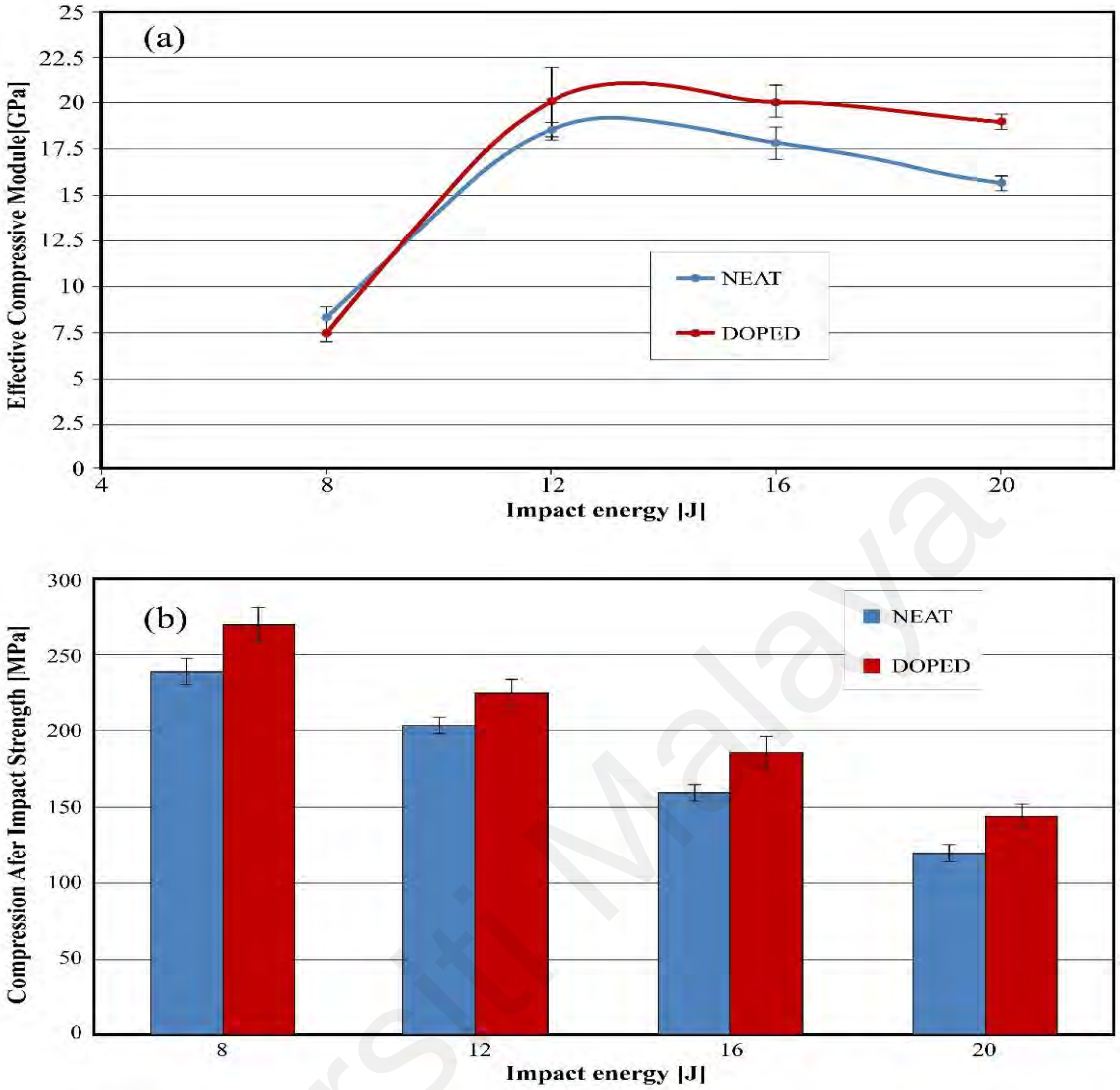

Figure 2.16: (a) Effective Compressive Modulus (b) Compression After Impact Strength on Neat and 0.5 wt. % MWCNTs Reinforced Epoxy (Kostopoulos et al., 2010)

2.7 CNTs-Based Epoxy Composite

Since the discovery of the CNTs, research has been conducted on the properties of SWCNTs and MWCNT and has observed the increase in mechanical, electrical, and thermal properties (Saba et al., 2016). CNTs are being used in the composite material as reinforced medium and significantly enhance the overall properties of the composite material due to their low density and high aspect ratio. In addition, CNTs increase the electric conductance, making them superlative candidates as a filler material in the composite (Islam et al., 2015). However, the use of SWCNTs over MWCNTs in the polymer composite needs further investigation. During tensile testing, the outer layer

carries most of the load. MWCNTs in the composite instead of SWCNTs develop a weak van der Waal bonding. It causes slipping of the layers leading to a decrement in the load-bearing capacity of the composite (Gojny et al., 2004). Due to the epoxy resin's strength, stability, and stiffness is widely used in composite material as a matrix material. Epoxy resin is a cross-linked polymer used in engineering applications and is an important thermosetting resin. Thus, based on the earlier literature, there is still a gap in the CNTs-based epoxy polymer composite research explored in the present work. Details investigation on the fabrication of CNTs-based epoxy polymer composite laminates together with their respective mechanical, physical, electrical, and thermal stability was investigated as reported in the following chapters.

2.8 Challenges Faced During Applications of CNTs-Based Composites.

Much research has been done to identify channellings or hurdles in composites' applications based on carbon nanotubes and overcome their effects on required properties. However, the literature has well documented and proven that producing carbon nanotubes at the industrial quantity and producing various polymer composites for commercial applications is particularly challenging. There are two main reasons: producing large quantities of carbon nanotube at consistent quality is difficult; furthermore, the production cost is very high. Then it comes difficult processability. This material is less usable for various industrial applications despite having extraordinary properties. Creating a homogeneous and uniform dispersion of carbon nanotubes in the polymer composite structures is extremely complicated, particularly in a basic polymer matrix system by applying compounding and other commercial techniques because of its excellent tendency to agglomerate (Baltopoulos et al., 2015). The resultant composite structure will exhibit positive reinforcement effects if uniform and stable dispersion of carbon nanotubes into a polymer matrix can be obtained. Therefore, suitable mixing and processing equipment must create a uniform and stable dispersion.

Due to the sp^2 hybridized bonds, the weak structural arrangement causes the carbon nanotubes' sliding because of the low-stress transfer at the interface (Bai & Allaoui, 2003). That is the reason for enhancement in modulus, maximum stress with carbon nanotubes considering the lowering in size, aggregation, and number (Bai & Allaoui, 2003). Many times, it has been observed that CNTs form aggregates or agglomerates upon high-stress values. To overcome this situation, ensuring the dispersion of carbon nanotubes, a beneficial calendar type dispersing tool is required (Gojny et al., 2004).

It was explored that the fiber breaks randomly if the composites incorporated with long fibres are subjected to loading under quasi-static state tension. This random fracture's main reason is fiber's poor quality that enforced the composite fiber rupture at very random stress even in favorable conditions showing the brittle nature of the material. The cause of this fracture caused can be explained using statistical methods (Jo et al., 2010). This nature of brittle fibers is usually associated with Weibull distribution, a very general configuration to characterize the performance of the long composite fibers (Jo et al., 2010). Another development issue is degassing when dealing with the nanocomposite formulation strategy. There can be trapped air bubbles in the composites, and as a result of high viscosity, pouring the mixed material into the mold can create cracks due to the specimen's failure under low strains (Jo et al., 2010). This technical issue must be resolved before the composite formulation process. It is well demonstrated in the literature and known in the materials community that uniform alignment of the composite matrix improves unidirectional properties like tensile strength, tensile modulus, compressive strength, and toughness.

Since carbon nanotubes stick together and form a bundle, most applications of CNT composites face processing challenges in dispersing nanotubes in the polymer matrix material. This issue is mitigated by ultrasonic processing, extrusion, high shear mixing, and melt spinning. However, there is still an urgent need to develop processes that control

orientation, positioning structure, and carbon nanotube length. Before applying CNTs, composites in various composite applications to provide fibrous reinforcement are challenging to manipulate corresponding to their size (Zhang et al., 2017). There have been numerous reports in the literature on this issue, but more research and innovations must be carried out to find the right solution. In several research, CNTs have been characterized to explore more about them for their better use and utilization by improving their mechanical electrical properties through optimal compounding of the fibers being utilized to make them. The characterization of CNTs is challenging when the CNTs show very high cohesiveness forming agglomeration and lower compatibility with the polymers. The properties of CNTs can be improved by controlling the agglomeration, but on the other hand, during drying, the forces of capillary action allow CNTs to join together (Hassanzadeh-Aghdam et al., 2018). The best elastic, tensile, and electrical properties allow them to be utilized in multiple applications of polymer-based nanocomposites. As CNTs are not highly compatible with polymers, many testing and characterizations have been published in several articles to explore more about the large-scale production or manufacturing of polymer-based composites.

The non-bonded energy and gap between CNTs and surrounding polyimide polymer were determined by Hassanzadeh-Aghdam et al. (Hassanzadeh-Aghdam et al., 2018) through the development of the three-phase micromechanical model. This model is comprised of effective interphase, polyimide polymer, and CNTs. Various parameters, including CNTs distribution, orientation, matrix material properties, aspect ratio, cross-sectional shape, volume fraction, and interphase characteristics, are considered to highlight the effective elastic properties of CNTs-reinforced polyimide nanocomposites. A multiscale model was also developed by Yang et al. (Yang et al., 2012) to investigate the impact of dimensions and deteriorated bonding of CNTs at the interface on elastic stiffness of CNTs-polymer nanocomposites. The interfacial separation was studied with

modifications in constitutive relations by adopting linear spring between the matrix and filler later. There is a limitation for the interfacial region to linear spring between the matrix and reinforcement in the radical area due to modification in constitutive relations. Poblete and Zhu (2019) showed that the characterization of interfacial shear stress transfer is important at nanoscale interfaces possessing various nanowire dimensions to guide the experimental design of elastic strain engineering. The van der Waals interactions between CNTs and polymers such as mechanical spring elements were studied by Wang et al. (Wang et al., 2011) based on fitting molecular mechanics results. The results showed that it is possible to model interactions based on the tube walls' external pressure. Due to limitations in the model, it is impossible to model the impact of debonding, relative sliding, and bonding between the matrix and fibers based on the mechanical properties. It is also impossible to identify and rely on predicting the CNTs-composites' mechanical properties because interfacial shear stress between the CNTs matrix and reinforcements was ignored in the models, along with the nanotube's axial direction. The models also neglected adhesion behaviors caused by non-linear effects between CNTs and the surrounding polymer matrix at large strains in radial and longitudinal directions. The overall elastic properties of the interfacial region can be predicted through a comprehensive understanding of the reinforcing mechanism. Therefore, previous studies have highlighted the importance of considering the effects at the nanoscale to fulfill the design, synthesis, and characterization of CNTs-polymer nanocomposites (Arash et al., 2015; Hassanzadeh-Aghdam et al., 2019; Singh & Kumar, 2018).

There have been extensive research and development activities about modifying and improving various composite interfacial properties of carbon nanotube reinforced polymer composites. Although many technical challenges have been solved over the years, there is still more to resolve. For example, the issue of interface adhesion of carbon nanofiber matrix should be solved before achieving the nanocomposite's full potential to

improve and conclude dispersion. Marriam et al. (Marriam et al., 2018) assessed the defective properties and structures of CNTs and generated a nanotubes configuration model. It was observed that SWCNTs were comparatively defect-free, while MWCNTs had added defects, like topological and structural imperfections. As a result, Nanotubes had to be more purposeful to get better compatibility and dispersion in a polymer matrix to improve the ultimate product (Sun et al., 2018). Furthermore, the right CNTs orientation is likely to result in CNTs-polymer composites with enhanced electrical conductivity and mechanical reinforcement; therefore, it is essential to control the alignment of CNTs towards the pre-determined direction for designing the composites.

All of the earlier described research studies have shown the effect of CNTs introduction to the polymer matrix-based nanocomposite. Furthermore, all properties and structural performance conclusions and results are inconsistent and look diverse and scattered. Due to this scattered data, it couldn't be used to design, control, and modify a particular set of properties for a specific nanocomposite material as many properties are not kept under consideration, especially the geometry of the geometrical properties of the CNTs. The main causes of this irrelevance of scattered results for the smooth and efficient designing process are the incompatibility interface delamination and gliding between the reinforcement and matrices, which ultimately reduces the composites' mechanical properties because of the weak bonding CNTs and matrixes. So, because of this factor of interfacial delamination of polymer and the CNTs at the interface, the composite at interface's overall performance cannot be judged or demonstrated for further design or modification.

CHAPTER 3: METHODOLOGY

This chapter outlines the methods used for the research and the materials employed in the study.

3.1 Research Methodology

An experimental research method is adopted for this study. The research seeks to collect quantitative (numerical) data to help analyze the role of CNTs on the fracture behavior of polymer composite and understand the underlying failure mechanisms. A deductive study approach is employed for this thesis to help in problem identification based on existing data (literature review); experimental data is then used to identify the cause and effect of the problem. The study is carried out in a laboratory set-up where standard developed testing procedures are used to test materials in the research. First, to understand HMWCNTs content on epoxy, a series of development studies was carried out systematically. Then, the fabricated nanocomposite laminates were subjected to various mechanical, thermal, and electrical testing to evaluate their properties. The Mode I and Mode II fracture toughness were investigated by conducting double cantilever beam (DCB) and end notched flexure (ENF) tests. In addition, low-velocity impact (LVI) and compression after impact (CAI) tests were carried out to investigate the mechanical responses of the nanocomposite laminates under static and impact loading conditions. This was followed by a detailed examination of the fracture surface with the help of field emission scanning electron microscope (FESEM) and ultrasonic C-scanning to investigate the underlying fracture and damage mechanism. Next, the nanocomposite laminates' electrical conductivity and thermal stability were carried out using thermogravimetric analysis (TGA) and differential scanning calorimetry (DSC) measurements.

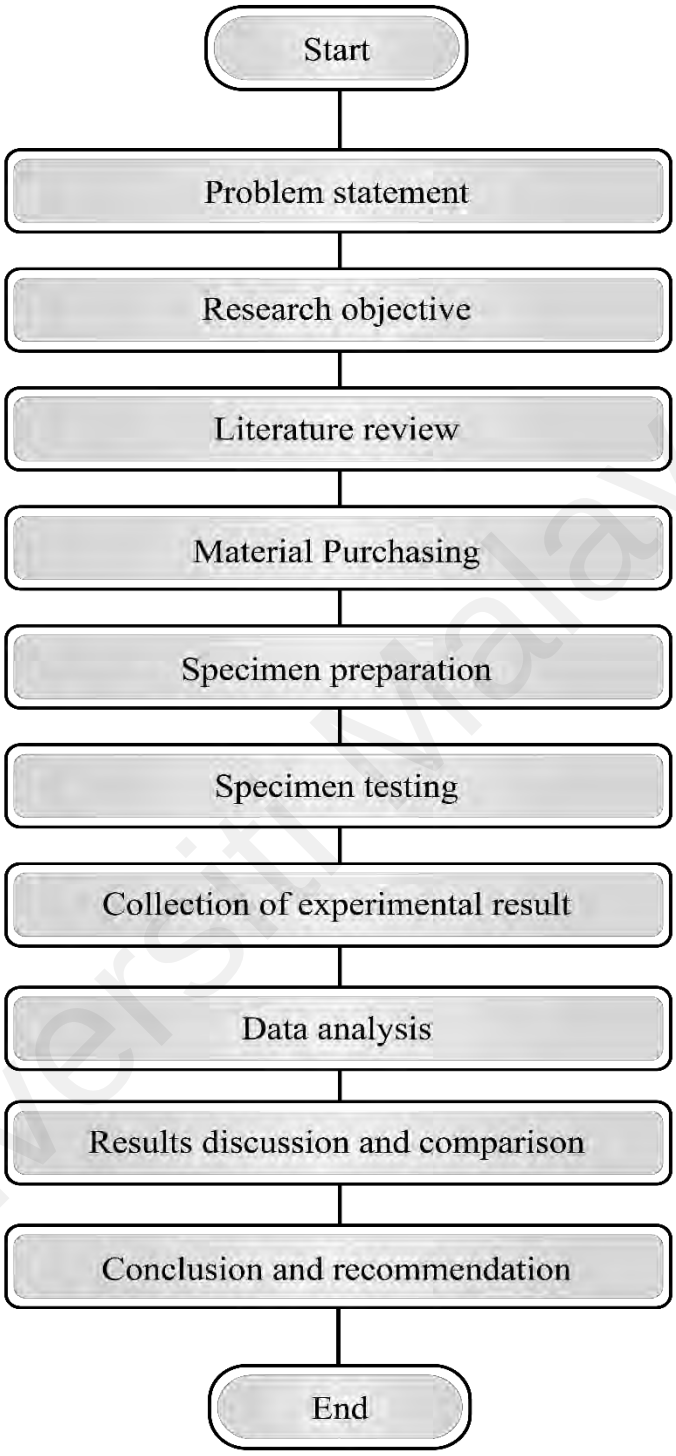

Figure 3.1: Research Flow Chart

3.2 Research Materials

This section elaborates the materials used in the present research and a detailed sample preparation methodology for different mechanical, electrical, and thermal testing.

Absolut care was taken towards sample preparation, which is essential for good reproducibility of the results and to ensure data accuracy and avoid artifacts.

3.2.1 Materials

The base resin used in the present research was EpoxAmiteTM 100 epoxy laminating system and 102 hardeners with a mix ratio of 3:1. These materials were commercially procured from Smooth-on. The helical multiwall carbon nanotubes (HMWCNTs) were procured from Cheaptubes.com (Grafton, VT 05146 USA) . In the HMWCNTs, about 80 wt. % was helical structure whereas the rest was in standard MWCNTs structure with outer diameter of 100-200 nm. A CYCOM 934 unidirectional carbon fibers epoxy prepreg was used in this study. The other auxiliary materials used during sample preparation include ethanol, Teflon film, sealant tape, breath bleeder cloth, vacuum bag film, release agent, Sikadur epoxy adhesive, and hinges.

3.2.2 Fabrication of Composite Panel

Before fabricating composite panels, HMWCNTs were dispersed in ethanol to ensure no agglomeration. The steps towards panel fabrication from the beginning of mixture preparation are described hereafter.

3.2.2.1 Mixture Preparation

In the present work, the dispersion of HMWCNTs in epoxy resin was carried out with the help of magnetic, mechanical stirring, and ultra-sonication to achieve good homogeneity. The HMWCNTs were initially mixed with a calculated solvent (ethanol) concentration in a beaker and placed baseplate with a magnetic stirrer, as shown in Figure 3.2a. The operation was carried out for 30 min at 1000 rpm. Then epoxy resin was added to the beaker with continued magnetic stirring at 1000 rpm for a further 1 hour followed by mechanical stirring for 1 hour by good mechanical mixture as shown in Figure 3.2b. After that, the mixture was placed in an ultrasonic bath for another 1 hour, as shown in

Figure 3.3. Finally, the mixture was put again on the magnetic stirrer at 1000 rpm for 30 min at 80 °C. The purpose of doing all these steps is to effectively break the agglomerates of HMWCNTs and make sure the solvent (ethanol) evaporated properly. After that, the mixture was degassed by placing the container in the vacuum chamber for 30 min, then adding hardener with gentle stirring. The present work investigated two different HMWCNTs-epoxy concentrations, namely, 0.2 wt. % and 0.4 wt. %. Thus, two different parameters were investigated during mixing: (i) rotational speed (rpm) and (ii) mixing time. It is important to use correct parameters as over rpm and duration may break down the HMWCNTs, and under rpm and duration may cause poor dispersion of the HMWCNTs in the mixture, which is undesirable.

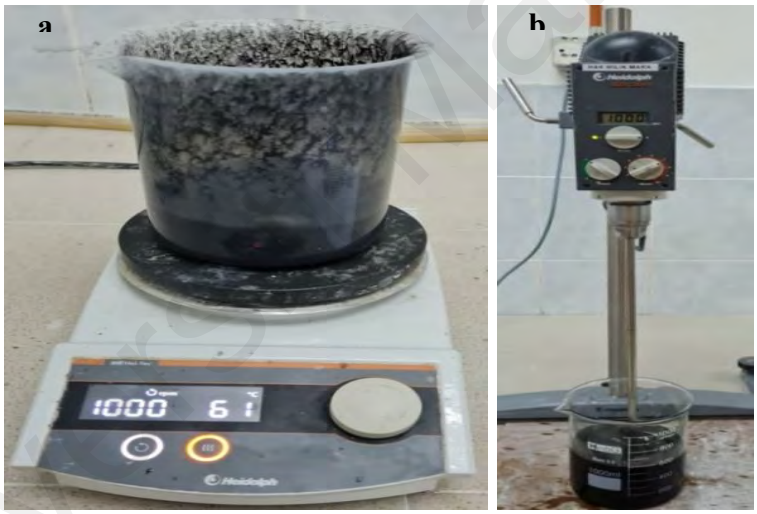

Figure 3.2: (a) Magnetic Stirrer Mixing of HMWCNTs with Solvent and (b) Mechanical Stirring

Figure 3.3: Ultrasonic Bath

3.2.2.2 Fabrication of Composite Laminate for DCB and ENF Test

A big roll of carbon fiber-epoxy prepreg (CYCOM 934 Epoxy) was procured commercially. CYCOM® 934 is a high flow curing epoxy resin with good wet and dry service and can be successfully processed by press molding. The standard curing time is about two hours at 177 °C, and no post-curing is required. Its room temperature tensile strength was 82.7 MPa, and flexural strength was 68.9 MPa. The glass transition temperature (*Tg*) is 197 °C with a density of 1.30 g/cm^3. Then the composite laminate was fabricated by these five steps as follows:

i. A frozen roll of prepreg was cut into 16 sheets (to achive the composite laminate thickness with no more than 5 mm) of 300 mm x 230 mm dimension. Then A3 paper was divided into equal size of rows and columns. In the middle of the A3 paper, the 8th and 9th CF-E prepreg were placed, and the HMWCNTs-epoxy-hardener mixture was applied on the surface of the two laminates equally using a dual-action airbrush, as shown in Figure 3.4. Next, a dual-action top-feed airbrush was used to spray the HMWCNTs-epoxy-hardener mixture on the composites with 0.35 MPa maximum pressure and a high flow rate of (16 L/min) air inlet valve. As a result, the mixture's viscosity was maintained in an optimum range for avoiding the HMCNTs deformation.

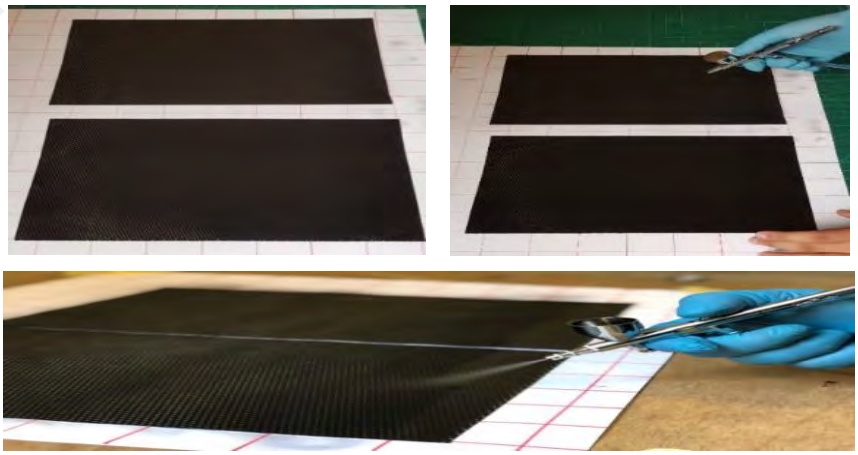

Figure 3.4: Coating of Composite Laminates

ii. It was then heat applied to the CF-E laminates in the oven for 15 min at 60 °C followed by fan drying to remove the leftover ethanol completely, as shown in Figure 3.5.

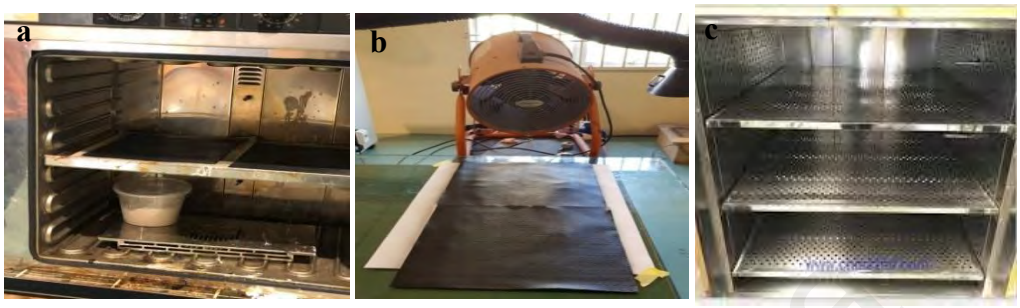

Figure 3.5: (a) Oven and (b) Fan Drying of Carbon Fibre-Epoxy Laminates (c) Hot Air Curing Oven

iii. Composite laminates (uncoated) were stacked up with seven layers and then placed on the top of the coated laminates. A Teflon film with 300 mm x 70 mm x 12 µm dimensions was placed between the 8^{th} and 9^{th} layers. An initial crack was induced during the testing with the help of Teflon film. The rest of the layers were continued stacking up till the final one.

iv. The prepared composite laminates were placed under a vacuum to remove entrapped air and consolidate the layup. Then the prepreg layups underwent debulking in a vacuum for 30 min. After these steps, a uniform laminated composite was obtained, as shown in Figure 3.6.

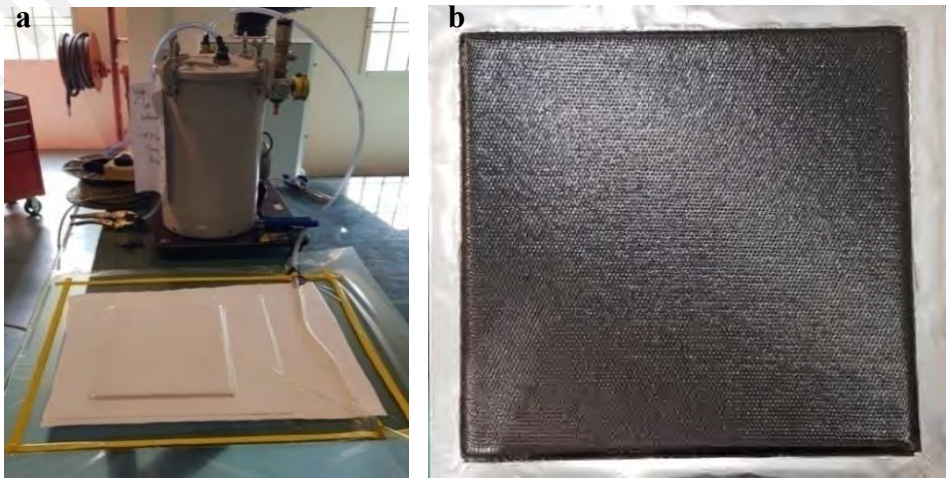

Figure 3.6: (a) Vacuum Debulking and (b) Prepared Composite Panel

v. The above composite planes were kept in a hot press machine, as shown in Figure 3.7, for the curing cycle. Then cooling of the composite panel was conducted at room temperature under natural cooling.

Figure 3.7: Hot Press Machine for Curing

After cooling, the sectioning of composite laminate was carried out in dimensions per ASTM standard for DCB and ENF testing. For DCB test samples, piano hinges were attached with Sikadur epoxy adhesive at the crack initiator location, and then correction fluid was used to paint the edges. Finally, several vertical lines were drawn to measure crack length.

3.2.2.3 Fabrication of Composite Laminate for LVI and CAI Tests

The preparation of composite laminate for the LVI and CAI test was similar to that of the DCB and ENF test, except for layup configuration. The configuration layup was unidirectional for DCB and ENF test samples, whereas it was $[45/0/-45/90^{o}]_{2S}$ for LVI and CAI test. The schematic of the whole process is shown in Figure 3.8.

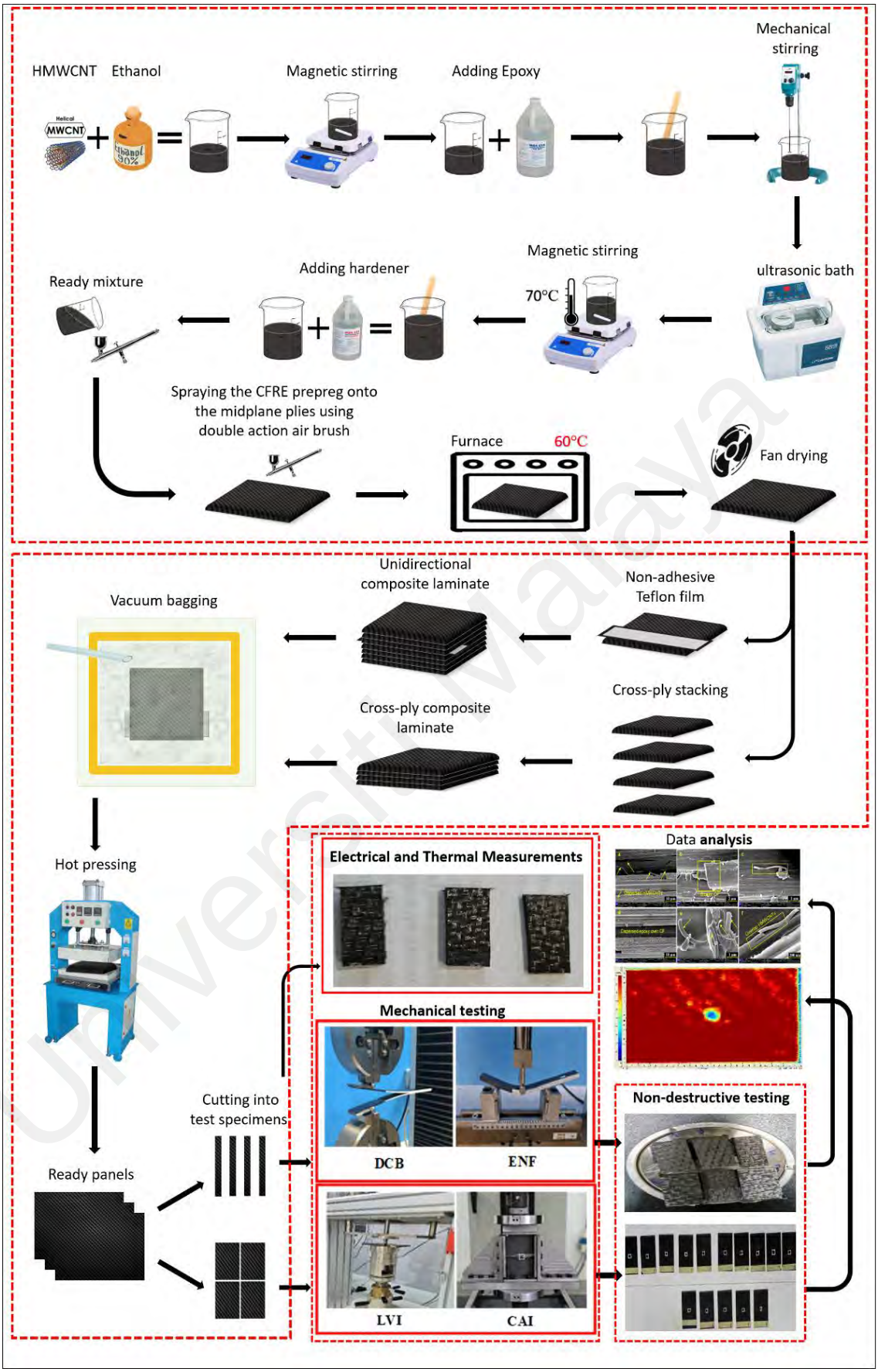

Figure 3.8: Schematic Representation of the Work Flow

3.2.3 Dimension of Test Specimens

The DCB test sample had 200 mm total length (L), 20 mm width (b), 50 mm initial crack length (a_0), and 4.8 mm thickness (h) with 12.7 μm thick Teflon film at the middle of the laminate according to ASTM D5528 standard. The ENF test samples had 200 mm total length (L), 20 mm width (b), and 4.6 mm thickness (h) with 12.7 μm thick Teflon film at the middle according to ASTM D7905 standard. The dimensions of the samples for LVI and CAI tests was (152 mm x 100 mm x 5mm) according to ASTM D7136 standard. A low-speed diamond cutting saw was used to cut the composite panel into desired dimensions, as shown in Figure 3.9.

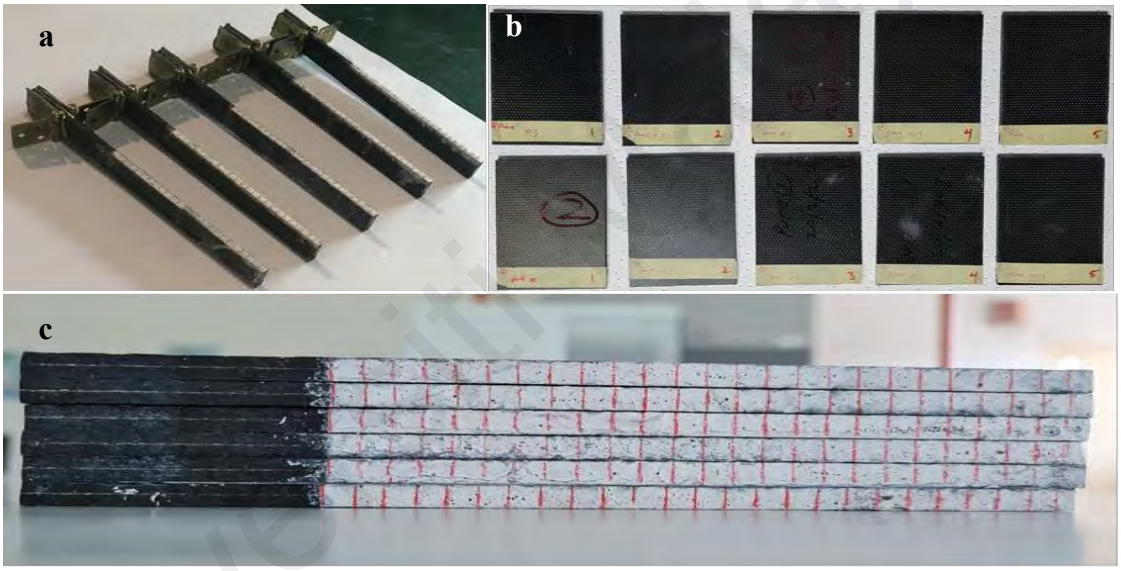

Figure 3.9: (a) Prepared Specimens for DCB Test, (b) Prepared Specimens for LVI and CAI Test and (c) Prepared Specimens for ENF Test

3.2.4 Characterization of Samples

The fabricated composite laminates were undergone different testing methods to evaluate their mechanical, thermal, and electrical properties. The employed test methods were classified into two broad categories: (i) Destructive and (ii) Non-Destructive testing, as described hereafter.

3.2.4.1 Destructive Testing

(a) ***Double Cantilever Beam (DCB) Test***

The double cantilever beam (DCB) test was utilized to know the Mode, I interlaminar fracture toughness, G_{IC}, of continuous fiber-reinforced composite materials, by ASTM D5528 standard and Shimadzu autograph precision universal testing machine (AG-X plus series) was used with 10 kN load cell as shown in Figure 3.10a together with DCB testing of sample in Figure 3.10b. Replicate samples with the number of five were used in every test. White correction liquid was used to paint one end of the crack during testing, and after every 5 mm from the initial crack tip, the thin vertical lines were marked. Then, the sample was placed in a line and the center relating to the longitudinal axis of the sample. The test was performed on displacement control mode at 5 mm/min crosshead speed. The recorded data during the test was load (P) and corresponding displacement (δ). The formula of loading points displacement divided by the load applied to calculate sample compliance (C).

The calculation of G_{IC} was carried out according to equation (3.1) [ASTM D5528]:

$$G_{IC} = \frac{nP\delta}{2ba} \qquad \text{Eq. (3.1)}$$

Where P denotes applied load, δ denotes load point displacement, b denotes the width of the sample, a is delamination length. N denotes experimental value calculated from log C versus log a plot. In this practice, G_{IC} is overestimated, as the rotation can take place at the delamination front during the experiment.

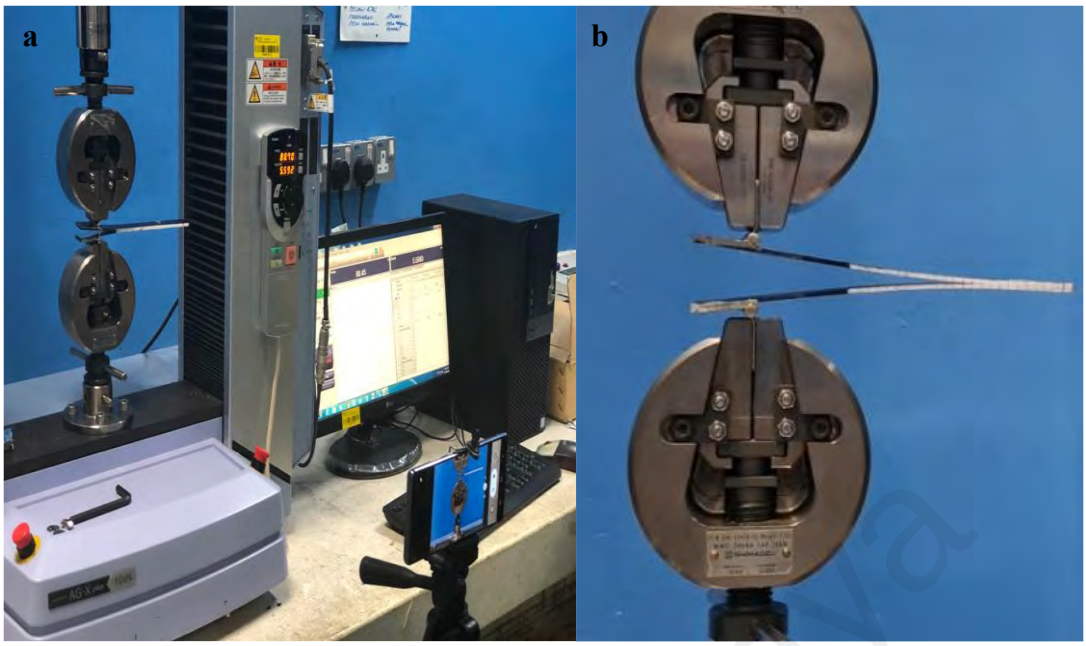

Figure 3.10: (a) Universal Testing Machine and (b) DCB Specimen Under Testing

Thus, equation (1) was modified into equation (3.2) [ASTM D5528]:

$$G_{IC} = \frac{nP\delta}{2b(a+\Delta)} \qquad \text{Eq. (3.2)}$$

Modified compliance method helps determine the delamination length by sample thickness *a/h* versus cubic root of compliance $C^{1/3}$ with the slope A_1. The interlaminar fracture toughness Mode I was then determined as equation (3.3) [ASTM D5528]:

$$G_{IC} = \frac{3P^2C^{2/3}}{2A_1bh} \qquad \text{Eq. (3.3)}$$

The double cantilever beam (DCB) test output is load versus displacement curves. Then these load versus displacement curves were employed to calculate the fracture toughness (G_{IC}) of the composite laminates according to the ASTM standard.

(b) End Notched Flexure (ENF) Test

The end-notched flexure (ENF) test was employed to know the Mode II interlaminar fracture toughness, G_{IIC}, of unidirectional fiber-reinforced polymer matrix composite

laminates under shear loading Shimadzu precision universal testing machine (AG-X plus series) with 10 kN load cell as shown in Figure 3.11a. A three-point bending fixture was used to perform the ENF test, which has loading roller and side supports and the displacement control at 1 mm/min crosshead speed. In the test, crack lengths were 50 mm; the peak force was loaded until the crack grew and the load dropped, as shown in Figure 3.11b. The ENF sample had a span length (S) of 100 mm according to the ASTM D7905 standard. The recorded data was load versus displacement to determine Mode II interlaminar fracture toughness, and G_{IIC} was calculated according to equation (3.4) [ASTM D7905]:

$$G_{IIC} = \frac{9a^2P^2}{16Eb^2h^3} \qquad \text{Eq. (3.4)}$$

Where h denotes half specimen thickness, P denotes maximum fracture test load of corresponded crack length, a denotes crack length, and b denotes sample width.

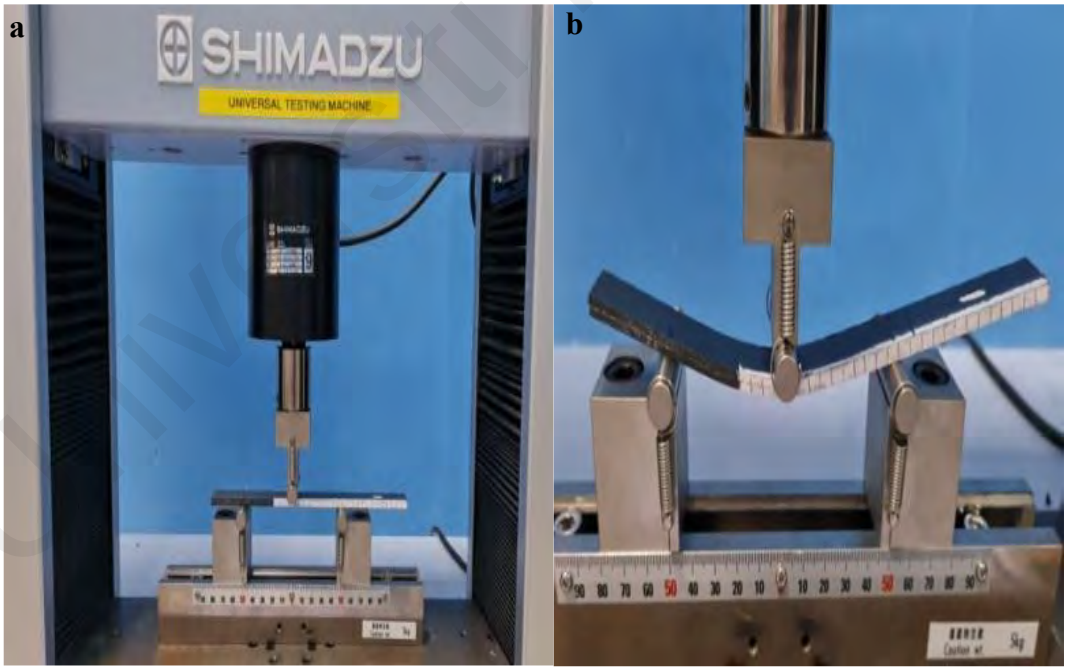

Figure 3.11: (a) Universal Testing Machine and (b) ENF Specimen under Load

The output from the end-notched flexure (ENF) test is load versus displacement curves. Then inter-laminar fracture toughness (G_{IIC}) of the composite laminates was calculated by these load versus displacement curves as per ASTM standard.

(c) Low-Velocity Impact (LVI) Test

A low-velocity impact test is used to determine the damage resistance of the material or to impose damages into the sample for subsequent damage tolerance testing. In this research, the drop weight impact method was utilized to examine the laminated composite behavior under LVI load according to the ASTM standard of D7136M-12. CEAST 9340 drop weight impact tester was used to carry out the drop weight test, as shown in Figure 3.12. Data acquisition systems DAS Junior, DAS 16000 were attached with the instrument via computer to analyze obtained data. The impactor utilizes a hemispherical nose striker with a 12 mm diameter and a total mass of 5.12 kg. The corresponding impact energy was 0 J, 15 J, and 25 J adjusted with impactor height, and the incident impact velocity was automatically controlled. The sample was placed with a cut-out ring hole in the impact support fixture, and a clamp was used to fix the sample during testing. In addition, a rebound brake was utilized to avoid the multiple unintentional impacts on the sample. Samples of composite laminates after the LVI test are shown in Figure 3.13.

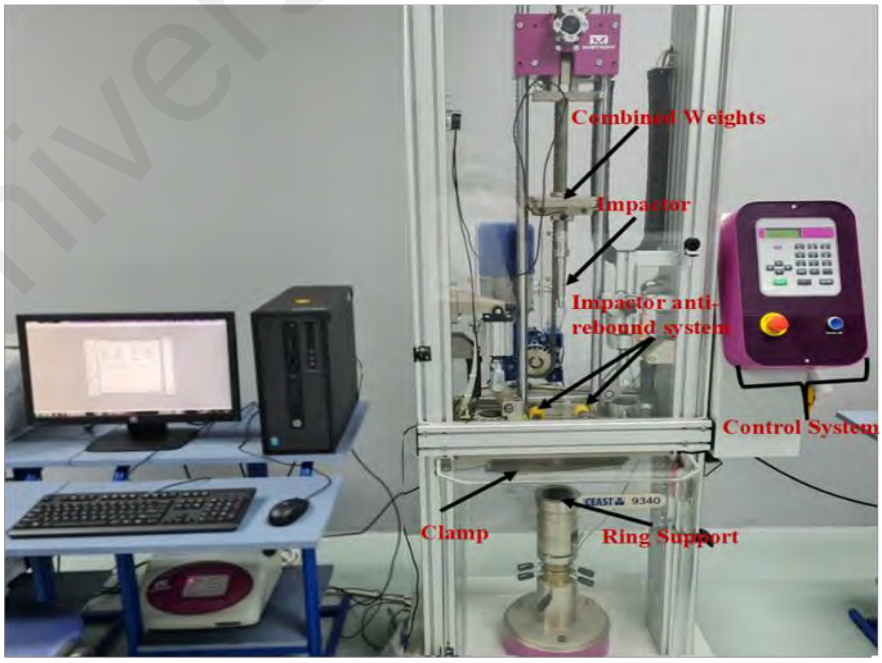

Figure 3.12: Drop Weight Impact Machine

The impact velocity of the impact device was determined according to equation (3.5) [ASTM D7136]:

$$v_i = \frac{(W_{12})}{(t_2 - t_1)} + g(t_i - \frac{(t_1 + t_2)}{2}) \quad \text{Eq. (3.5)}$$

Where, v_i = impact velocity, W_{12}= distance between upper and lower flag prongs, t_1 and t_2 = time lower and upper flag prong passed detector respectively, and t_i = initial time contact. The displacement versus time graph was represented by equation (3.6) [ASTM D7136]:

$$\delta(t) = \delta_i + v_i t + \frac{gt^2}{2} - \int_0^t (\int_0^t \frac{F(t)}{m} dt) dt \quad \text{Eq. (3.6)}$$

Where δ = impactor displacement at time t and δ_i Impact displacement from reference location at time t. The absorbed energy versus time graph was represented by equation (3.7) [ASTM D7136]:

$$E_a(t) = \frac{m(v_i^2 - v(t)^2)}{2} + mg\delta(t) \quad \text{Eq. (3.7)}$$

Where E_a = absorbed energy at the time.

Figure 3.13: Composite Laminates after LVI Testing

The output from the low-velocity impact (LVI) test comes in the form of (i) force versus time curves, (ii) displacement versus time curves, and (iii) energy versus time curves. Then the data from these curves were used to calculate the developing energy measurement of the polymer composite concerning different HMWCNTs loading the laminates according to the ASTM standard. Laminated composite structures in service are likely to suffer from impact loading in many forms, such as tool drops, debris impact, and bird impact

*(d) **Compression After Impact (CAI) Test***

The Compression determined the compression residual strength properties of composite laminates after impact, which have undergone quasi-static indentation per drop-weight impact according to ASTM standard D7137. An Instron machine (5984 series) was used to test with a force capacity of 150 kN, as shown in Figure 3.15a. The test was conducted according to ASTM standard D7137. All the impacted and unimpacted samples were undergone compression loadings by this standard specification with a 1.25 mm/min speed rate, as shown in Figure 3.14b. The direct contact between loading surfaces and the aligning with the platens was ensured by the specimen/fixture assembly subjected to preloading. After that, compression force was decreased and set to re-zero to stable the whole instrumentations.

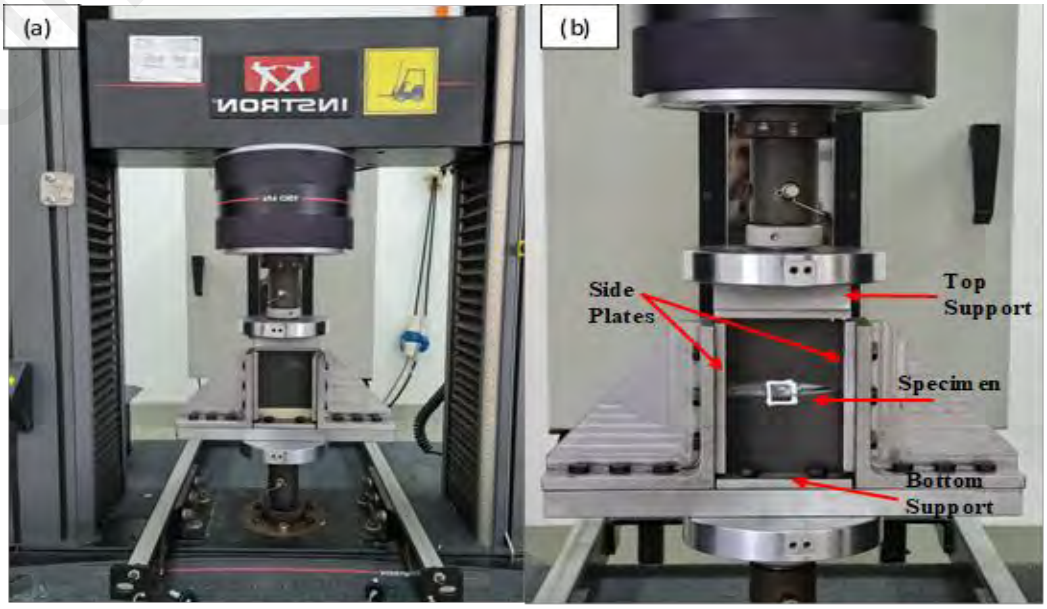

Figure 3.14: (a) CAI Test Machine and (b) Specimen Under Loading

The ultimate compressive residual strength was determined according to equation (3.8) [ASTM D7137]:

$$F^{CAI} = {}^{P_{max}}/_{A} \qquad \text{Eq. (3.8)}$$

F^{CAI} denotes ultimate compressive residual strength, MPa, P_{max} is maximum force before failure, and A is the cross-sectional area, mm^2.

The output from the compression after impact (CAI) test comes from compression force versus displacement curves. Then the data from these curves were used to determine the compressive strength of the polymer composite concerning different HMWCNTs loading the laminates according to the ASTM standard.

(e) ***Thermal Stability Test***

Thermogravimetric analysis (TGA) and differential scanning calorimeter (DSC) was employed to know the thermal stability of the composite laminate. TGA analysis was used to determine the amount of volatile material in the sample by observing the weight change by heating the sample at a constant rate. DSC is employed to know the material behavior concerning temperature and time. In this analysis, heat flow in the sample was measured, which occurred when heated, cooled, or held isothermally at a constant temperature. A thermos-gravimetric analyzer (TGA Q50 V20.13 Build 39) was used for TGA analysis. Alumina crucible was used to place the sample in the analyzer for pyrolysis in a Nitrogen environment with a 60 mL/min flow rate and a 20 °C/min heating rate. The temperature of the experiment was from room temperature to 800 °C.

Differential scanning calorimetry (DSC) testing was done in a DSC analyzer (DSC Q20 V24.11 Build 124). Alumina crucible was used to place the sample in the analyzer and tested from room temperature to 250 °C in N_2 and O_2 environments with a 50 mL/min flow rate at a heating rate of 10 °C/min. The outcome of the thermal stability test gives us the information related to the thermal stability of the composite laminates in terms of

(i) wt. % change versus temperature and (ii) heat flow rate versus temperature. The curves' analysis shed light on the phases changes of the composite being investigated and how stable they are at a given temperature.

(f) ***Electrical Conductivity***

Volume resistivity was measured as electrical resistance through an insulating material cube. The test was carried out according to F 390 standard, and the volume resistivity of the composite laminate was determined by a four-point probe, as shown in Figure 3.15.

Figure 3.15: Volume Resistivity Testing

The outcome of the electrical conductivity tests is the respective volume resistivity of the composite laminates concerning different HMWCNTs loading the composite.

3.2.4.2 Non-Destructive Characterization

(a) ***Field Emission Scanning Electron Microscopy (FESEM)***

Fractured surfaces of the samples were analyzed in Zeiss crossbeam 340 field emission scanning electron microscope (FESEM), as shown in Figure 3.16. Before analysis, the surface of the samples was coated by puttering gold to avoid charge accumulation. The FESEM micrographs were then obtained, and the surface morphologies and mechanism of fracture damages of all the fractured surfaces were investigated.

Figure 3.16: (a) Field Emission Scanning Electron Microscope and (b) Analysis of Fractured Surfaces

The outcome of scanning electron microscopy investigation is the physical proof of the damaged areas of the composites after another mechanical testing, in terms of photographs, which are commonly known as fractography in literature. Furthermore, analysis of such fractography helps us unravel the underlying fracture mechanism such as ductile fracture, brittle fracture, or mix-fracture that prevail in the composites.

(b) Ultrasonic Scanning (C-scan)

Internal delamination damages produced by impact testing in composite laminates were determined by ultrasonic inspection (C-scan) measurements at 100 MHz before the compression test, as shown in Figure 3.17. The instrument model was a UPK-24 immersion system (pulse-echo) from Physical Acoustics (Mistras), and the probe size was 25-inch diameter at 2.25MHz. The instrument was controlled via TwinTM software, and the scanning concept was based on Snell's law. C-scan provides information about the in-plane view correlated with the residual material strength.

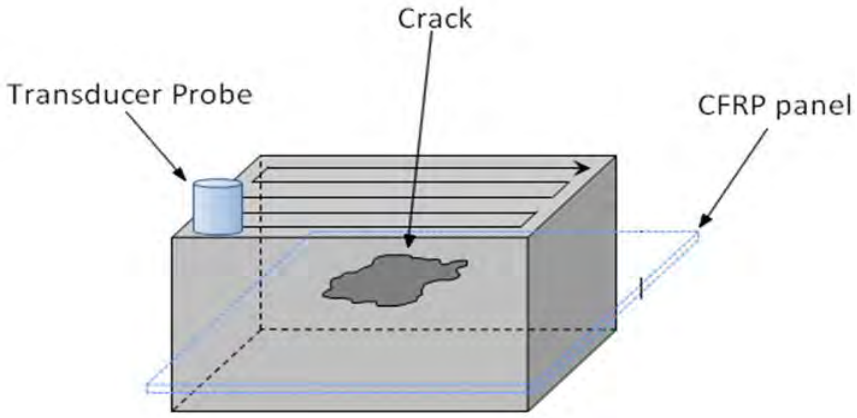

Figure 3.17: Ultrasonic Raster Scanning to Prepare a C-scan of a Specimen Containing an Internal Flaw

The outcome of ultrasonic scanning (C-scan) is assessing internal damage of the composite laminates during the mechanical testing in terms of counter graphs. It shows the extent of internal damage of the composite laminates, which are not otherwise detectable. The experimental parameters used during this study were selected based on extensive literature review and ensured that the used parameters are not over-selected can overshadow the properties of HMWCNTs. For instance, oxide/ceramic reinforcing particles' properties are different from that of CNTs. Hence, experimental parameters normally used for oxide/ceramic reinforced polymer reinforced composite are not applicable for CNTs reinforced polymer matrix composites.

Similarly, the epoxy resin also has a certain limit of operating conditions, beyond which degradation occurred due to the inherent limitation of the resin properties. For instance, an increase of temperature beyond a certain limit may affect the viscosity of the region, which will have a detrimental effect on the composite's mechanical properties. Similarly, improper rpm selection during mixing may cause HMWCNTs breakdown/aggregation.

CHAPTER 4: RESULTS AND DISCUSSION

This thesis chapter represents the results obtained on laminated composite samples as described in the preceding chapters.

4.1 Double Cantilever Beam (DCB) Test Results

DCB test was carried out according to section 3.4.1.1. Three types of samples were consisted: (i) control (without any HMWCNTs), (ii) 0.2 wt. % HMWCNTs and (iii) 0.4 wt. % HMWCNTs loaded. A set of five samples from each composition was tested to obtain accurate results. The data obtained from DCB tests is shown in Figure 4.1 in force versus displacement curves. As seen from Figure 4.1, the load was increased linearly and reached a critical value gradually. The load suddenly tends to decrease after the critical values to ~50 N for control ~70 N for 0.2 wt. % HMWCNTs-epoxy and ~105 N for 0.4 wt. % HMWCNTs-epoxy composite at displacement range about 4-6 mm. This is due to the delamination initiation and cracks propagation. The delamination growth was unstable in all the tests at the beginning. That can be ascribed to adding the Teflon layer causing artificial delamination at the middle plane in every sample. After that, though, the load decreases gradually with the delamination propagation and the middle plane interface until 20 mm, indicating stable delamination growth.

Figure (a) represents results for control; Figure (b) represents results for cand Figure (c), which represents 0.4 wt. % HMWCNT- epoxy composite. Each Figure contains DCB test results for all five samples from each composition. The specimen codes for each sample are also shown in the diagrams, e.g., C-1 for sample 1 of control, HMWCNT021 for sample 1 of 0.2 wt. % HMWCNTs-epoxy, and HWCNT 041 for sample 1 of 0.4 wt. % HMWCNT- epoxy. The codes are well shown in Table 4.1.

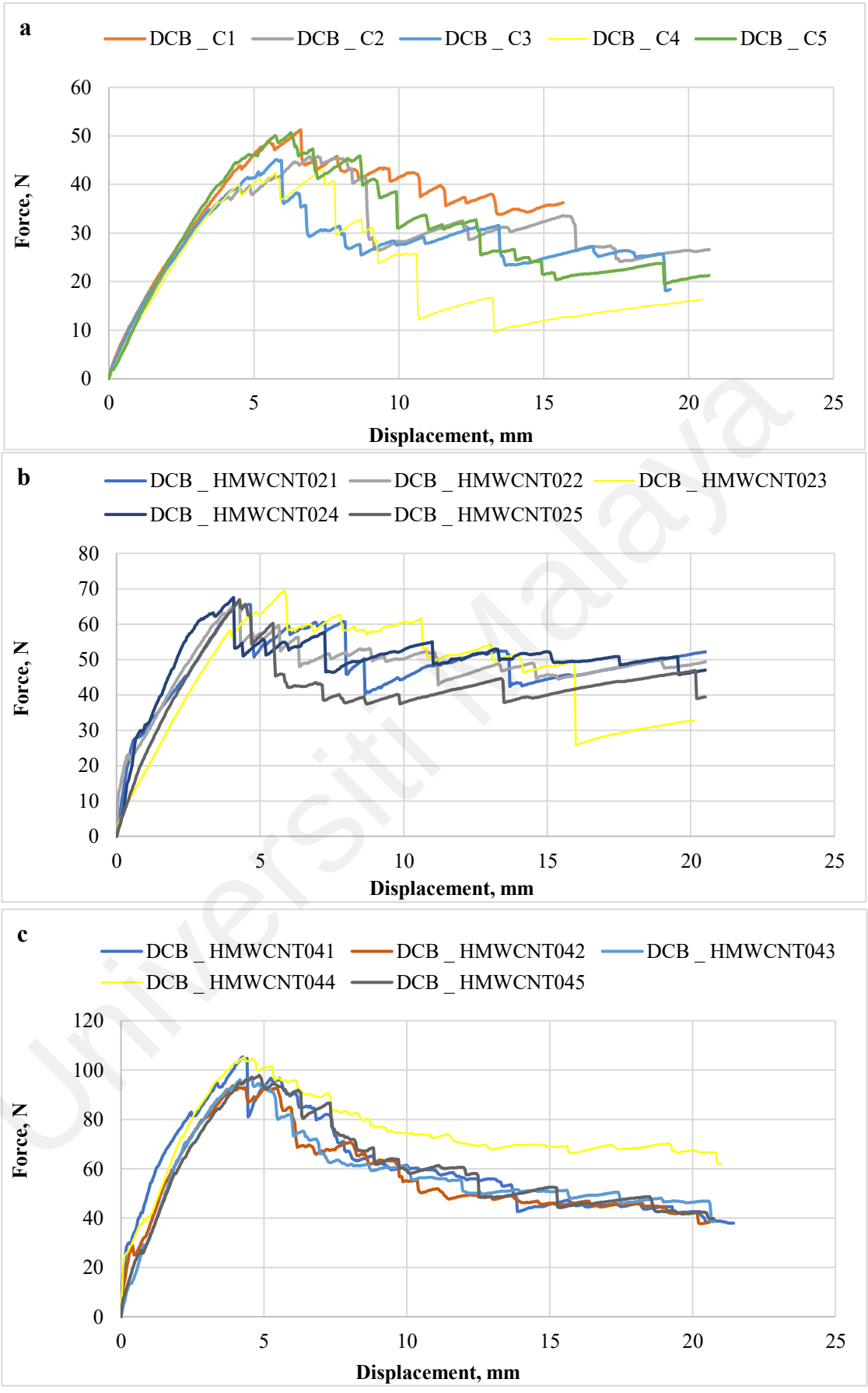

Figure 4.1: Force versus Displacement Graphs Obtained during DCB Tests on Different Samples: (a) Control, (b) 0.2 wt. % HMWCNTs-epoxy, and (c) 0.4 wt. % HMWCNTs-epoxy Composite

Interlaminar Fracture Toughness (G_{IC})

The crack initiation ($G_{IC/Initiation}$) is defined as the linear deviation of a composite failure process, and the crack propagation ($G_{IC/propagation}$) is the mean values at plateau area attained from the samples, which were presented in Table 4.1, 4.2, and 4.3 for control, 0.2 wt. % HMWCNTs-epoxy and 0.4 wt. % HMWCNTs-epoxy samples, respectively, corresponding the average values of interlaminar fracture toughness (G_{IC}) and standard deviations. The mode-I interlaminar fracture toughness properties were evaluated by using four modes. These consisted of a Modified Compliance Calibration Method (MCC), a Compliance Calibration Method (CCM), Modified Beam Theory (MBT), and the Original Beam theory (OBT).

Table 4.1: Interlaminar Fracture Toughness (GIC) of Control Samples

Specimen Code	Interlaminar Fracture Toughness, G_{IC} (kJ/m^2)							
	Initiation				Propagation			
	OBT	MBT	CCM	MCC	OBT	MBT	CCM	MCC
DCB_C1	0.4926	0.2342	0.2917	0.2613	0.4304	0.2483	0.2549	0.2631
DCB_C2	0.4695	0.1951	0.2616	0.2656	0.3883	0.1983	0.2138	0.2456
DCB_C3	0.3879	0.2422	0.2771	0.2589	0.3009	0.2163	0.2149	0.2207
DCB_C4	0.3523	0.3076	0.3841	0.3988	0.2659	0.2400	0.2899	0.3049
DCB_C5	0.4247	0.3901	0.4068	0.399	0.3640	0.3416	0.3487	0.3448
Average	0.4059	0.2644	0.3113	0.3044	0.3587	0.2591	0.2740	0.2837
Standard Dev.	0.0701	0.0722	0.0673	0.0737	0.0631	0.0554	0.0559	0.0480

TTable 4.2: Interlaminar Fracture Toughness (GIC) of 0.2 wt. % HMWCNTs-epoxy Samples

Specimen Code	Interlaminar Fracture Toughness G_{IC} (kJ/m^2)							
	Initiation				Propagation			
	OBT	MBT	CCM	MCC	OBT	MBT	CCM	MCC
DCB_HMWCNT021	0.4181	0.3222	0.3133	0.3225	0.5142	0.4277	0.3965	0.4220
DCB_HMWCNT022	0.4064	0.2230	0.2658	0.3250	0.5044	0.3265	0.3299	0.3997
DCB_HMWCNT023	0.5951	0.3025	0.3734	0.3326	0.6173	0.3805	0.3874	0.3944
DCB_HMWCNT024	0.3921	0.2391	0.2922	0.3089	0.5385	0.3756	0.4013	0.4202
DCB_HMWCNT025	0.4270	0.3086	0.3467	0.3335	0.3653	0.2915	0.2965	0.3075
Average	0.4477	0.2791	0.3183	0.3245	0.5079	0.3604	0.3623	0.3887
Standard Dev.	0.0833	0.0447	0.0427	0.0099	0.0912	0.0525	0.0466	0.0470

Table 4.3: Interlaminar Fracture Toughness (G_{IC}) of 0.4 wt. % HMWCNTs-epoxy Samples

Specimen Code	Interlaminar Fracture Toughness G_{IC} (kJ/m^2)							
	Initiation				Propagation			
	OBT	MBT	CCM	MCC	OBT	MBT	CCM	MCC
DCB_HMWCNT041	0.6698	0.5884	0.7390	0.7687	0.6020	0.5515	0.6642	0.6928
DCB_HMWCNT042	0.5643	0.5274	0.5645	0.5965	0.5581	0.5323	0.5583	0.5535
DCB_HMWCNT043	0.6373	0.5126	0.5720	0.5897	0.6097	0.5219	0.5473	0.5399

DCB_HMWCNT044	0.7077	0.4872	0.5742	0.5901	0.8332	0.6388	0.6761	0.6848
DCB_HMWCNT045	0.6978	0.5214	0.5987	0.6229	0.6685	0.5403	0.5736	0.5710
Average	0.6554	0.5274	0.6097	0.6336	0.6543	0.5570	0.6039	0.6084
Standard Dev.	0.0577	0.0373	0.0733	0.0767	0.1074	0.0470	0.0613	0.0742

Graphical representation of average values of interlaminar fracture toughness propagation and initiation is shown in Figure 4.2 and Figure 4.3, respectively.

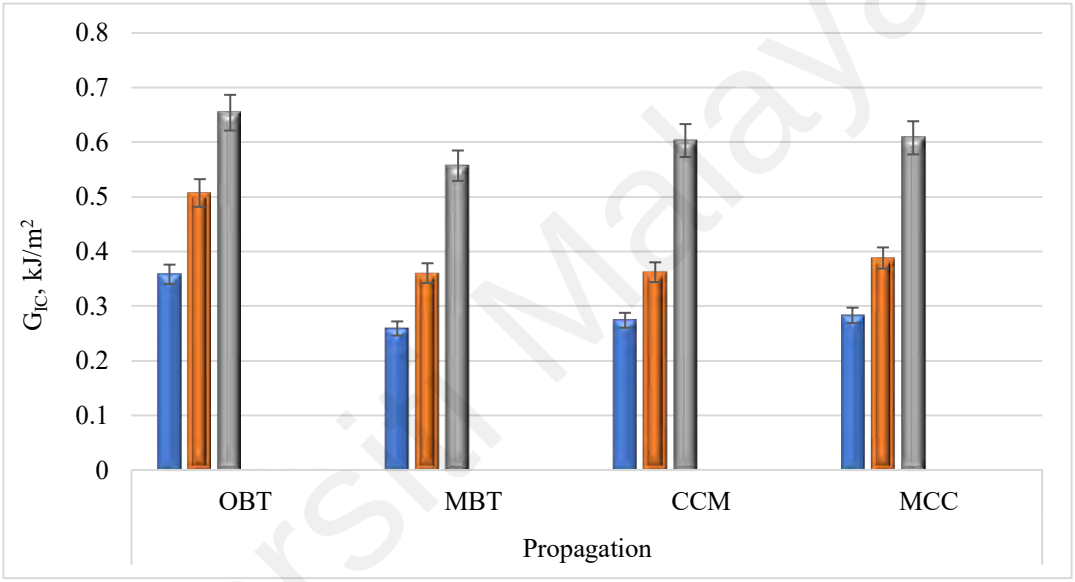

Figure 4.2: Interlaminar Fracture Toughness G_{IC} (kJ/m^2) for Propagation

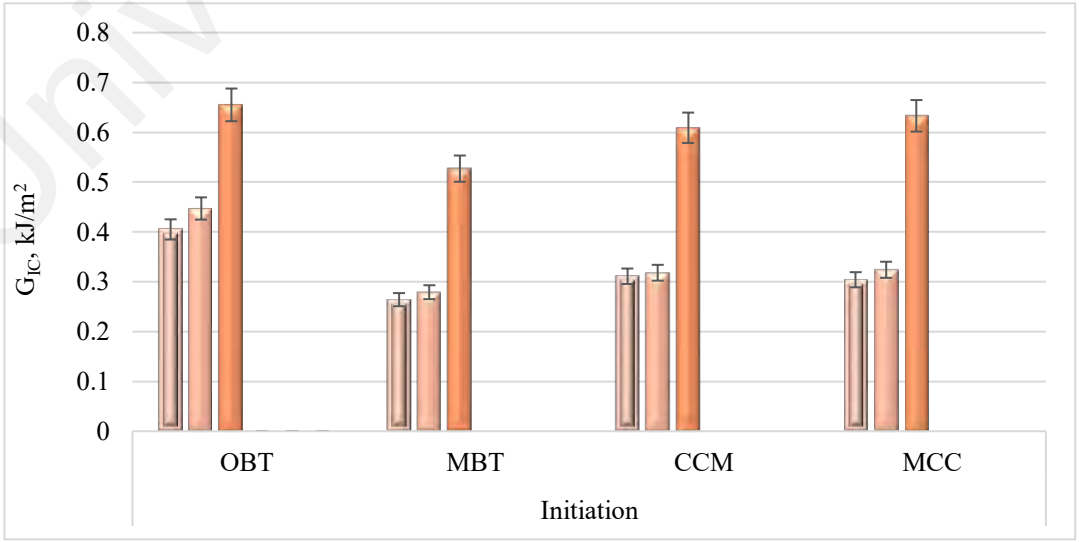

Figure 4.3: Interlaminar Fracture Toughness G_{IC} (kJ/m^2) for Initiation

The increased percentages of interlaminar fracture toughness G_{IC} of all compositions are shown in Table 4.4. The maximum observed value was 0.4 wt. % HMWCNTs-epoxy composite in initiation and propagation, while 0.2 wt. % HMWCNTs-epoxy has a lower increment than the 0.4 wt. % HMWCNTs-epoxy composite. The resistance curve (*R*-curve) of interlaminar fracture toughness Mode I versus crack length is shown in Figures 4.4, 4.5, and 4.6, respectively, for control, 0.2 wt. % HMWCNTs-epoxy and 0.4 % HMWCNTs-epoxy composite. The incorporation of HMWCNTs resulted in an increase in fracture toughness compared with the control sample.

Table 4.4: Increment Percentage of Interlaminar Fracture Toughness G_{IC} for all Compositions

HMWCNTs Content (wt.%)	Interlaminar Fracture Toughness G_{IC}							
	Increment in Initiation %				Increment in Propagation %			
	OBT	MBT	CCM	MCC	OBT	MBT	CCM	MCC
0.2	10.3703	5.6818	2.2508	6.5789	41.6201	39.1505	32.1167	37.1024
0.4	61.7284	99.6212	95.8199	108.2237	82.6815	115.0579	120.0730	114.8410

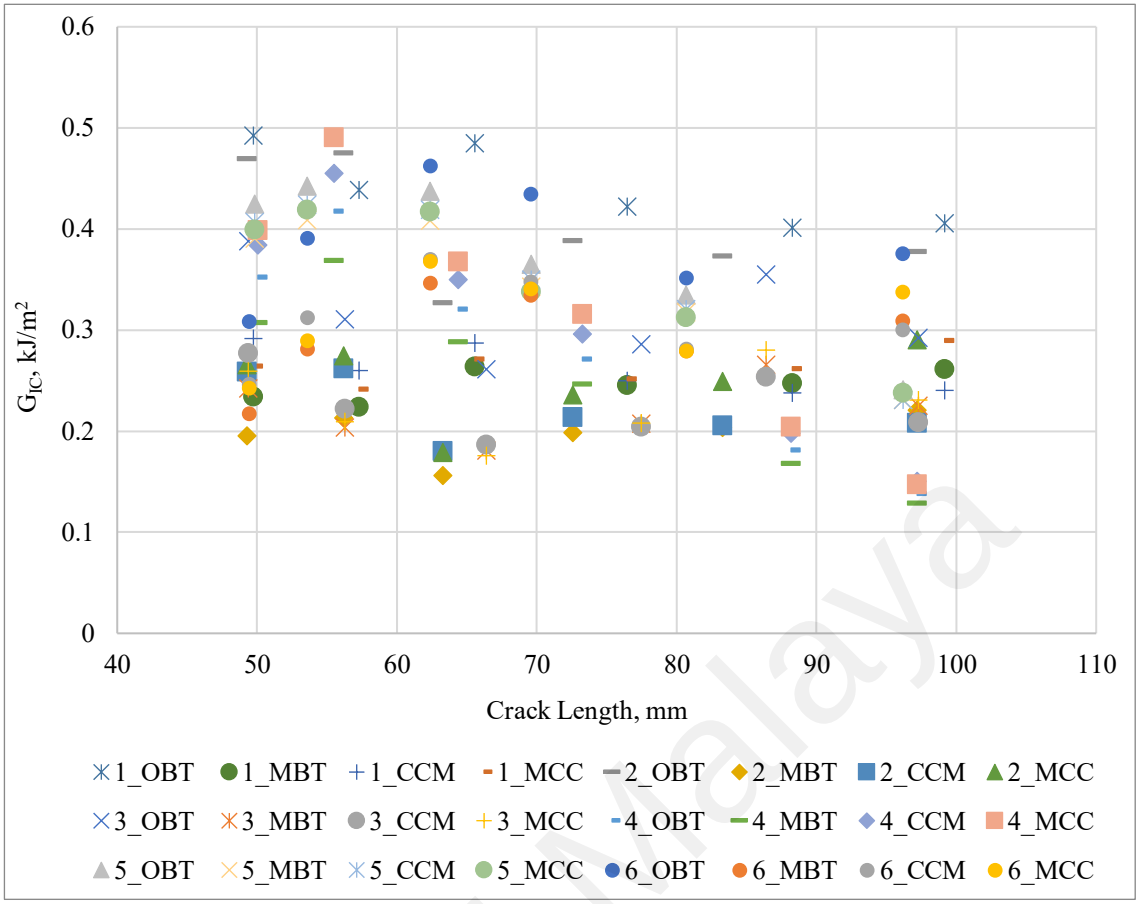

Figure 4.4: R Curves for DCB Samples for Control

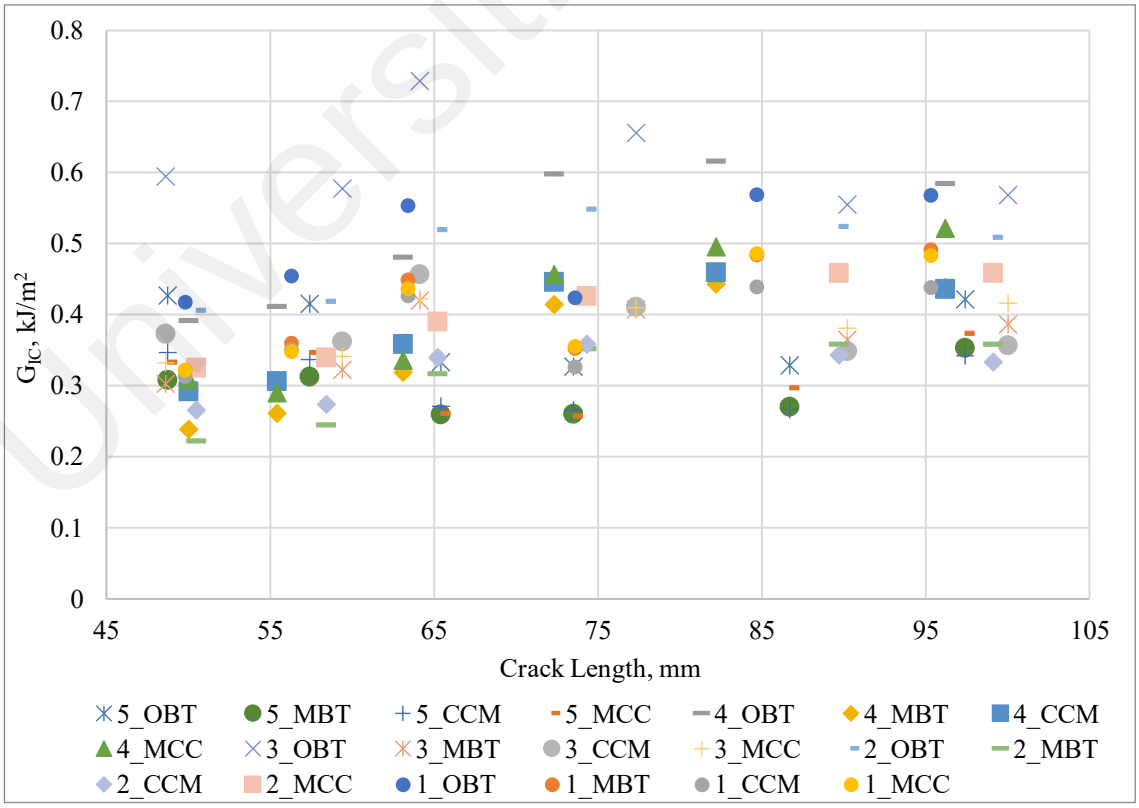

Figure 4.5: R Curves for DCB Samples for 0.2 wt. % HMWCNTs-epoxy Composite

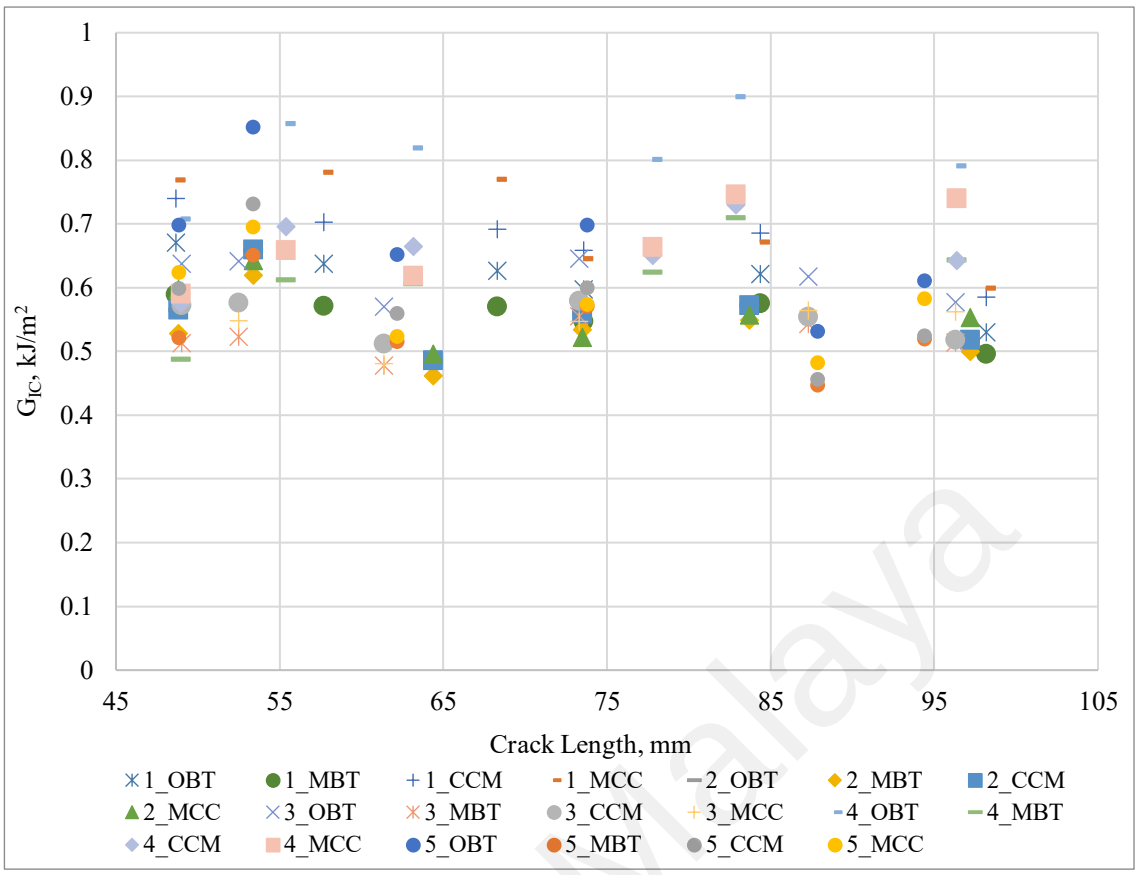

Figure 4.6: R Curves for DCB Sample for 0.4 wt. % HMWCNTs-epoxy Composite

In the DCB test, the tip of the notch between the central plies was the location of the largest stress concentration, and cracked development occurred from this notch. When specimens undergo load application, the crack propagation occurs until the partial release of the stress corresponds to some intermediate equilibrium state. After that, additional loading will further propagate the crack, leading to complete sample breakage. This procedure helps to calculate $G_{IC,}$ which is resultant from the high jumps in load and not causing the sharp decrease in the load value (Seyhan et al., 2008), as Compston et al. has explained in detail (Compston et al., 1998). According to Hine et al. (1989), the unstable crack propagation in fiber-reinforced polymer composites is due to high toughness at local regions. Therefore, when the tougher region was attained by crack tip (due to either a tougher matrix region or fiber bridging), crack propagation slowed down until the stored elastic energy build-up was at a sufficient level for re-initiating the crack propagation (Sacchetti et al., 2018). During re-initiation, the stored elastic energy is normally greater

than required for stable crack propagation; therefore, the crack propagates inconsistently until sufficient input energy is not left for further growth and arrests. Other factors contribute towards stick-slip crack growth like blunting and resharpening of cracks and an imbalance between static and dynamic toughness. The fiber bridging was observed during crack propagation, as illustrated in Figure 4.1.

The average vales of G_{IC} for control sample was 0.405 kJ/m^2 for OBT, 0.264 kJ/m^2 for MBT, 0.311 kJ/m^2 for CCM and 0.304 kJ/m^2 for MCC. When HMWCNTs was added, as shown in Table 4.1-4.3, it can be seen that the laminate has relatively higher value: 0.447 kJ/m^2 for OBT, 0.279 kJ/m^2 for MBT, 0.318 kJ/m^2 for CCM, and 0.324 kJ/m^2 for MCC in the case of 0.2 wt. % HMWCNTs-epoxy and 0.655 kJ/m^2 for OBT, 0.527 kJ/m^2 for MBT, 0.609 kJ/m^2 for CCM and 0.633 kJ/m^2 for MCC in the case of 0.4 wt. % HMWCNTs-epoxy. Indeed, the delamination resistances observed for both composites are notably higher than that of the control sample. The values of interlaminar fracture toughness during steady-state crack propagation are considerably higher than for crack initiation. In Table 4.4, the percentages of increase in fracture toughness values show that the highest increase was observed for 0.4 wt. % HMWCNTs-epoxy composite recorded at 120%. Similarly, the R-curve of Mode I fracture toughness values as a function of crack length in Figures 4.4-4.6 showed that crack length for the control sample was lower than composite samples. This increase in all Mode I interlaminar fracture toughness values are attributed to the fact that fiber bridging has occurred during crack propagation.

From the discussion mentioned above, it is evident that the composite laminates perform better than that of control samples in DCB tests. This improvement was achieved due to improved intermolecular bond and homogenous dispersion of HMWCNTs in the epoxy. This results in effective load transfer from matrix to fibre-HMWCNTs and enhances the overall strength of the composite. To be explained further, if HMWCNTs have poor dispersion quality, then the mixture of composites could pull out during

delamination and thus decrease the maximum fracture toughness (Kim et al., 2004). Thus, the experimental results confirmed that the interfacial chemical interactions between the HMWCNTs and epoxy form a strong interfacial bonding by dispersion technique that achieved improved fracture toughness.

4.2 End Notched Flexure (ENF) Test Results

ENF test was carried out according to section 3.4.1.2 to find Mode II interlaminar fracture toughness. To get accurate results, a set of five samples from each composition were tested, and the corresponding load versus displacement graphs are shown in Figure 4.7. As demonstrated in Figure 4.7, almost similar behavior was observed in all the samples. The linear increase in applied load was observed in the crack initiation to propagation specified by the deviation observed in the elastic region—the slope of load versus displacement curve for 0.4 wt. % HMWCNTs-epoxy samples have the highest value among others because of higher CNTs content, as further explained in the upcoming section.

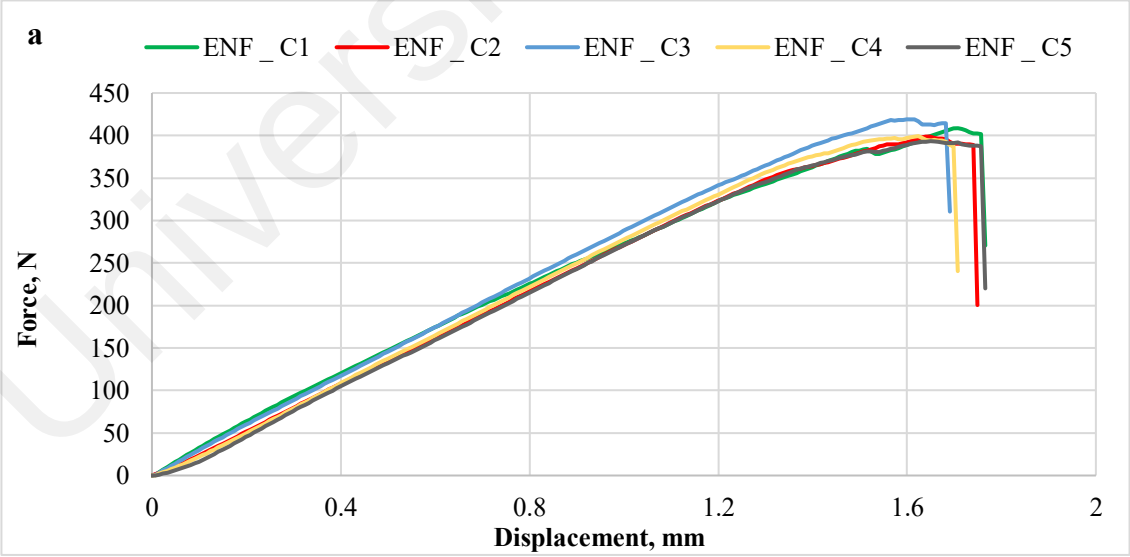

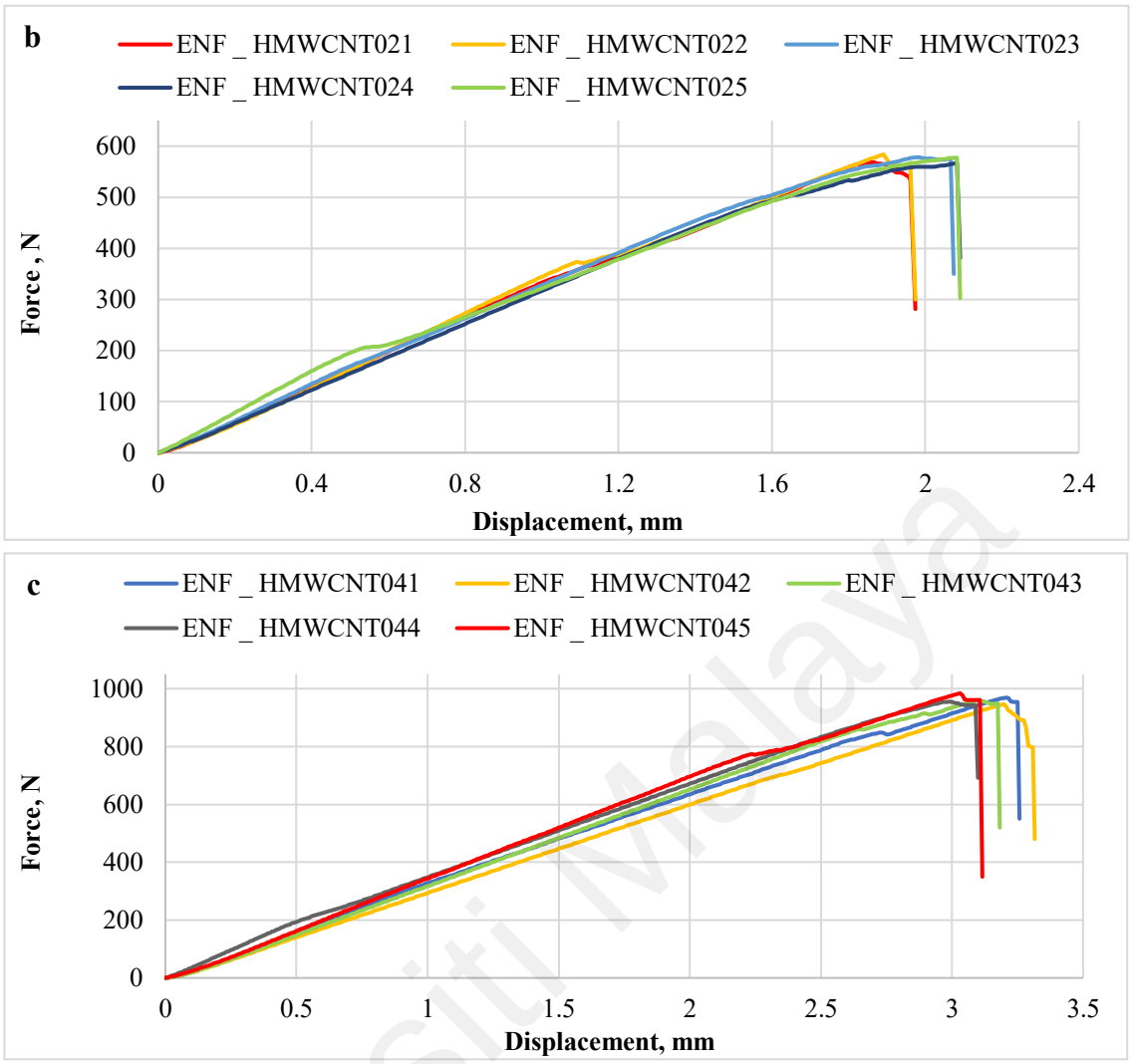

Figure 4.7: Force versus Displacement Graphs Obtained during ENF Tests of Different Samples: (a) Control, (b) 0.2 wt. % HMWCNTs-epoxy, and (c) 0.4 wt. % HMWCNTs-epoxy Composite

Interlaminar Fracture Toughness (G_{IIC})

Incorporating HMWCNTs has increased fracture toughness (G_{IIC}) compared with the control specimen. Tables 4.5, 4.6, and 4.7 illustrate the fracture toughness values for Mode II of all tested specimens.

Table 4.5: Interlaminar Fracture Toughness (G_{IIC}) of Control Sample

Specimen Code	Interlaminar Fracture Toughness G_{IIC} (kJ/m^2)					
	a	P	E	b	h	G_{IIC} (kJ/m^2)
ENF_C1	30	408.15	24333.7	20.53	2.10	0.8878
ENF_C2	30	398.70	23334	20.60	2.09	0.8902

ENF_C3	30	419.20	24708.9	20.50	2.11	0.9120
ENF_C4	30	397.65	23380.1	20.50	2.10	0.8797
ENF_C5	30	391.68	21532.2	20.53	2.11	0.9109
Average						0.8961
Standard Dev.						0.0145

Table 4.6: Interlaminar Fracture Toughness (G_{IIC}) of 0.2 wt. % HMWCNTs-epoxy Samples

Specimen Code	Interlaminar Fracture Toughness G_{IIC} (kJ/m^2)					
	a	P	E	b	h	G_{IIC} (kJ/m^2)
ENF_HMWCNT021	30	567.70	26845.9	20.73	2.20	1.3281
ENF_HMWCNT022	30	579.80	27850	20.63	2.23	1.2947
ENF_HMWCNT023	30	576.14	25162.4	20.66	2.21	1.4495
ENF_HMWCNT024	30	567.60	26453.1	20.60	2.21	1.3460
ENF_HMWCNT025	30	558.52	25885.8	20.66	2.20	1.3423
Average						1.3521
Standard Dev.						0.0580

Table 4.7: Interlaminar Fracture Toughness (G_{IIC}) of 0.4 wt. % HMWCNTs-epoxy Samples

Specimen Code	Interlaminar Fracture Toughness G_{IIC} (kJ/m^2)					
	a	P	E	b	h	G_{IIC} (kJ/m^2)
ENF_HMWCNT041	30	945.07	33676.8	20.60	2.30	2.6004
ENF_HMWCNT042	30	940.22	29200.9	20.63	2.31	2.9214
ENF_HMWCNT043	30	935.67	32428	20.50	2.29	2.7081
ENF_HMWCNT044	30	946.36	36810.1	20.56	2.30	2.3948
ENF_HMWCNT045	30	955.22	37073.3	20.66	2.31	2.3681

Average		2.5986
Standard Dev.		0.2295

Figure 4.8 shows graphical representation of the average values which is 0.88 kJ/m^2, 1.35 kJ/m^2 and 2.61 kJ/m^2 for control, 0.2 wt. % HMWCNTs-epoxy and 0.4 wt. % HMWCNTs-epoxy composite.

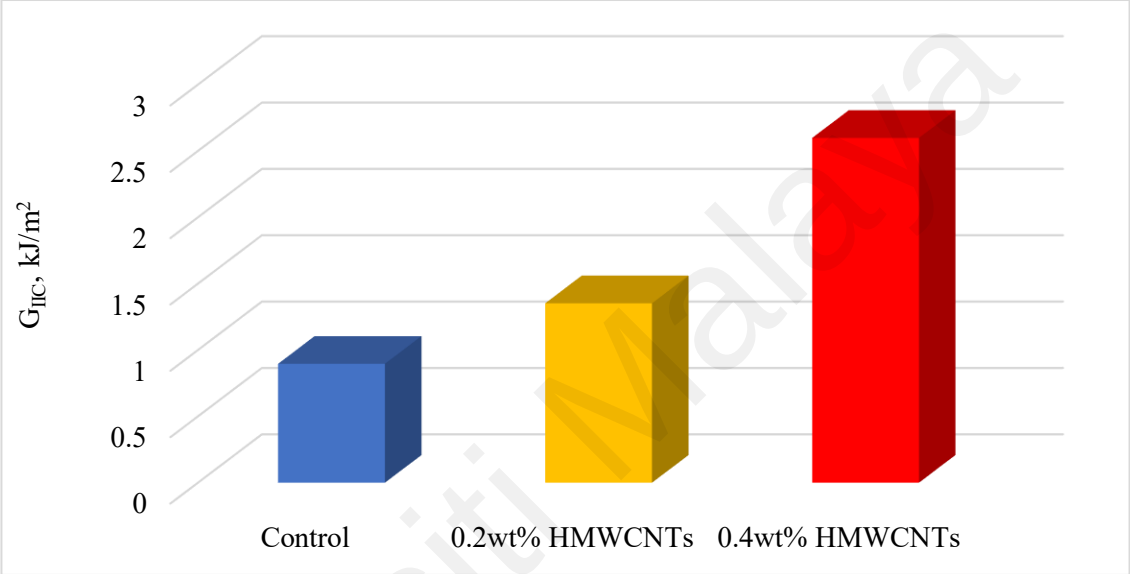

Figure 4.8: Average Values of Interlaminar Fracture Toughness

Based on the outcomes of the ENF test (Figure 4.7 and Tables 4.5-4.7), the values of G_{IIC} were considerably higher than the values of G_{IC} as expected. The values of Mode II interlaminar fracture toughness, 0.2 wt. % HMWCNTs-epoxy and 0.4 wt. % HMWCNTs-epoxy is greater than the control sample. As illustrated in Figure 4.8, Mode II interlaminar fracture toughness for the control sample was calculated as 0.887 kJ/m^2 for 0.2 wt. % HMWCNTs-epoxy was 1.352 kJ/m^2 and for 0.4 wt. % HMWCNTs-epoxy was 2.611 kJ/m^2. By analyzing complete sets of experimental results, it is confirmed that the fracture toughness values of CF-E laminates have increased compared with the reference material by adding 0.2 wt. % and 0.4 wt. % HMWCNTs. The increase in fracture toughness values is due to the energy dissipation mechanism integrated into the material structure at the

crack propagation stage. The cause of the energy absorptions is attributed to a high HMWCNTs proportion in CF-E laminates.

Furthermore, the delamination occurred in the control sample due to the tensile crack in the polymer matrix associated with the carbon fiber bridging resulting in resisting the delamination growth at the crack tip. The same mechanism was observed in the case of composite laminates; however, another mechanism was also observed with extra energy consumption, i.e., the bridging of HMWCNTs at the interface of crack tip resulted in higher resistance to crack propagation. As individual HMWCNTs have higher strength than that of the epoxy or carbon fiber, thus it can tolerate a higher level of stress at the crack tip and, in a given situation, may arrest/divert the track tip. As a result, the overall composite withstands a higher level of external loading before ultimate failure.

4.3 Low-Velocity Impact (LVI) Test Results

LVI test was conducted according to section 3.4.1.3. There were two different energy levels (15 J and 25 J) for each set of specimens for impact tests, and the outcome of the tests is shown in Figure 4.9 in terms of force versus time responses. It has been observed that impact force increases with the beginning, and when it reaches the maximum point, it tends to decrease slowly and return to zero. At a 0-2 ms interval, the curve rises and shows a high-frequency oscillation region that indicates the contact of samples and impactor. It can be said that some irregularity in curves was observed, which shows the

damage formation like delamination. After that, the load starts to drop and shows unloading of samples due to damage presence and reaches zero.

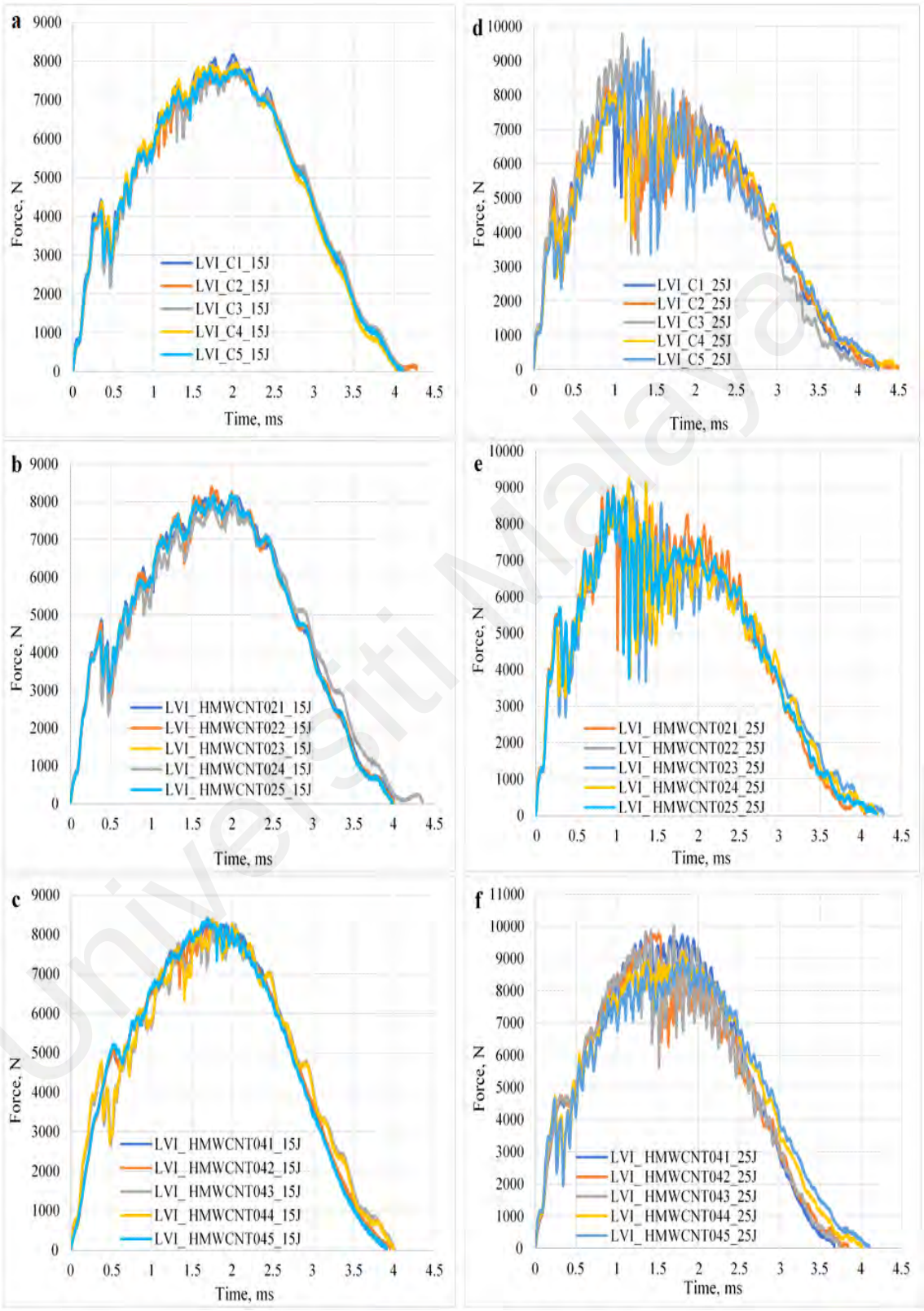

Figure 4.9: Force versus Time Curves from LVI Tests: (a-c) At 15 J (Control, 0.2 % HMWCNTs-epoxy and 0.4 % HMWCNTs-epoxy, respectively) and (d-f) at 25 J (Control, 0.2 % HMWCNTs-epoxy and 0.4 % HMWCNTs-epoxy, respectively)

The displacement versus time response of the LVI test is sown in Figure 4.10. The trend of graphs declares that the difference observed in impact energy level is almost similar; however, HMWCNTs-epoxy laminates demonstrate a slightly higher than control samples.

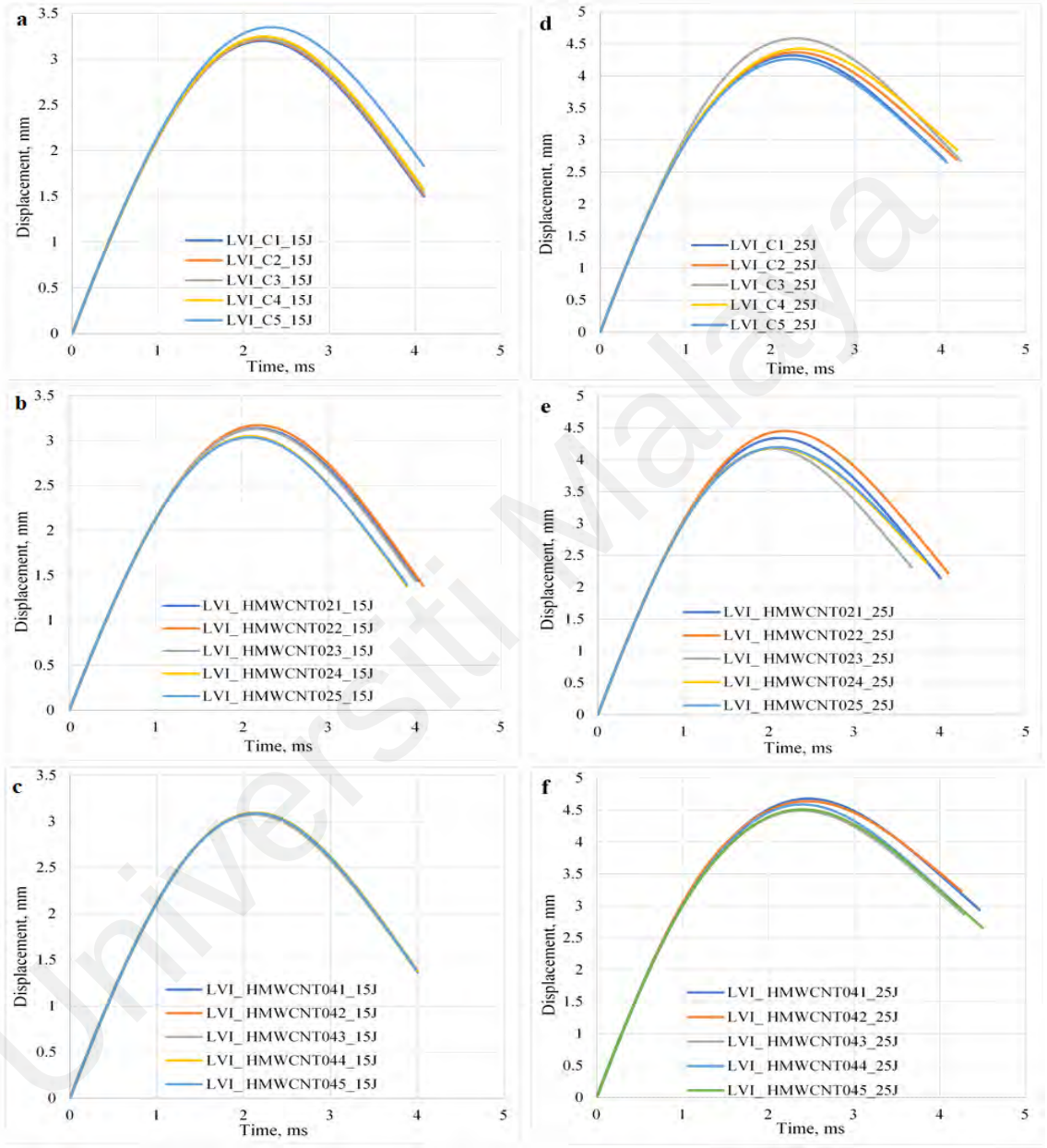

Figure 4.10: Displacement versus Time Curves from LVI Tests: (a-c) At 15 J (Control, 0.2 % HMWCNTs-epoxy and 0.4 % HMWCNTs-epoxy, respectively) and (d-f) at 25 J (Control, 0.2 % HMWCNTs-epoxy and 0.4 % HMWCNTs-epoxy, respectively)

Absorbed energy indicates the energy level of the curve when it becomes constant with time. As shown in Figure 4.11, initially (at t = 0 s), the impactor delivered its kinetic energy to the sample and stored it partially as elastic deformation in the sample. The rest

dissipated by friction, heat, and sound. After reaching to maximum non-perforation impact level, the energy absorption curves show the stop moment of the impactor after the complete transfer of impactor energy to samples. Then, the stored elastic strain energy of the specimen is returned to the impactor till separation and represents a little drop in a curve (at t = 3s) in both graphs, showing a decreasing rate of decline. The final energy value shows the total energy absorbed/dissipated by samples, mostly in damage formation in the samples.

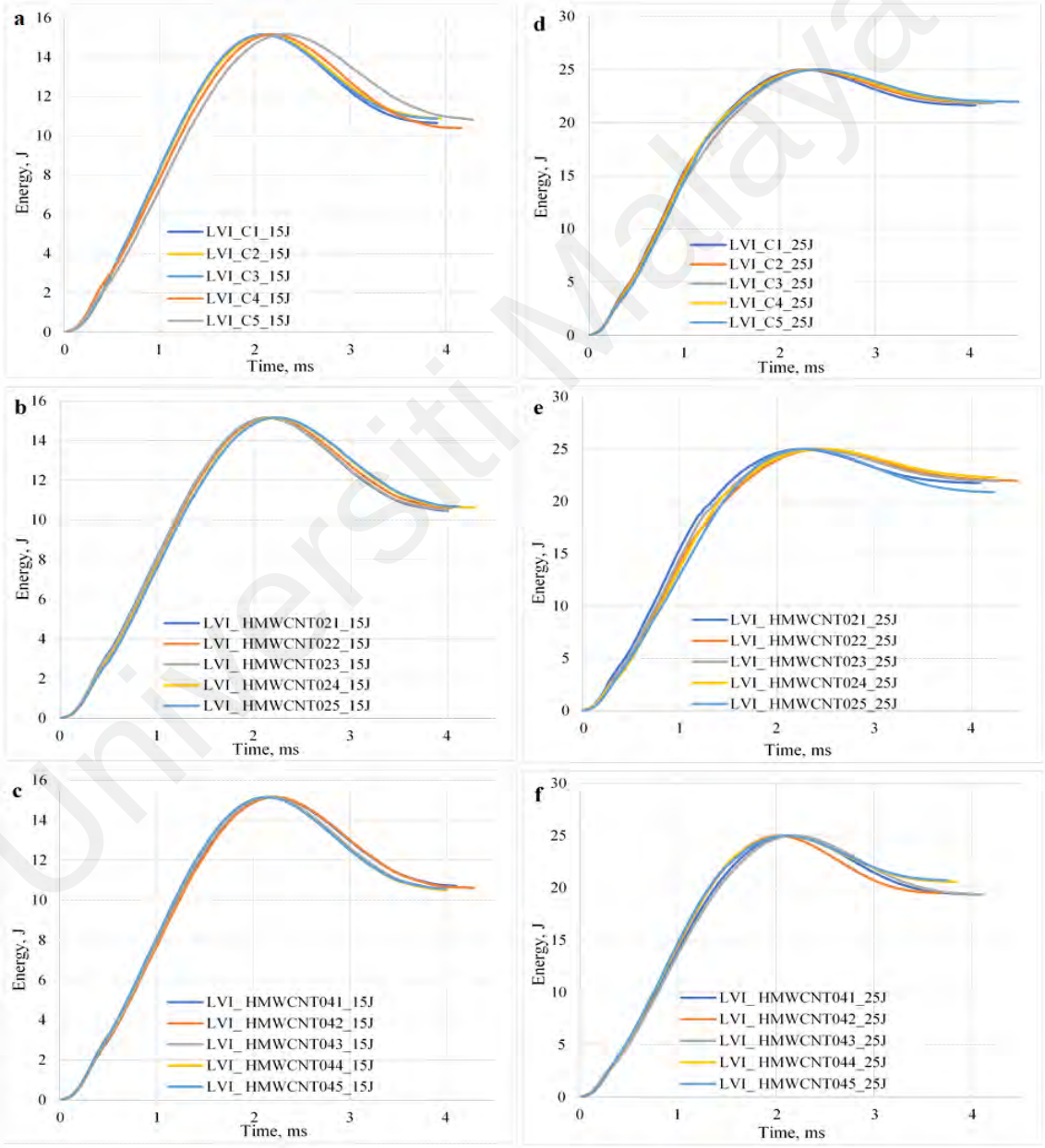

Figure 4.11: Energy versus Time Curves from LVI Tests: (a-c) At 15 J (Control, 0.2 % HMWCNTs-epoxy and 0.4 % HMWCNTs-epoxy, respectively) and (d-f) at 25 J (Control, 0.2 % HMWCNTs-epoxy and 0.4 % HMWCNTs-epoxy, respectively)

Figure 4.12 shows the graph of the developing energy of control, 0.2 wt. % HMWCNTs-epoxy and 0.4 wt. % HMWCNTs-epoxy laminates at the energy level of 15 J and 25 J. The graph shows the lowest energy for control and a slight increase in 0.2 wt. % HMWCNTs-epoxy and highest for 0.4 wt. % HMWCNTs-epoxy samples.

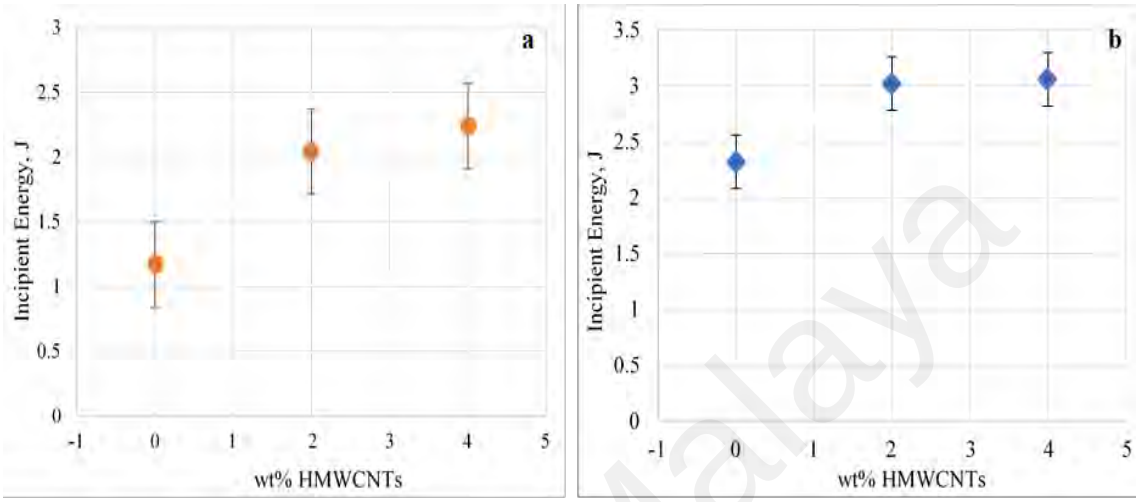

Figure 4.12: Incipient Energy Measured for Different HMWCNTs Content of Composite: (a) 15 J and (b) 25 J

Figure 4.13 shows the control's absorbed energy versus impact graphs, 0.2 wt. % HMWCNTs-epoxy and 0.4 wt. % HMWCNTs-epoxy laminates. The graph shows the lowest energy for control and a slight increase in 0.2 wt. % HMWCNTs-epoxy and highest for 0.4 wt. % HMWCNTs-epoxy composites, as expected.

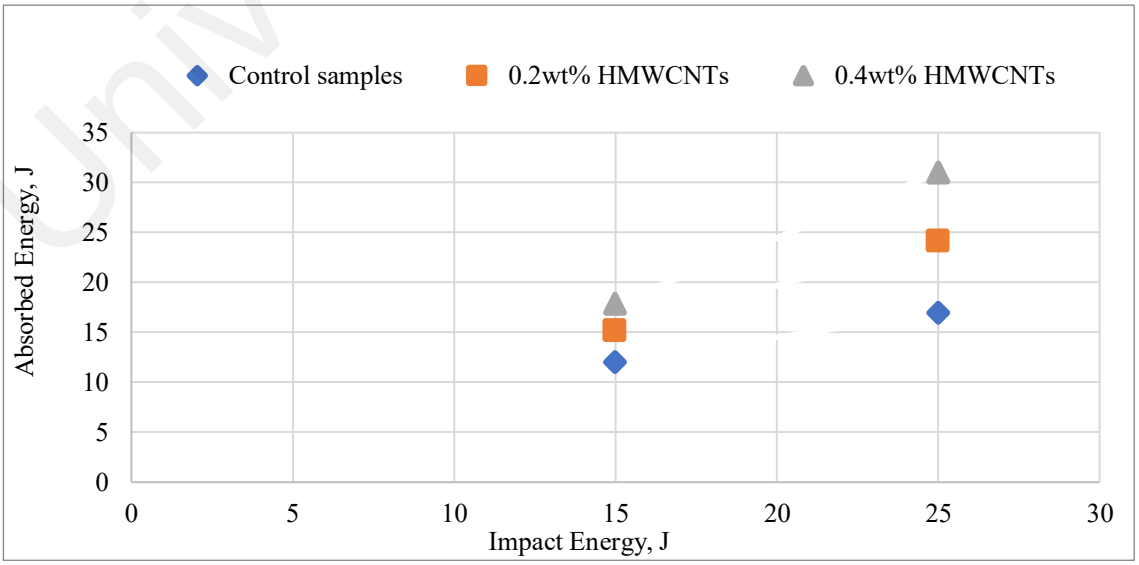

Figure 4.13: Absorbed Energy versus Impact Energies

The impact test results explained the parameters like the value of forces at first damage, impact energy, maximum forces, and non-recoverable energy dissipation by samples to impact energy and the response of absorbed energy with time. There are three types of impact: (i) rebound occurs with low energy absorbed, (ii) the impactor stops without rebounding, and (iii) the impactor perforation through the sample. The maximum load that an impactor can impact the samples the entire time is the peak load, while the energy of the sample at maximum impact load is the peak energy.

The composite's damage mechanism under low-velocity impact is not related to the laminate layup (unidirectional or woven plies). It consists of the low energy indentation, tensile damages on the back surfaces (decreased the composite local stiffness), and then the penetration because of layers shearing through the thickness due to crack initiation and propagating of delamination. These modes were dependent on many factors such as energy, impact velocity, impactor properties, laminate properties, and the boundary condition. Impactor properties comprise shapes, sizes, and tip geometry. Laminate properties comprise a type of layup, constituent properties (matrix and fiber and other additives), fabrication process, and laminate size (width, length, and thickness). Boundary conditions comprise whether the plate edges are free, fixed, or supported edges or combinations. Impact load versus time responses provide a qualitative indication of the response of laminates and damage. In load versus time response, the sharp drop in load shows severe damages in laminates, while the localized damages are indicated by slopes change in graphs.

In addition, damage initiation, also known as damage resistance, greatly depends on incipient energy. Damage resistance is material's ability to withstand the incident, resisting damages and energy at the time of first change occurs in load– time plot at the slope of ascending section is known as developing energy. The failure initiation of fiber-

matrix at the interface is indicated by this energy or matrix element failure near the opposite of the impacted face (Mahdi et al., 2013).

Figure 4.13 shows the force versus time response at 15 J and 25 J at two different energy levels. The graphs show that the impact force increases with the beginning, and when it reaches the maximum point, it tends to decrease slowly and return to zero. At time 0-2 ms, the curve starts to rise and shows a region of high-frequency oscillation, which indicates the contact of samples and impactor. It can be said that some irregularity in curves was observed, which shows the damage formation like delamination. After that, the load starts to drop and shows unloading of samples due to damage presence and reaches zero (Hosur et al., 2007). The response observed was smooth without any sudden dropping in loads. After the process of progressive damages, there was no penetration. Oscillation indicates loadings and unloading of the impactor and the progressive damage.

The smooth curves mean less server damage in the samples (Hosur et al., 2007). The peak load of the control sample was lower than both composites. This implies that the composites have higher impact resistance than the control sample. Similarly, the displacement versus time response of the LVI test in Figure 4.10 confirms the absence of any perforation through the sample (Ismail et al., 2019).

Energy absorbed by samples due to damage formation and the friction between sample and impactor is known as absorbed energy. (Icten, 2015). Absorbed energy can be thoroughly analyzed by energy versus time graphs (Vaidya, 2011), as shown in Figure 4.11. Initially, at t = 0 s, the impactor delivered its kinetic energy to the sample and stored it partially as elastic deformation in the sample. The rest dissipated by friction, heat, and sound. After reaching maximum, the non-perforation impact level, energy absorption curves show the stop moment of impactor after complete transfer of impactor energy to samples. Then, the stored elastic strain energy of the specimen is returned to the impactor till separation and represents a little drop in the curve.

The final energy value shows the sample's total energy dissipated/absorbed mostly due to damage formation. It is to be mentioned that the free vibration energy of samples is very small and negligible because of the quasi-static condition of LVI tests (Tan et al., 2013). But the impactor's energy at the perforation impact level is high enough to break through the sample. Therefore, there is no sign of decline in the curve, and the majority of absorbed energy is dissipated through damage propagation in the samples. Furthermore, as the impactor with unconverted potential energy still travels, the samples' highest energy is always lesser than the total impact or energy. This highest energy represents the impact perforation threshold energy of the composites (Shyr and Pan, 2003).

As shown in Figure 4.12, incipient energy is the ability of a material to endure an event resisting damages, also known as damage resistance. This is the energy when the first change in slope occurs in a graph (Iqbal et al., 2009). This energy specifies the initiation of interfacial failure of fiber and matrix or matrix failure close to the opposite of the impacted face, hence, initiating fracture in the laminates. The trend observed for all the composites, as shown in Figure 4.13, was lowest for control, slightly high for 0.2 wt. % HMWCNTs-epoxy and highest for 0.4 wt. % HMWCNTs-epoxy composites. Thus, the composite laminates can absorb more energy than that of control samples, thanks to the higher tensile strength of the HMWCNTs.

4.4 Compression After Impact (CAI) Test

Compression after impact test is necessary to examine the damage propagation in laminates before total failure. The mean value of all three samples by the CAI test are shown in Table 4.8. The compression forces and compression strength were observed for 0.2 wt.% HMWCNTs and 0.4 wt. % HMWCNTs in 0 J, 15 J, and 25 J impact energy is higher than the control sample.

Table 4.8: CAI Experimental Force and Compressive Strength Values for all Specimens

Specimen code	Experiments force kN_0 J	Experiments force kN_15 J	Experiments force kN_25 J	Compressive strength MPa_0 J	Compressive strength MPa _15 J	Compressive strength MPa _25 J
CAI_C1	61.69	45.12	29.83	121.93	87.34	54.84
CAI_C2	64.31	43.17	32.30	127.10	85.23	65.13
CAI_C3	60.50	39.39	29.64	121.77	79.44	58.52
CAI_C4	57.50	49.87	28.36	115.84	400.57	57.19
Average	61.00	44.39	30.03	121.66	88.14	59.92
Standard Dev.	2.82	4.36	1.64	4.60	8.93	3.54
CAI_HM WCNT021	78.48	66.32	59.14	157.95	121.12	119.16
CAI_HM WCNT022	87.82	70.17	58.77	175.30	130.57	119.71
CAI_HM WCNT023	90.80	71.67	58.28	185.32	130.76	118.82
CAI_HM WCNT024	86.34	69.78	53.40	174.47	141.48	108.99
Average	85.86	69.48	57.40	173.26	131.07	116.69
Standard Dev.	5.26	2.25	2.68	11.33	8.47	5.14
CAI_HM WCNT041	91.18	82.92	69.44	485.71	168.55	141.15
CAI_HM WCNT042	100.00	82.58	68.92	199.80	165.01	132.15
CAI_HM WCNT043	100.00	82.61	70.74	199.60	161.65	130.35
CAI_HM WCNT044	103.10	84.40	68.57	205.79	161.99	131.22
Average	98.57	83.13	69.42	197.72	164.30	133.72
Standard Dev.	5.13	0.86	0.94	8.50	3.20	5.00

The compression versus displacement curve obtained after the impact test at three different energy levels 0 J, 15 J, and 25 J of all samples is shown in Figure 4.14. The curve shows the linear behavior of compression and displacement after the initial phase characterized by a small load applied. The curves show the same trend: an increase in displacement with the increase in compression force until maximum force value has reached, followed by compression force. The maximum force values were different for

different samples. The undamaged samples (Figure 4.14) had a higher maximum force value than damaged samples, implying that undamaged samples can withstand high impact energy. In the case of 25J, the increase in the 0.2% and 0.4% HMWCNT is not so significant because higher energy has already assisted the sample to nearly reach its stiffness limit of 0.2%.

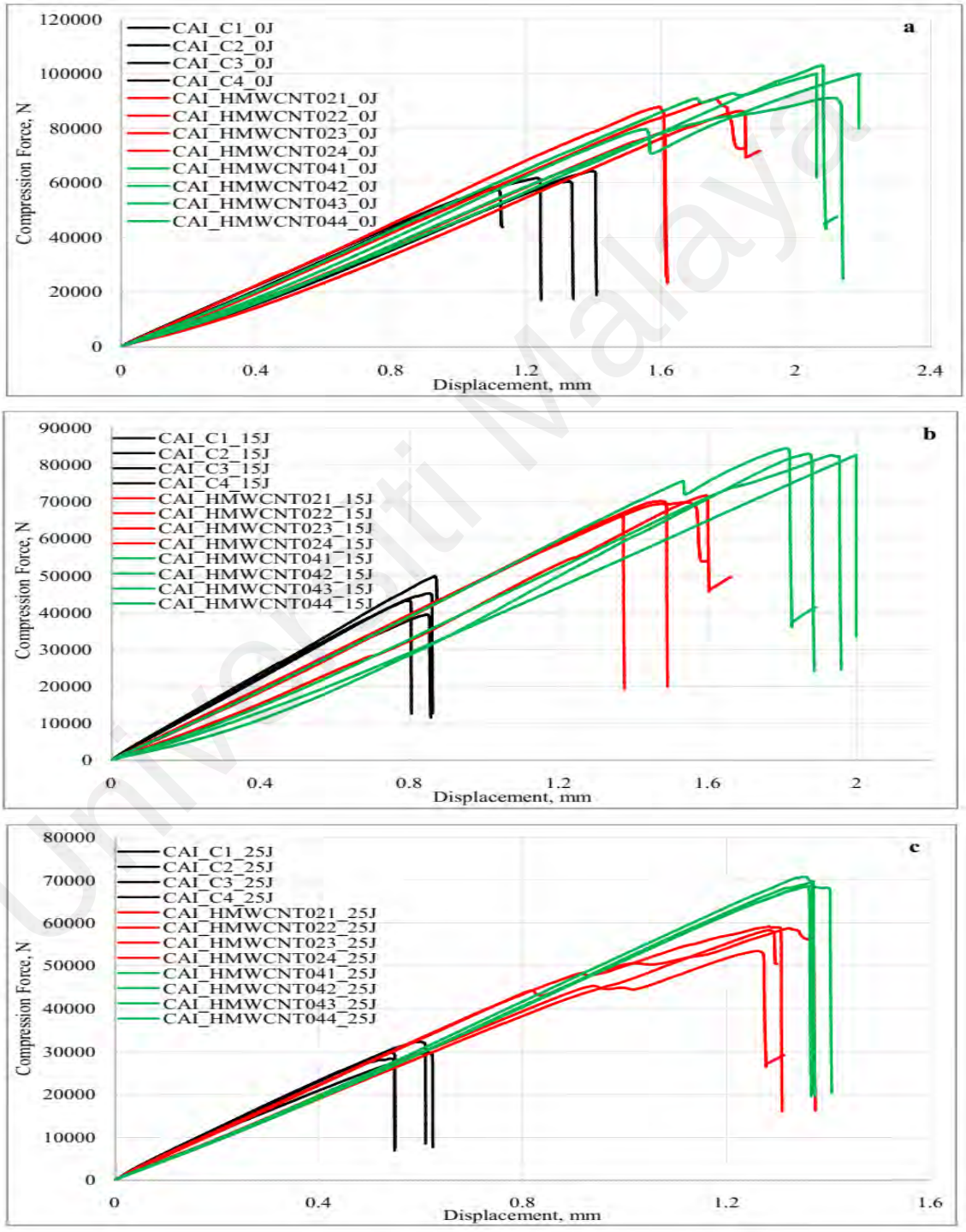

Figure 4.14: Compression Load versus Displacement Behaviour at: (a) 0 J, (b) 15 J and (c) 25 J

Based on the compression outcomes after impact testing (Table 4.8), it can be stated that the higher compressive values were observed on 0.4 wt. % HMWCNTs-epoxy laminates because of control shear cracking and structural delamination by the presence of the reinforcement (Sanchez-Saez et al., 2005). The compressive strength is the ability of the material to survive loads without elongation. The compression versus displacement curve for impacted and unimpacted samples obtained after the impact test at different energy levels 0 J, 15 J, and 25 J of all samples can be seen in Figure 4.14 (a-c). The curve shows the linear behavior of compression and displacement after the initial phase characterized by the low applied load. The curves were shown to have the same trend as displacement increase with increased impact energy; when the maximum force value has been achieved, the curve drops. Although the maximum force of 0.4 wt. % HMWCNTs-epoxy was the highest than 0.2 wt. % HMWCNTs-epoxy and control samples. Control samples had the lowest impact resistances than HMWCNTs-epoxy composite laminates.

The higher peak load of HMWCNTs-epoxy is due to the effective load transfer mechanism between fibers and matrices, as HMWCNTs offer a bridging effect. The sample deflection and peak load attaining time are directly related to composite laminates stiffness. Minimum displacement obtained for the control sample can be attributed to the fact that normally, high ductile material requires high time to reach peak load and deflect more under the same energy levels. In addition, HMWCNTs improve the stiffness of the composite, which tends to show smaller deflection amounts (Rahman et al., 2013, Rahman et al., 2012, Salam et al., 2013). When the maximum elastic limit for deformation crosses the impact energy level, the residual energies are now for plastic deformations. The polymer composites are typically brittle; hence, plastic deformations do not occur under loading conditions. Thus, the excess energy is dissipated by damage mechanisms like indentations on top surfaces, shear fractures in laminate, matrix failures, fiber

breakage, interfacial failure of laminates, and penetration through the laminate (Kostopoulos et al., 2010).

4.5 Electrical Conductivity

The volume resistivity of the control, 0.2 wt. % HMWCNTs-epoxy and 0.4 wt. % HMWCNTs are shown in Figure 4.15. Volume resistivity observed around 7.94 Ω.cm, 5.78 Ω.cm for control and 0.2 wt. % HMWCNTs-epoxy respectively and 2.01 Ω.cm for 0.4 wt.% HMWCNTs-epoxy specimens. The lowest resistivity among all the laminates was observed for 0.4 wt. % HMWCNTs-epoxy because of more conductive of HMWCNTs amount in an insulating matrix, when resistivity is low, conductivity is high . The difference in electrical conductivity of composites laminates was due to the different HMWCNTs.

Moreover, during the fabrication method, HMWCNTs could be broken into smaller tubes, resulting in little porosity of bucky papers and causing higher HMWCNTs concentration that implies conductivity improvement. HMWCNTs provide a conductive phase in the composite polymeric matrix and add high aspect ratios that encourage conduction at lower loadings than spherical or irregularly shaped fillers.

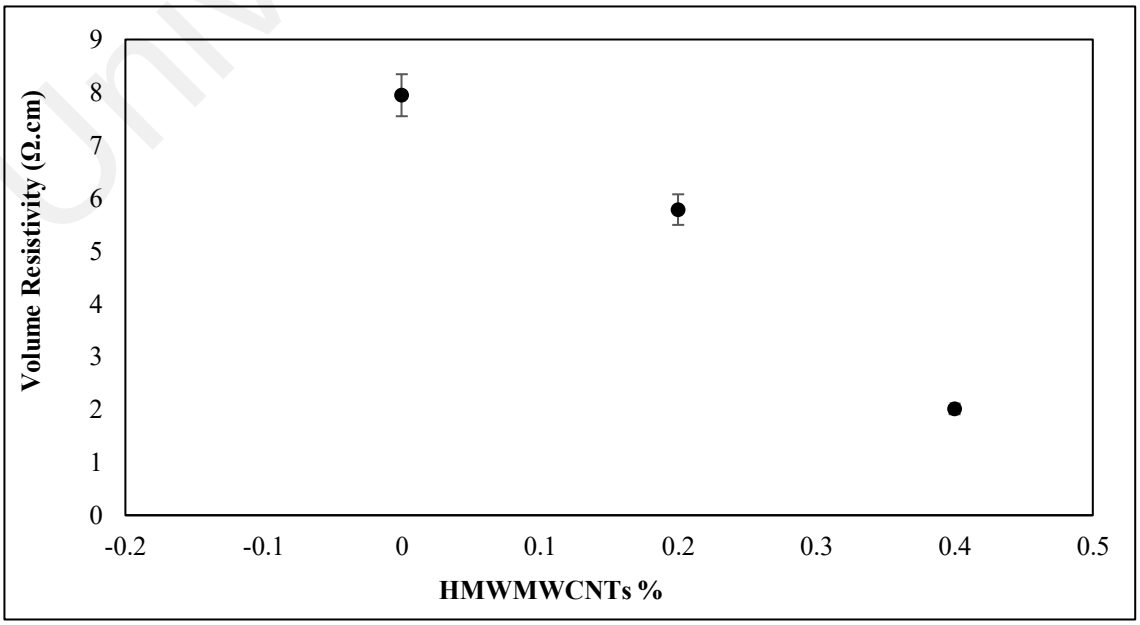

Figure 4.15: Volume Resistivity of Samples

4.6 Thermal Stability

4.6.1 Thermogravimetric Analysis (TGA)

TGA analysis was carried out on the control sample, 0.2 wt. % HMWCNTs-epoxy and 0.4 wt. % HMWCNTs-epoxy as shown in Figure 4.16. Samples showed an initial mass loss, notwithstanding a minor difference related to the greatest degradation temperatures of this initial mass loss curve. Such an increase in temperature from the control sample (321.4 °C) with the addition of HMWCNTs, led to 325.5 °C (0.2 wt. % HMWCNTs-epoxy) and 327.5 °C (0.4 wt. % HMWCNTs-epoxy).

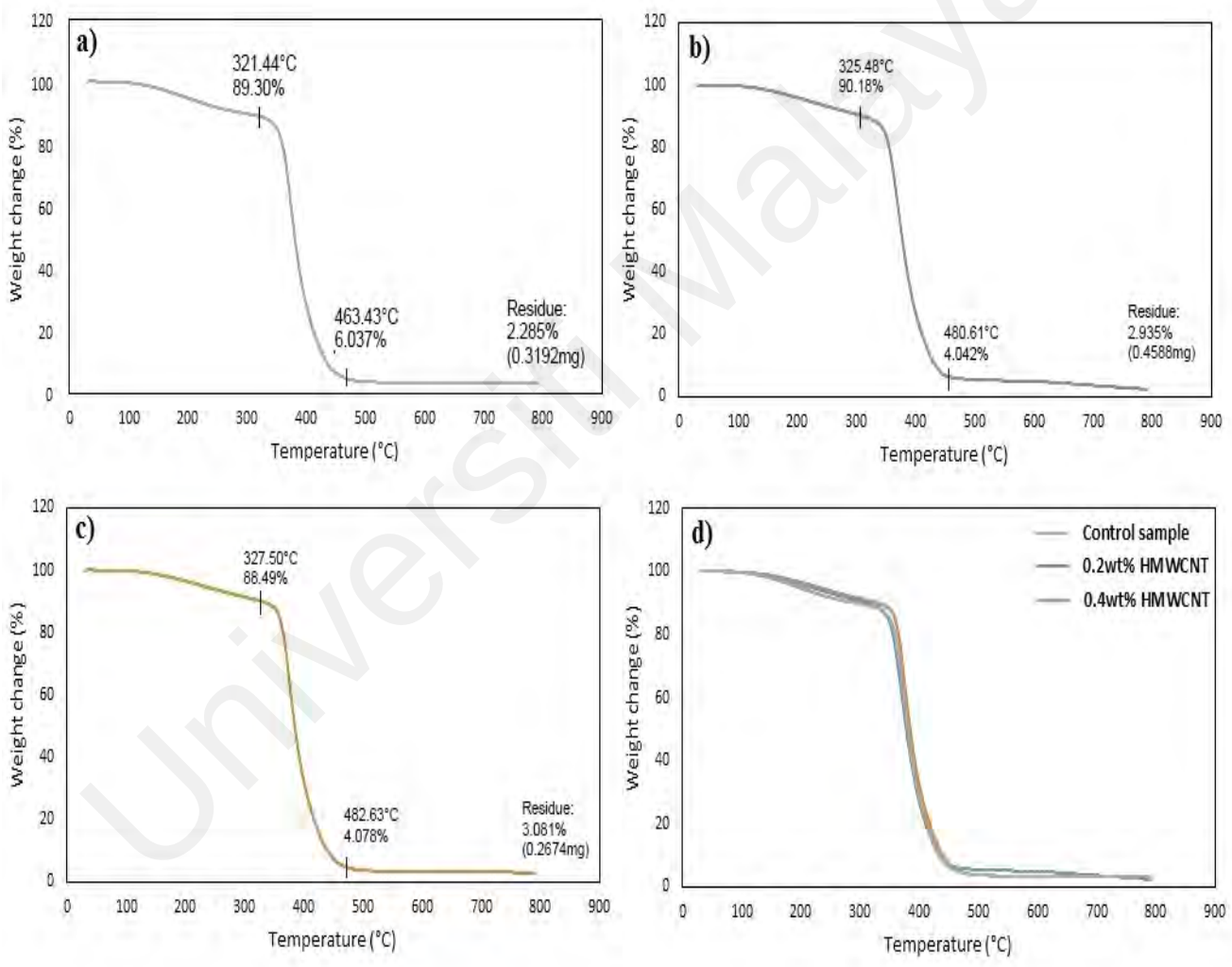

Figure 4.16: Thermogravimetric Analysis of (a) Control, (b) 0.2 wt. % HMWCNTs-epoxy, (c) 0.4 wt. % HMWCNTs-epoxy Samples and (d) Comparison of all Graphs

This event was attributed to moisture elimination in the secondary alcoholic group upon dehydration of epoxy materials, which results in an unsaturated structure. This

unsaturation process forms weak aliphatic C–O bonds and C–N bonds (Noël et al., 1988; Wu et al., 2002; Zhou et al., 2020). Then, at temperatures above 300 °C, the second degradation phase occurs, 321 – 463 °C for control, 325 – 481 °C for 0.2 wt. % HMWCNTs-epoxy and 327 – 483 °C for 0.4 wt. % HMWCNTs-epoxy samples. This second mass loss is associated with aromatic epoxy decompositions (Noël et al., 1988; Wu et al., 2002; Zhou et al., 2020). Degradation of laminates is the last phase that occurred at the end of the aromatic degradation stage, at 463 °C for the control sample (residual mass of 2.29 wt. %), at 481 °C for 0.2 wt. % HMWCNTs-epoxy (residual mass of 2.94 wt. %) and at 483 °C for 0.4 wt. % HMWCNTs-epoxy (residual mass of 3.09 wt.%). Regarding HMWCNTs, the residual mass is due to the metal catalyst particles from the synthesis method (Mansfield et al., 2010). The residual mass increases with HMWCNTs content in the samples as more catalyst particles are added. The stability in samples is highly affected by the HMWCNTs content, as the increase in degradation temperature in all the stages confirmed that fact. This could be explained by the strong bond between epoxy and HMWCNTs can delay small molecules diffusion from the resin matrix at higher temperatures, leading to improved thermal stability (Zhou et al., 2007). Some studies have shown a decrease in decomposition temperature in epoxy composites with increasing HMWCNTs-to-resin ratio (Ciecierska et al., 2013; Loos et al., 2008; Zhou et al., 2007) because of the better thermal conductivity of the composites by adding HMWCNTs. In Figure 4.16, this effect has not been observed for the specimens and implies that adding HMWCNTs, in this case, does not negatively affect thermal stability but rather exerts the opposite effect. TGA carried out in oxidizing conditions resulted in decomposition at around 650°C of most carbon-based materials (Mahajan et al., 2013; Noël et al., 21988; Liu et al., 2012). The 0.4 wt. % HMWCNTs-epoxy laminates degraded 3°C later than that of 0.2 wt. % HMWCNTs-epoxy composite. This is due to the strong

bond between epoxy and HMWCNTs that delayed the molecular diffusions from the resin matrix at higher temperatures and resulted in better thermal stability.

The derivative curves of the TGA (dW%/dT) analysis of the samples are illustrated in Figure 4.17. At temperatures higher than 300°C, a very well-defined degradation peak was observed in all the samples, which indicates the main degradative temperature of every sample: control sample structural disruption occurs at 375°C, followed by 0.2 wt. % HMWCNTs-epoxy (379°C) and 0.4 wt. % HMWCNTs-epoxy (383°C). This showed

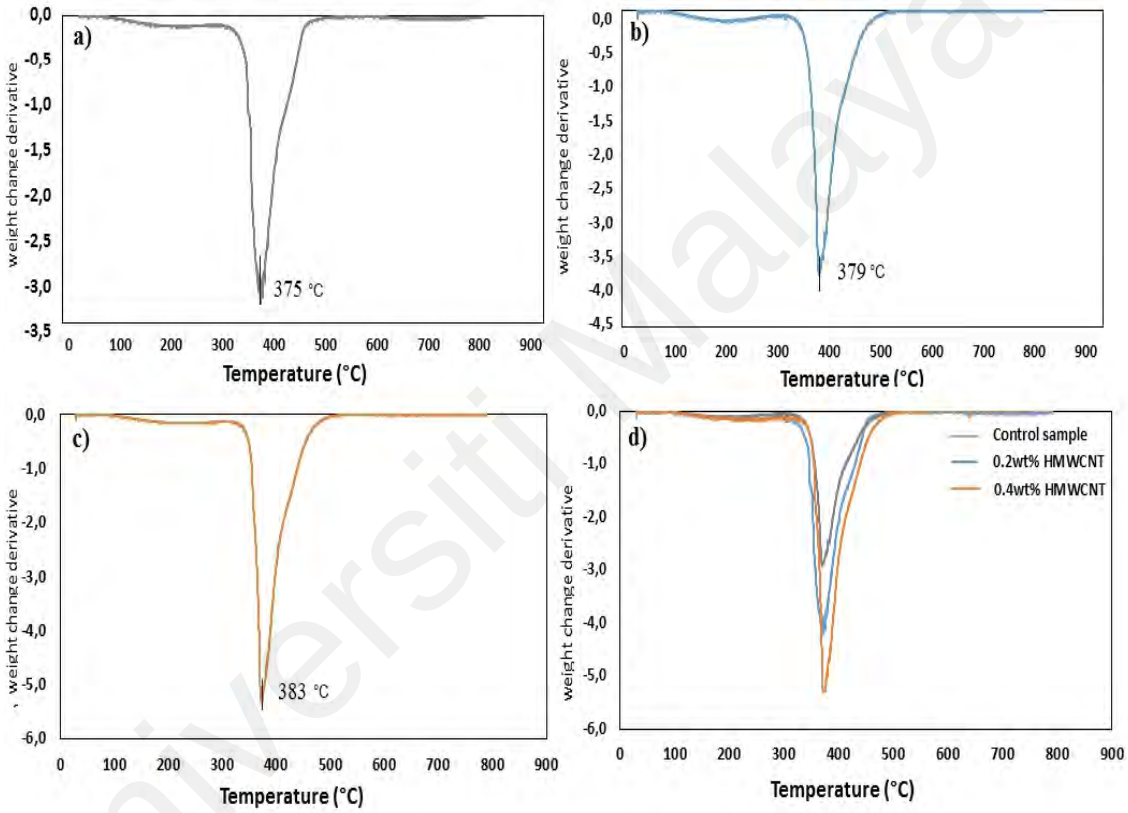

Figure 4.17: Derivative Curves Calculated from the Thermal Gravimetric Analysis Profiles of (a) Control, (b) 0.2 wt. % HMWCNTs-epoxy, (c) 0.4 wt. % HMWCNTs-epoxy Samples and (d) Comparison of all Graphs

4.6.2 Differential Scanning Calorimetry (DSC)

The DSC analysis was done on the control sample, 0.2 wt. % HMWCNTs-epoxy and 0.4 wt. % HMWCNTs-epoxy composite laminates. The phase transition dynamics were analyzed in the control sample and then compared with the other samples, as shown in Figure 4.18. The heat flow curves show a steep endothermic deviation at the start of the

experiment's temperatures. It is related to the initial mass loss events occurring from 50 to 300°C in all the specimens (Figure 4.16).

Differential calorimetric analysis showed that upon HMWCNTs addition, *Tg* has shifted to a higher temperature, as shown in Figure 4.18. The heat flow curves show a steep endothermic deviation at the start of the experiment's temperatures. It is related to the initial mass loss events occurring from 50 to 300°C in all the specimens (Figure 4.16). At lower temperatures, the cause of loss of heat is related to the compounds evaporating

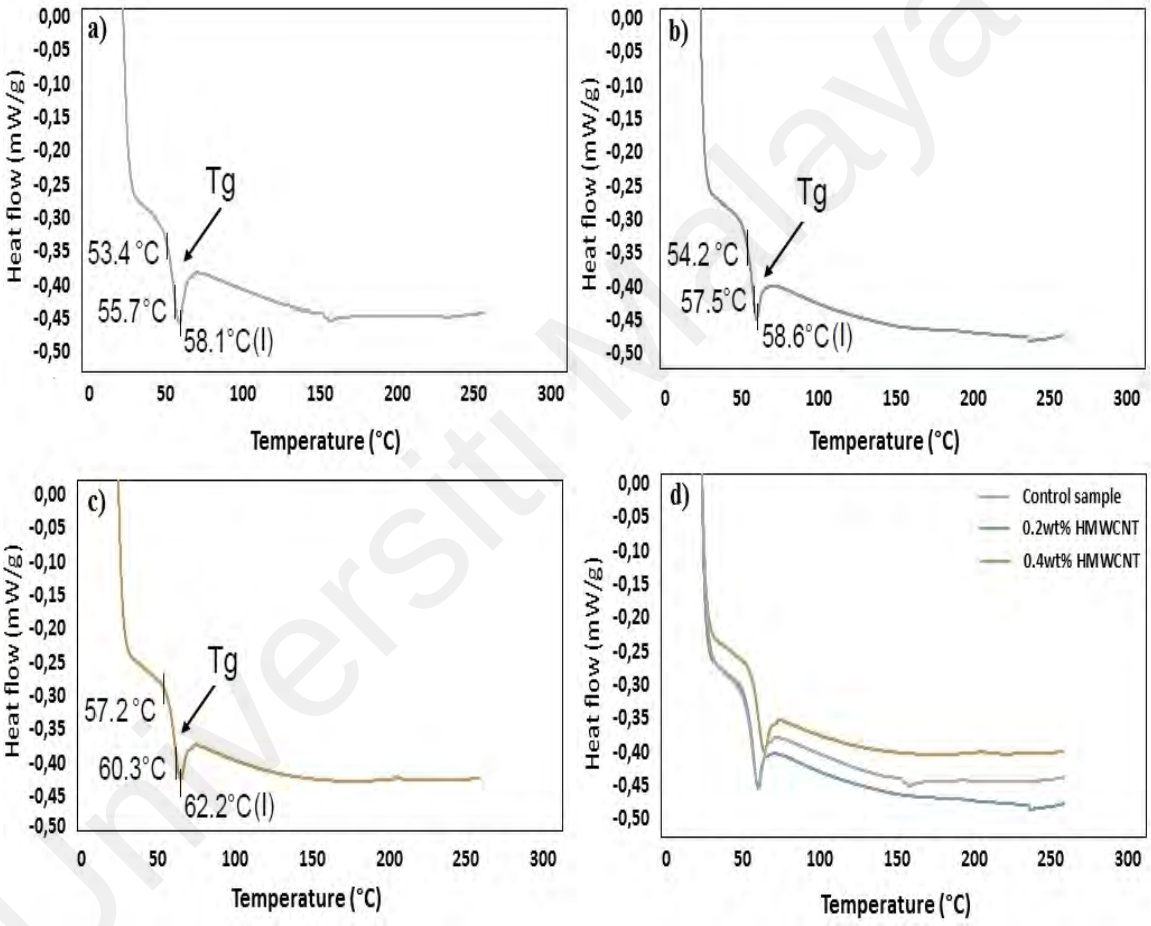

Figure 4.18: Differential Scanning Calorimetric Analysis of (a) Control, (b) 0.2 wt. % HMWCNTs-epoxy, (c) 0.4 wt. % HMWCNTs-epoxy Composite and (d) Comparison of all Graphs

The endothermic peak shown in the curves indicates the glass transition events. Since one did not observe in TGA curves, these endothermic peaks are not associated with mass loss but rather with the glass transition temperatures (*Tg*). The *Tg* was identified as 55.7 °C for the control sample and 57.5 °C for 0.2 wt. % HMWCNTs-epoxy and 60.3 °C for

0.4 wt. % HMWCNTs-epoxy composite. This resulted in the Tg peak has shifted towards higher temperature by adding a certain mass of HMWCNTs. This current observation is supported by the reports concerning pure epoxy resins and their composite materials (Allaoui et al., 2009; Ciecierska et al. 2013; Loos et al. 2008; Maljaee et al. 2017). The change in the composite composition affects this temperature and by the factors like temperature, time, heat load, and degree of orientation (Startsev et al. 2020; Michels et al., 2015).

The addition of HMWCNTs with amino groups resulted in higher glass transition temperature. The reason can be the reaction between amino groups located on the surface of HMWCNTs and epoxide groups from epoxy resin. The high specific surface area of HMWCNTs can also affect the matrix properties. Therefore, the probable reason for significant changes in composite laminates' mechanical and thermal properties is the high surface area of HMWCNTs and interaction between carbon nanotubes and polymer macromolecules (Ciecierska et al., 2013).

4.7 FESEM Characterization of HMWCNTs and Polymer Composite

FESEM micrographs of HMWCNTs from powder are shown in Figure 4.19. The diameter of the nanotubes is in the range of 5-10 nm and could belong up to 100's of a micron.

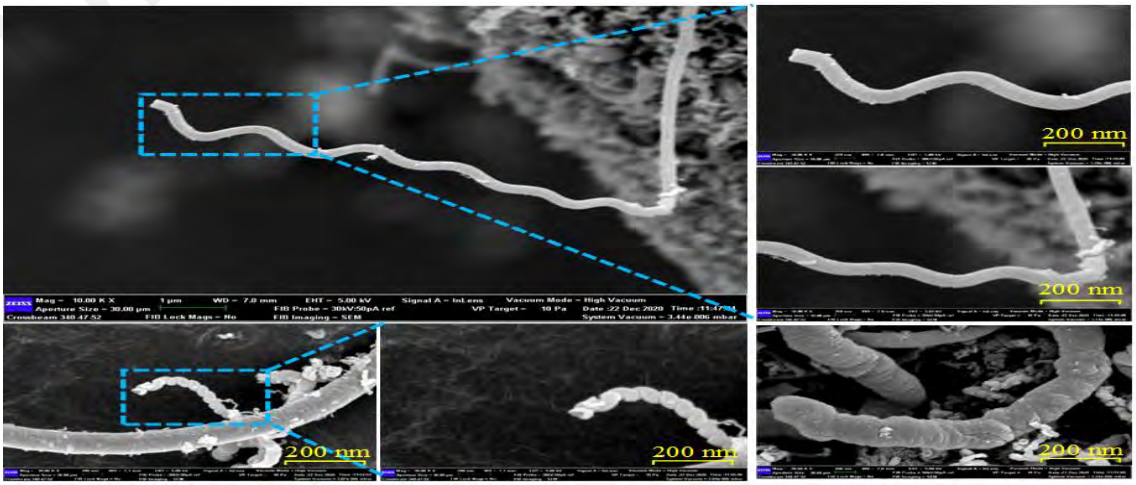

Figure 4.19: Micrographs of HMWCNTs from Powder

FESEM images of the fractured surface after DCB and ENF tests were taken at different magnifications and shown in Figure 4.20 for the control sample, which exhibits good dispersion of carbon fiber in laminated epoxy, dispersed epoxy over CF, and broken

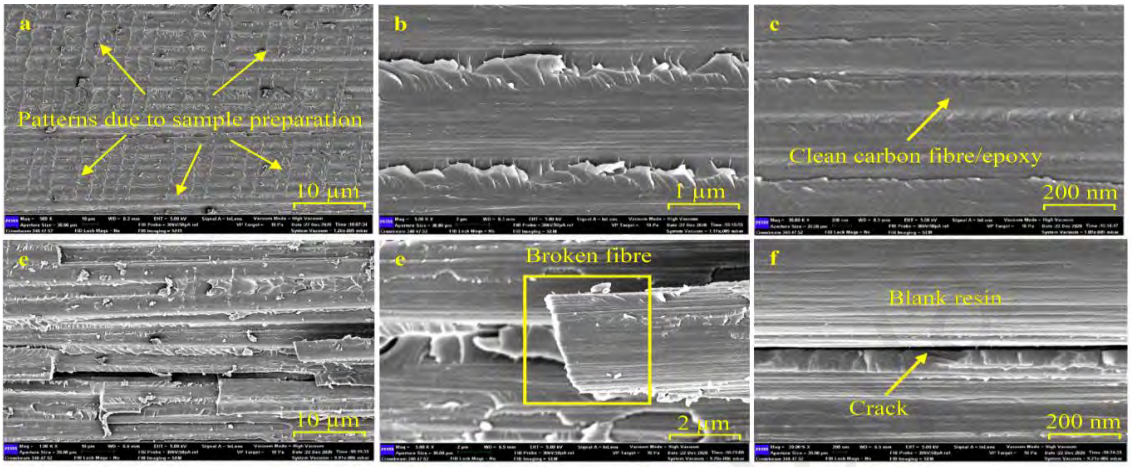

Figure 4.20: FESEM Images of Fracture Surface for Control Sample

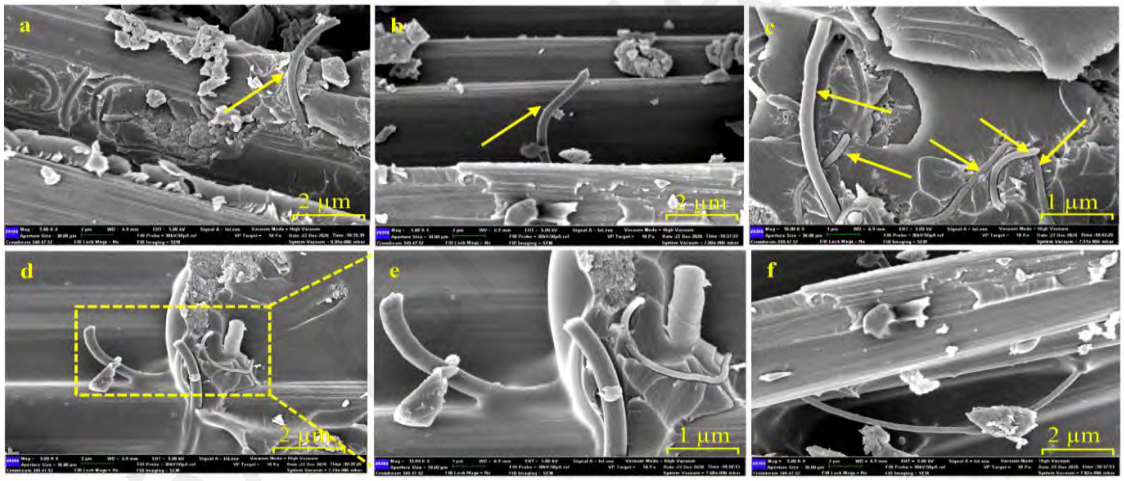

Figure 4.21: (a-b) Elongated HMWCNTs, (c-e) Good Dispersion of HMWCNTs in Epoxy, (f) Single Strand of HMWCNTs Visible in Image after DCB Tests

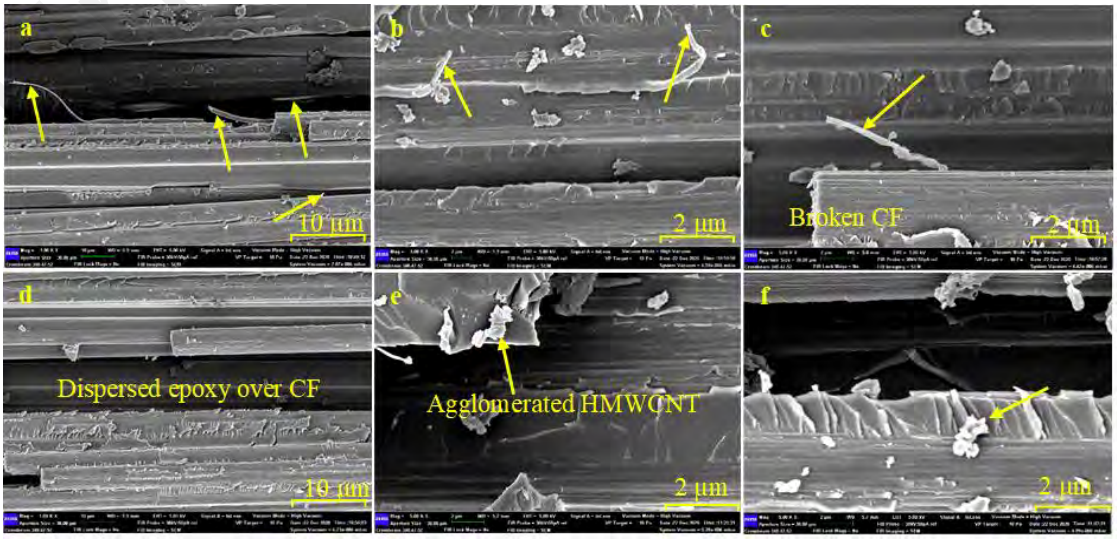

Figure 4.22: (a-c) Good Dispersion of HMWCNTs, (d) Dispersed Epoxy Over CF, (e-f) Agglomerated HMWCNTs after ENF Tests

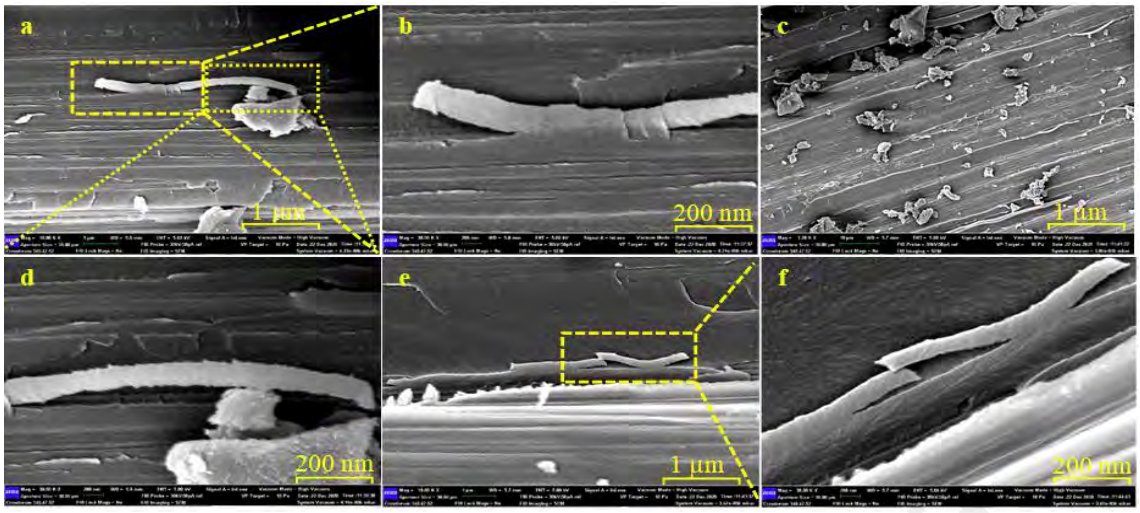

Figure 4.23: (a-b, d) Image of CF-E Matrix with HMWCNTs Dispersed in Epoxy, (c) CF-E Matrix, (e-f) Two Overlapping HMWCNTs after Compression Tests

The fractography of the samples is shown in Figure 4.19-4.23, together with micrographs of HMWCNTs in Figure 4.19. In Figure 4.20, the micrograph of the control sample shows a smooth and featureless appearance. Furthermore, the carbon fibers in control samples are completely free of any retained matrix, showing that failure occurred along with the interface of fiber and matrix, which resulted in a relatively lower fracture toughness value. Figure 4.21 shows some roughness of a higher degree, which indicates matrix polymer deformation. It can also be seen that within the matrix, some cohesive failure has occurred, and therefore high interlaminar fracture toughness value has been observed. Figure 4.22 exhibits good dispersion of HMWCNTs in epoxy and aggregation of HMWCNTs due to dispersion technique. Figure 4.23 shows the fractured surface of HMWCNTs-epoxy composite laminates, and the broken CFs and HMWCNTs are attached to the fibers that have been pulled out from the matrix (Figure 4.23d-e). Therefore, higher interlaminar fracture toughness has resulted compared to the control sample.

Furthermore, it can be seen that by adding the number of HMWCNTs in the composites, the composite's strength increases, which results in higher surface roughness. This confirms the embedment of HMWCNTs in the epoxy matrix because the crack

interface is in areas of relatively smoother surfaces. Moreover, there was evidence of fewer HMWCNTs agglomerates over the fracture surface due to optimum dispersion in the dispersion process. The bridging of HMWCNTs and pulling-out at fractured zones of the carbon fiber-epoxy composite laminates can be seen in the figures (Figure 20-23). Due to bridging mechanisms and better compatibility of CF-epoxy matrix and HMWCNTs, the composite laminates have considerably better interlaminar fracture toughness.

4.8 Ultrasonic C-Scan

Figure 4.24 shows the C-scan images of all the samples impacted at an energy level of 15 J and 25 J. In Figure 4.24, the blue-white area represents the damaged area where the projectile hit. The white area exhibits the breakage and delamination of the laminates that occurred at almost all the interfaces through the thickness of the samples. The blue area represents the splitting and delamination of the back-face rather than internal damages. The other colors represent some possible additional damages. It is worth mentioning that area with smaller diameters is observed for all the samples of 15 J, whereas no damage or minor damage can be seen for the case of 0.4 wt. % HMWCNTs-epoxy laminates.

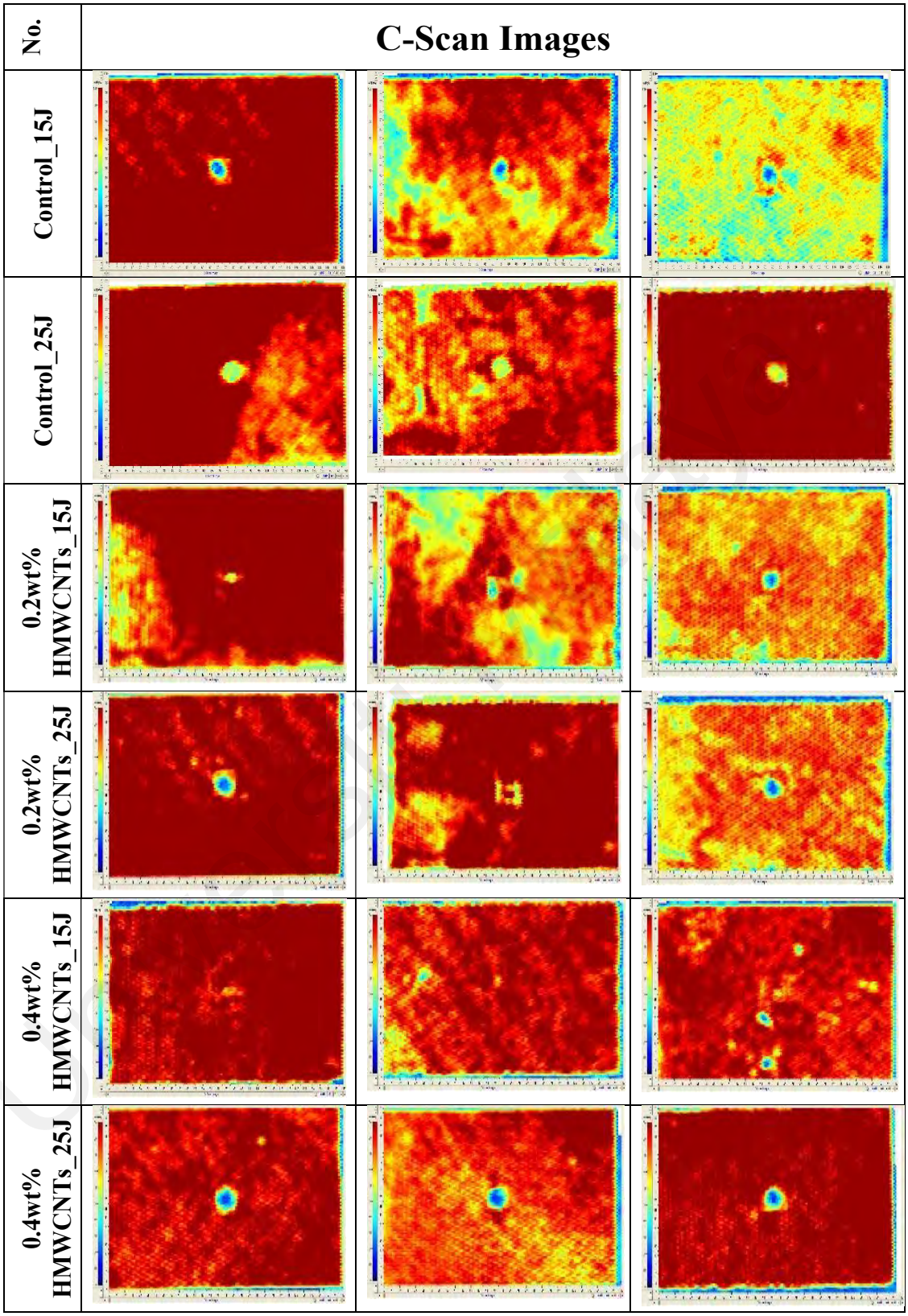

Figure 4.24: C-scan Images of all the Samples Impacted at Energy level of 15 J and 25 J; Blue-White Section Represents Damage Area Hit by a Projectile, the White Area Exhibits Delamination of the Laminates, Blue Area Represents Splitting and Delamination of the Back-Face

Damaged Area

The damaged areas obtained from the tower drop weight for different samples at the energy level of 15 J and 25 J are given in Table 4.9 and Table 4.10, respectively. The maximum damaged area was observed on the control sample, whereas the least damaged area was observed for 0.4 wt. % HMWCNTs-epoxy composite as shown in Figure 4.25.

Table 4.9: Impacted Area of the Samples as Evaluated by C-Scan and the % Decrement Compared to Control Sample for 15 J

Samples No.	Control (15 J)	0.2 wt. % HMWCNTs (15 J)	% Decrease	0.4 wt. % HMWCNTs (15 J)	% Decrease
1	35.92 mm^2	24.01 mm^2	33.15	23.32 mm^2	35.07
2	43.2 mm^2	28.94 mm^2	33.00	4.44 mm^2	89.07
3	50.94 mm^2	29.78 mm^2	41.53	11.86 mm^2	76.71
Average	43.35 mm^2	27.57 mm^2	35.89	13.20 mm^2	66.95

Table 4.10: Impacted Area of the Samples as Evaluated by C-Scan and the % Decrement Compared to Control Sample for 25 J

Samples No.	Control (25 J)	0.2 wt. % HMWCNTs (25 J)	% Decrease	0.4 wt. % HMWCNTs (25 J)	% Decrease
1	110.4 mm^2	58.41 mm^2	47.09	56.88 mm^2	48.47
2	91.92 mm^2	64.11 mm^2	30.25	53.86 mm^2	41.40
3	78.75 mm^2	62.63 mm^2	20.46	49.98 mm^2	36.53
Average	93.69 mm^2	61.71 mm^2	32.6	53.57 mm^2	42.13

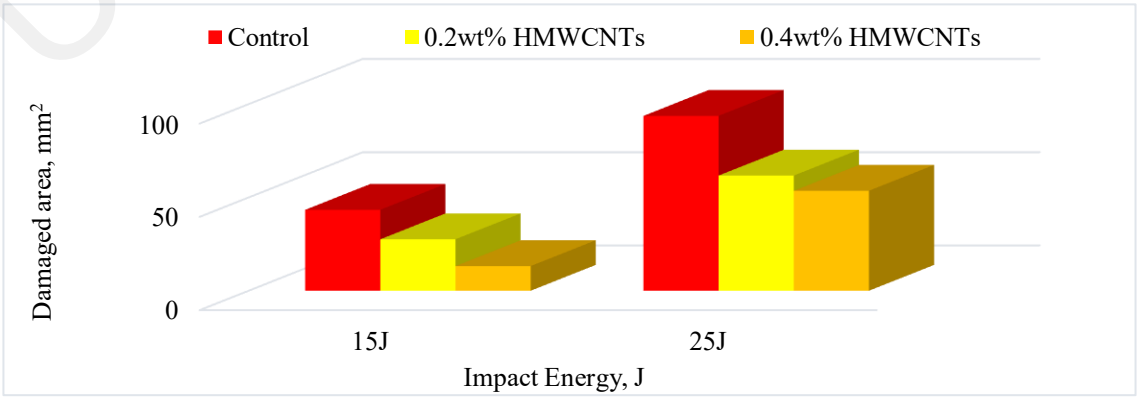

Figure 4.25: Damaged Area from Specimens Tested with Impact Energies 15 J and 25 J

The control sample has the highest damages area, as expected, while the 0.2 wt. % HMWCNTs-epoxy has a relatively less damaged area, and the least damaged area was observed for 0.4 wt. % HMWCNTs-epoxy composite. At lower level 15 J, the lower peak load can be attributed to the fact that composites were not fully capable. However, at the higher energy level of 25 J, the laminates carried the highest load they could have attained, and the damaged area observed was higher than the observed at 15 J (Mahdi et al., 2013). This is because higher fracture energy is required for the imitation of delamination. The impact in the matrix and crack first caused damage generated by tensile or shear stress in the middle or back-wall layers, then delamination grows from the crack tips between layers. After the high energy impact, the damaged area was grown, and the initiated cracks in the back-wall layers were developed until the front-face layers because of significant delamination. It is evident from Figure 4.11 that peak load increased with the increase in impact energy when the impact energy level increased from 15 J to 25 J. Therefore, in Table 4.8 and Figure 4.13, the lower absorbed energy at 15 J indicates that composites structures had not undergone their full capacity. Higher energy values were obtained in all samples when subjected to a higher load.

4.9 Analytical Modeling of Mechanical Properties

An analytical modeling approach has been proposed to investigate the trend of change in mechanical properties with respect to HMWCNTs content. In addition, data from literature was also included with due references for comparison purpose. As there was no data available in literature on HMWCNTs-epoxy composite, thus, data on CNTs-epoxy composite was included for comparison. The analytical modeling was carried out with second order polynomial fit together with root mean square values, which represent the goodness of the fit as presented hereafter.

Figure 4.26 shows the fitting of interlaminar fracture toughness G_{IC} (kJ/m^2) for propagation on HMWCNTs/epoxy composite. The respective equations for fitting are given in equations 4.1-4.5.

For OBT:

$$y = -0.035x^2 + 0.753x + 0.3587 \text{ with } R^2 = 1 \quad \text{Eq. (4.1)}$$

For MCC:

$$y = 1.5046x^2 + 0.1957x + 0.2894 \text{ with } R^2 = 1 \quad \text{Eq. (4.2)}$$

For CCM:

$$y = 1.9162x^2 + 0.0583x + 0.274 \text{ with } R^2 = 1 \quad \text{Eq. (4.3)}$$

For MBT:

$$y = 1.1913x^2 + 0.2683x + 0.2591 \text{ with } R^2 = 1 \quad \text{Eq. (4.4)}$$

From literature data (Karapappas et al., 2009):

$$y = 1.05x^2 - 0.305x + 0.3 \text{ with } R^2 = 1 \quad \text{Eq. (4.5)}$$

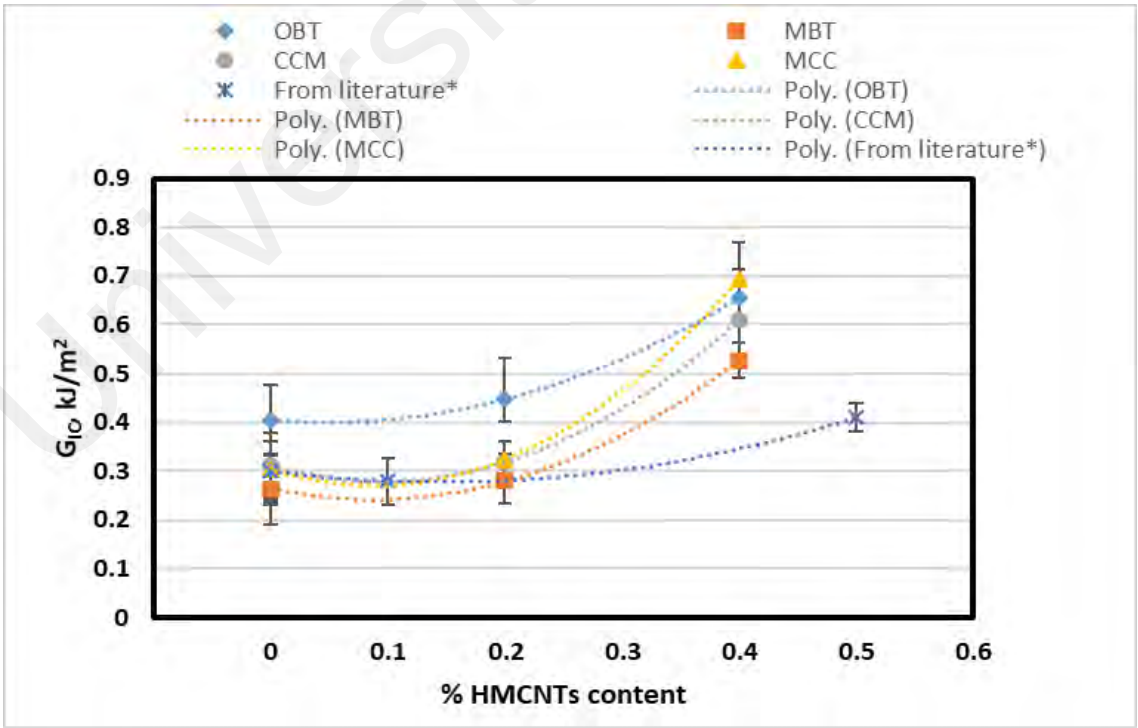

Figure 4.26: Fitting of Interlaminar Fracture Toughness G_{IC} (kJ/m^2) for Propagation with Respect to HMWCNTs Content for (OBT, MBT, CCM & MCC)

The general tread is that, there is an increment of G_{IC} values with the increase of HMWCNTs content on the epoxy matrix. The findings of present work is also supported by the data reported in literature, as data from literature was also plotted in Figure 4.26 and exhibits the similar tread. The goodness of the fitting can also be seen in equations 4.1-4.5, as the root mean square value is 1. Similarly, the fitting of interlaminar fracture toughness G_{IC} (kJ/m^2) for initiation on HMWCNTs/epoxy composite is shown in Figure 4.27 with respective equations for fitting are given in equations 4.6-4.10. The similar tread was observed, that is, the mechanical properties increase with the increase of HMWCNTs content.

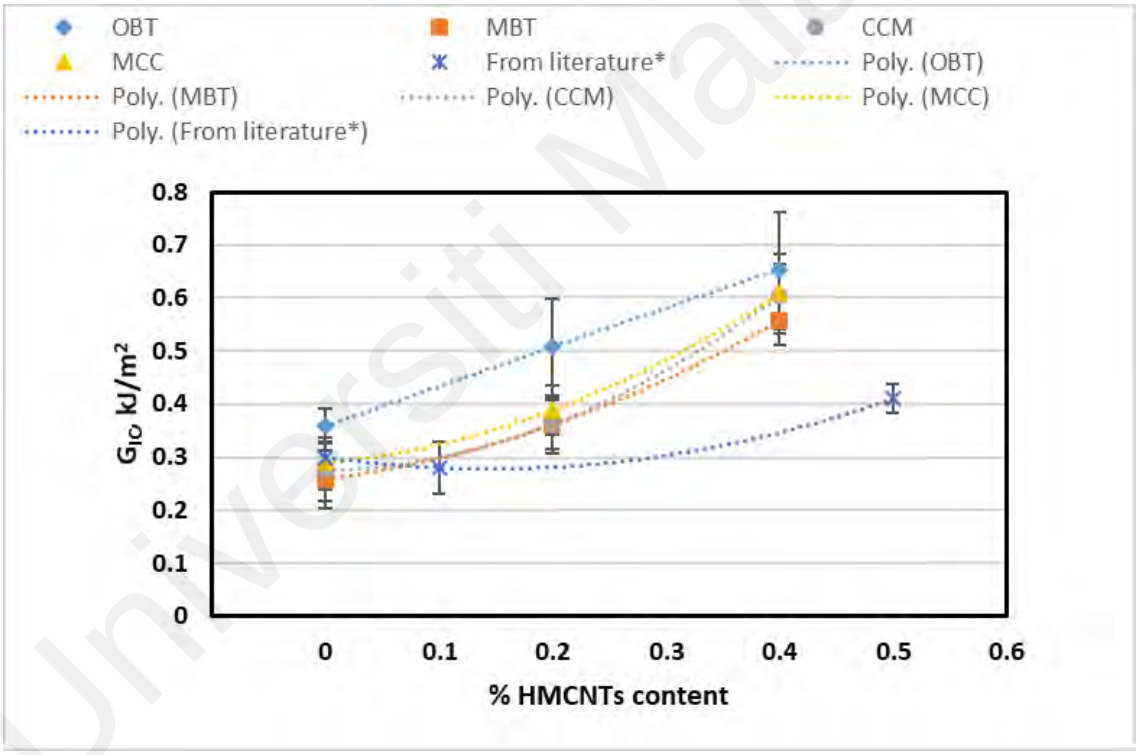

Figure 4.27: Fitting of Interlaminar Fracture Toughness G_{IC} (kJ/m^2) for Initiation with Respect to HMWCNTs Content for (OBT, MBT, CCM & MCC)

For OBT:

$$y = 2.0738x^2 - 0.2057x + 0.4059 \text{ with } R^2 = 1 \qquad \text{Eq. (4.6)}$$

For MCC:

$$y = 4.3595x^2 - 0.7714x + 0.3044 \text{ with } R^2 = 1 \qquad \text{Eq. (4.7)}$$

For CCM:

$$y = 3.555x^2 - 0.676x + 0.3113 \text{ with } R^2 = 1 \quad \text{Eq. (4.8)}$$

For MBT:

$$y = 2.92x^2 - 0.5105x + 0.2644 \text{ with } R^2 = 1 \quad \text{Eq. (4.9)}$$

From literature data (Karapappas et al., 2009):

$$y = 1.05x^2 - 0.305x + 0.3 \text{ with } R^2 = 1 \quad \text{Eq. (4.10)}$$

The fitting of interlaminar fracture toughness G_{IIC} (kJ/m^2) on HMWCNTs/epoxy composite is shown in Figure 4.28 with respective equations for fitting are given in equations 4.11 & 4.12. The similar tread was observed, that is, the mechanical properties increase with the increase of HMWCNTs content.

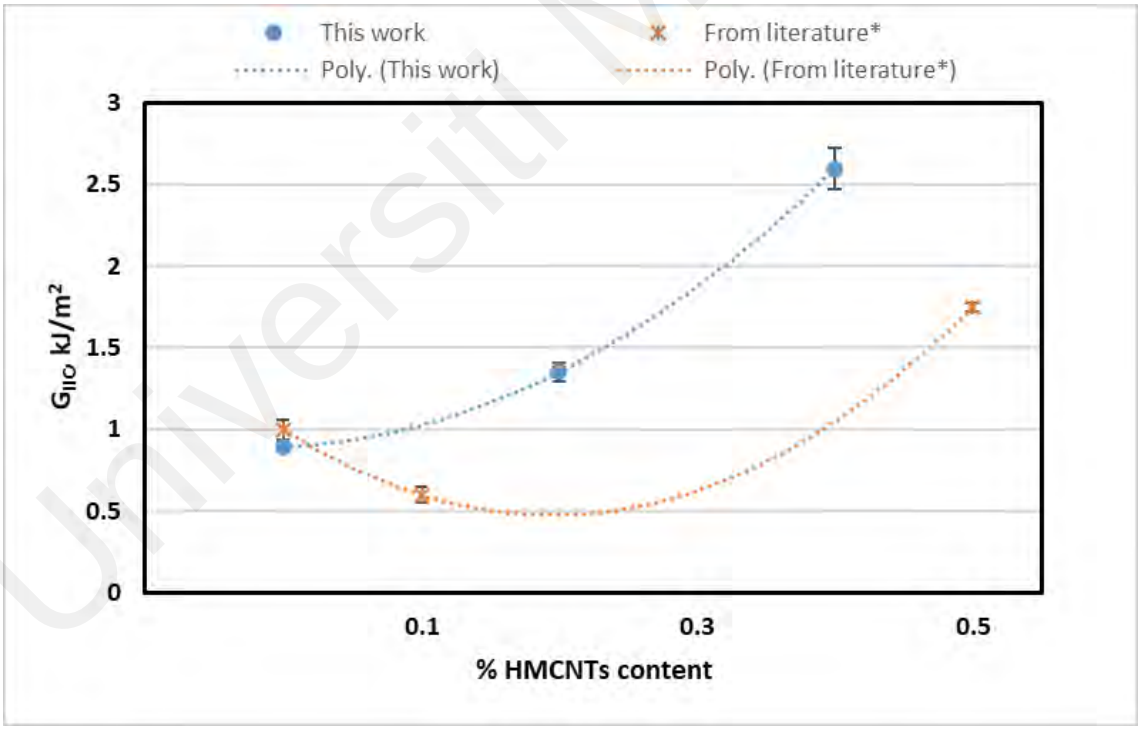

Figure 4.28: Fitting of Interlaminar Fracture Toughness G_{IIC} (kJ/m^2) with Respect to HMWCNTs Content

For this work:

$$y = 9.8812x^2 + 0.3038x + 0.8961 \text{ with } R^2 = 1 \quad \text{Eq. (4.11)}$$

From literature data (Gojny et al., 2005):

$$y = 13.75x^2 - 5.375x + 1 \text{ with } R^2 = 1 \qquad \text{Eq. (4.12)}$$

It is interesting to note that, the mechanical properties of epoxy composites investigated in the present study exhibits higher values compared to those as reported in literature. The reason behind that, in the present work HMWCNTs was used as reinforcing element compared to normal CNTs on the samples reported in literature. This demonstrate the superiority of HMWCNTs as reinforcing element in epoxy composite than that of normal CNTs.

The fitting of incipient energy on HMWCNTs/epoxy composite is shown in Figure 4.29 with respective equations for fitting are given in equations 4.13-4.15. The absorbed energy by the composite increase with the increase of HMWCNTs loading. Withstanding that, the fitting of the graphs exhibits the similar tread as supported by the literature data.

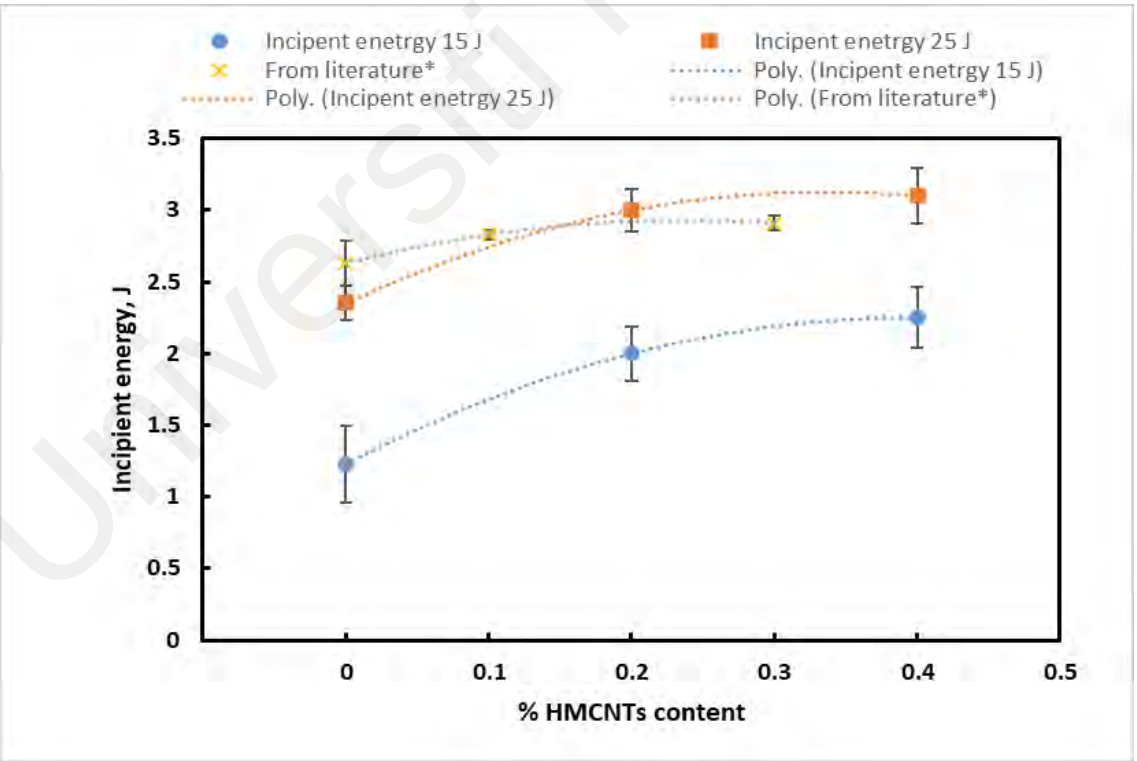

Figure 4.29: Fitting of Incipient Energy with Respect to HMWCNTs Content

Incipient energy at 15 J:

$$y = -6.5x2 + 5.15x + 1.23 \text{ with } R^2 = 1 \qquad \text{Eq. (4.13)}$$

Incipient energy at 25 J:

$$y = -6.875x^2 + 4.625x + 2.35 \text{ with } R^2 = 1 \quad \text{Eq. (4.14)}$$

From literature data (Mahdi et al., 2017):

$$y = -5.3333x^2 + 2.5333x + 2.63 \text{ with } R^2 = 1 \quad \text{Eq. (4.15)}$$

4.10 Results Summary

On attaining critical values, DCB test results showed a decrease in load to around ~50 N for control ~70 N for 0.2 wt. % HMWCNTs-epoxy and ~105 N for 0.4 wt. % HMWCNTs-epoxy at a 4-6 mm displacement due to delamination and crack propagation initiation. All the tests showed an unstable growth of delamination at the start.

For ENF test results, fracture toughness G_{IIC} increased with incorporating HMWCNTs in comparison with control specimen. The average interlaminar fracture toughness observed for control samples was 0.887 kJ/m^2 for 0.2 wt. % HMWCNTs-epoxy was 1.352 kJ/m^2 while the maximum for 0.4 wt. % HMWCNTs-epoxy was noticed 2.611 kJ/m^2.

LVI results showed that the peak load of the control sample was lowest than both laminates composites. As expected, the trend observed for all the composites was lowest for control, slightly high for 0.2 wt. % HMWCNTs-epoxy and highest for 0.4 wt. % HMWCNTs-epoxy composite.

The CAI results showed that the compression forces and compression strength were observed for 0.2 wt. % HMWCNTs-epoxy and 0.4 wt. % HMWCNTs-epoxy can withstand higher load without being elongated, and therefore, this composite has the highest impact resistance. On the other hand, the control sample had the lowest impact resistances than the composite laminates.

The volume resistivity of the control sample was around 7.94 Ω.cm, 5.78 Ω.cm for 0.2 wt. % HMWCNTs-epoxy and 2.01 Ω.cm for 0.4 wt. % HMWCNTs-epoxy composites.

The 0.4 wt. % HMWCNTs showed the lowest resistivity among all the laminates due to increased conductive fillers HMWCNTs an insulating matrix.

Thermogravimetric analysis of composite laminates showed that 0.4 wt. % HMWCNTs-epoxy laminates degraded 3 °C later than 0.2 wt. % HMWCNTs-epoxy shows the somewhat strong bond between epoxy and HMWCNTs that can delay molecular diffusion from resin matrix at higher temperature and result in enhanced thermal stability (Ali et al., 2021).

Differential calorimetric analysis showed that upon HMWCNTs addition, *Tg* shifts to a higher temperature. The addition of HMWCNTs with amino groups resulted in higher glass transition temperature.

From the morphology analysis of fractured surfaces by FESEM, it is clear that upon increasing the number of HMWCNTs in the composite laminate, the composites' tensile strength improves, leading to higher surface roughness. This confirms the embedment of HMWCNTs in the epoxy matrix as the crack interface predominantly in areas of a relatively smoother surface. Furthermore, the evidence of fewer HMWCNTs agglomerates over the fracture surface was observed because of the optimal dispersion over the prepreg during the dispersion process.

C-scan images showed the damaged areas of all the samples at both energy levels of 15 J and 25 J. The control sample had the highest damages area, while the 0.2 wt. % HMWCNTs had relatively less damaged area, and the least damaged area was observed for 0.4 wt. % HMWCNTs.

The analytical modeling was carried out with second order polynomial fit together with root mean square values, which represent the goodness of the fit.

Based on the above-mentioned results and discussion, it can be concluded that, HMWCNTs-epoxy composite exhibits improved mechanical, physical and thermal

properties and could find extended applications in broad area of engineering and technology.

4.11 Reference Material Comparison

As illustrated in Figure 4.8, Mode II interlaminar fracture toughness for the control sample was calculated as 0.887 kJ/m^2 for 0.2 wt. % HMWCNTs-epoxy was 1.352 kJ/m^2 and for 0.4 wt. % HMWCNTs-epoxy was 2.611 kJ/m^2. This value in fracture toughness of CF-E laminates has increased compared to that of the reference material (Yokonzeki et al., 2007; Karapapas et al., 2009) by adding 0.2 wt. % and 0.4 wt. % HMWCNTs.

The thermal stability results for the samples differ from that of the reference material (Ciecierska et al., 2013; Loos et al., 2008; Zhou et al., 2007) as a better thermal conductivity value of the composites is expected by adding HMWCNTs in-sample results. However, as shown in Figure 4.16, this effect has not been observed for the specimens for this research. Therefore, it implies that adding HMWCNTs, in this case, does not affect the thermal stability negatively but rather exert the opposite effect.

The research test results for electrical conductivity show a decrease in resistivity volume with an increase in aspect ratio, as shown in Figure 4.15. In terms of electrical conductivity, these results suggest an increase in conductivity with an increase in aspect ratio in CNTs which meets the current literature expectations as reported earlier (Estelle et al., 2015; Sasty et al., 2008). Moreover, during the fabrication method, HMWCNTs could be broken into smaller tubes, resulting in little porosity of bucky papers and causing higher HMWCNTs concentration that implies conductivity improvement. This is also similar to the literature provided by Xiao et al. (2018) that the uniform dispersion of CNTs enhances their electrical properties.

Based on the compression outcomes after impact testing (Table 4.8), it can be stated that the higher compressive values were observed on 0.4 wt. % HMWCNTs-epoxy laminates because of control shear cracking and structural delamination by the presence

of the reinforcement (Sanchez-Saez et al., 2005). Minimum displacement obtained for the control sample can be attributed to the fact that normally, high ductile material requires high time to reach peak load and deflect more under the same energy levels. In addition, HMWCNTs improve the composite's stiffness, which tends to show smaller amounts of deflection (Rahman et al., 2013, Rahman et al., 2012, Salam et al., 2013).

Damage area results exhibited, least damage for 0.4 wt. % HMWCNTs-epoxy composite as shown in Figure 4.25. The control sample has the highest damages area, as expected, while the 0.2 wt. % HMWCNTs-epoxy has a relatively less damaged area, and the least damaged area was observed for 0.4 wt. % HMWCNTs-epoxy composite. At lower level 15 J, the lower peak load can be attributed to the fact that composites were not fully capable. However, at a higher energy level of 25 J, the laminates carried the highest load they could have attained, and the damaged area observed was higher than the observed at 15 J (Mahdi et al., 2013).

The compression versus displacement curve for impacted and unimpacted samples at different energy levels 0 J, 15 J, and 25 J, as presented in Figure 4.14 (a-c), shows linear behavior of compression and displacement after the initial phase by the low applied load. In addition, the curves showed an increase in displacement with an increase in impact energy. This strength behavior of composite laminates presented in this study corresponds to Josh et al.'s (2012) research, who found that composite laminates face substantial reductions in strength when loaded under compression because of local uncertainties rising from the widespread damage.

CHAPTER 5: CONCLUSION AND FUTURE RECOMMENDATIONS

5.1 Conclusions

The present work investigated the mechanical, thermal, and electrical behavior of HMWCNTs reinforced epoxy-carbon fiber composites. As reported in the introduction and literature review sections, most of the work on HMWCNTs reinforced epoxy-composite involves direct mixing of HMWCNTs in the polymer matrix and then fabrication of the composite laminates. However, in the present work, the mixture of HMWCNTs-epoxy-hardener was spray coated on individual carbon fiber epoxy composite sheets. This innovative approach reduces the breakage and entanglement of the HMWCNTs and ensures the effective distribution of the HMWCNTs. Furthermore, this particular method of sample fabrication enables us to determine the direct contribution of the HMWCNTs on the improvement of the mechanical properties of the composite. As evident from chapter 4 (results and discussion), this work's outcome is promising.

For this research, HMWCNTs-epoxy laminates were prepared by mixed method to have better dispersion with the composition of 0.2 wt. % HMWCNTs and 0.4 wt. % HMWCNTs. The Mode I and Mode II fracture toughness was examined by DCB and ENF, respectively, with LVI and CAI test, thermal stability, electrical conductivity, FESEM imaging, and C-scanning. The research objectives of the study were to investigate the effect of adding HMWCNTs of different concentrations on the underlying failure mechanisms of the fabricated nanocomposite laminates; investigate the deformation and damage characteristics involved in the impact and after an impacted event of the fabricated nanocomposite laminates; evaluate the thermal and electrical properties of the fabricated nanocomposite laminates, and characterize the fracture surface and the damaged area of the nanocomposite laminates under monotonic and

impact loading conditions, and to correlate it with underlying failure mechanism. The following sections summarise how these objectives were met in this research.

- **Attainment of objective 1: To investigate the effect of adding HMWCNTs of different concentrations on the fabricated nanocomposite laminates (inter and intra-laminar failure)**

DCB test showed that when critical values were attained, the load suddenly tended to decrease to around ~50 N for control ~70 N for 0.2 wt. % HMWCNTs-epoxy and ~105 N for 0.4 wt. % HMWCNTs-epoxy at 4-6 mm displacement due to delamination and crack propagation initiation. All the tests showed an unstable growth of delamination at the beginning. That can be ascribed as the artificial delamination caused by the Teflon layer in every sample at the middle plane. Thus, it is demonstrated from the experimental results and analysis that the interfacial chemical interaction between the epoxy and HMWCNTs was created strong enough by the dispersion technique that improves fracture toughness.

ENF examination declared that fracture toughness G_{IIC} has increased with incorporating HMWCNTs in comparison with control specimen. The average interlaminar fracture toughness observed for control samples was 0.887 kJ/m^2 for 0.2 wt. % HMWCNTs-epoxy was 1.352 kJ/m^2 while the maximum for 0.4 wt. % HMWCNTs-epoxy was noticed 2.611 kJ/m^2

- **Attainment of objective 2: To investigate the deformation and damage characteristics involved in the fabricated nanocomposite laminates' impact and after an impacted event**

LVI results showed that the peak load of the control sample was lowest than both laminates composites. This implies that HMWCNTs-epoxy laminates have high impact resistance than the control sample. The developing energy specifies the initiation of interfacial failure of fiber and matrix or matrix failure close to the opposite of the

impacted face, hence, the start of damage in the laminates. As expected, the trend observed for all the composites was lowest for control, slightly high for 0.2 wt. % HMWCNTs-epoxy and highest for 0.4 wt. % HMWCNTs-epoxy composite. The CAI results showed that the compression forces and compression strength were observed for 0.2 wt. % HMWCNTs-epoxy and 0.4 wt. % HMWCNTs-epoxy can withstand higher load without being elongated, and therefore, this composite has the highest impact resistance. The control sample had the lowest impact resistances than the composite laminates.

- **Attainment of objective 3: To evaluate the fabricated nanocomposite laminates' thermal and electrical properties**

The volume resistivity of the control sample was around 7.94 Ω.cm, 5.78 Ω.cm for 0.2 wt. % HMWCNTs-epoxy and 2.01 Ω.cm for 0.4 wt. % HMWCNTs-epoxy composites. The 0.4 wt. % HMWCNTs showed the lowest resistivity among all the laminates due to the increase in the conductive fillers HMWCNTs an insulating matrix. Thermogravimetric analysis of composite laminates showed that 0.4 wt. % HMWCNTs-epoxy laminates degraded 3 °C later than 0.2 wt. % HMWCNTs-epoxy shows the somewhat strong bond between epoxy and HMWCNTs that can delay molecular diffusion from resin matrix at higher temperature and result in enhanced thermal stability. Differential calorimetric analysis showed that upon HMWCNTs addition, *Tg* has shifted to a higher temperature. The addition of HMWCNTs with amino groups resulted in higher glass transition temperature.

- **Attainment of objective 4: To characterize the fracture surface and the damaged area of the nanocomposite laminates under monotonic and impact loading conditions and correlate it with the underlying failure mechanism**

From the morphology analysis of fractured surfaces by FESEM, it is clear that upon increasing the number of HMWCNTs in the composite laminate, the composites' tensile

strength improves, leading to higher surface roughness. This confirms the embedment of HMWCNTs in the epoxy matrix as the crack interface predominantly in areas of a relatively smoother surface. Furthermore, there was evidence of fewer HMWCNTs agglomerates over the fracture surface because of the optimal dispersion over the prepreg during the dispersion process. C-scan images showed the damage areas of all the samples at both energy levels of 15 J and 25 J. The control sample had the highest damages area, as expected, while the 0.2 wt. % HMWCNTs had relatively less damaged area, and the least damaged area was observed for 0.4 wt. % HMWCNTs. At lower level 15 J, the lower peak load can be attributed to the fact that composites were not fully capable. However, at the higher energy level of 25 J, the laminates carried the highest load they could have attained64, and the damaged area observed was higher than the observed at 15 J for all the samples.

5.2 Research limitations

In present study, two different loading of HMWCNTs namely, 0.2 wt. % and 0.4 wt.%, on epoxy composite was fabricated and investigated together with neat epoxy, that is, without any reinforcement in it. Thus, basically there was only three points for each property. Due to this, finite element analysis (FEA) was not possible to perform; and therefore, second order polynomial fitting of the data points with respective root mean square values were performed. Withstanding this limitation, the present curve fittings can be regarded as an information on the general trend of the improvement of the mechanical properties of the composite, which is supported in comparison of the data reported in the literature. To get the precise modeling, such as FEA, more experimental data are required, by varying the HMWCNTs content in the epoxy composite, and suggested as future work.

The study relied so much on experimental lab research which is highly subjective as there are possibilities of human error that could occur at some point hence .The research

was also time consuming as each variable had to be isolated and tested and some variables had to be combined. This process was lengthy and required a large amount of financial and personal resources to purchase the materials to be used during the testing's. Dealing with machinery and chemicals requires high level of alertness and extreme care. Working with machinery and chemicals exposed us to risks such being injured or being poisoned by the chemical used to clean samples. Moreover, the scope of the present research is limited concerning the fracture and impact loading of the polymer composite and the electrical and thermal characteristics of the polymer composites.

5.3 Future Recommendations

The following future work is recommended:

- To further increase the number of HMWCNTs loading in the composite and find the optimum content representing the optimum mechanical, thermal, and electrical properties.
- Further mechanical experiments are required to find the elasticity E_{11} and E_{22}, shear module $G_{12,}$ and Poisson ratio υ_{12}, which will offer the complete mechanical aspects of such composites.
- It is necessary to carry out the computer-aided simulation to find out the effect of HMWCNTs loading on the mechanical properties of the composite laminates. Simulation work may also help determine the optimum HMWCNTs loading and carry out the subsequent experimental work accordingly to verify the outcome of the simulation work.

REFERENCES

Afzal, A., Nawfal, I., Mahbubul, I. M., & Kumbar, S. S. (2019). An overview on the effect of ultrasonication duration on different properties of nanofluids. Journal of Thermal Analysis and Calorimetry, 135(1), 393-418.

Ajayan, P. M., Stephan, O., Colliex, C., & Trauth, D. (1994). Aligned Carbon Nanotube Arrays Formed by Cutting a Polymer Resin—Nanotube Composite. Science, 265(5176), 1212–1214.

Ajayan, Pulickel M., Schadler, L. S., Giannaris, C., & Rubio, A. (2000). Single-walled carbon nanotube-polymer composites: Strength and weakness. Advanced Materials, 12(10), 750–753.

Ajayan, Pulickel M., & Tour, J. M. (2007). Nanotube composites. Nature, 447(7148), 1066–1068.

Ali, A., Andriyana, A., Hassan, S. B. A., & Ang, B. C. (2021). Fabrication and Thermo-Electro and Mechanical Properties Evaluation of Helical Multiwall Carbon Nanotube-Carbon Fiber/Epoxy Composite Laminates. Polymers, 13(9), 1437.

Allaoui, A. & El Bounia, N.-E. (2009). How carbon nanotubes affect the cure kinetics and glass transition temperature of their epoxy composites? – A Review. Express Polymer Letter, 3, 588–594.

Amraei, J., Jam, J. E., Arab, B., & Firouz-Abadi, R. D. (2019). Effect of interphase zone on the overall elastic properties of nanoparticle-reinforced polymer nanocomposites. Journal of Composite Materials, 53(9), 1261–1274.

Andresen, C., Demuth, C., Lange, A., Stoick, P., & Pruszko, R. (2012). Biobased automobile parts investigation. A Report Developed for the USDA Office of Energy Policy and New Uses.

Andrews, R., Jacques, D., Qian, D., & Rantell, T. (2002). Multiwall carbon nanotubes: Synthesis and application. Accounts of Chemical Research, 35(12), 1008–1017.

Aqel, A., Abou El-Nour, K. M., Ammar, R. A., & Al-Warthan, A. (2012). Carbon nanotubes, science and technology part (I) structure, synthesis and characterisation. Arabian Journal of Chemistry, 5(1), 1-23.

Arai, M., Noro, Y., Sugimoto, K., & Endo, M. (2008). Mode I and mode II interlaminar fracture toughness of CFRP laminates toughened by carbon nanofiber interlayer. Composites Science and Technology, 68(2), 516–525.

Arash, B., Park, H. S., & Rabczuk, T. (2015). Mechanical properties of carbon nanotube reinforced polymer nanocomposites: A coarse-grained model. Composites Part B: Engineering, 80, 92–100.

Arora, N., & Sharma, N. N. (2014a). Arc discharge synthesis of carbon nanotubes: Comprehensive review. Diamond and Related Materials, 50, 135–150.

Arora, N., & Sharma, N. N. (2014b). Arc discharge synthesis of carbon nanotubes: Comprehensive review. Diamond and Related Materials, 50, 135–150.

Arora, N., & Sharma, N. N. (2017). Effect of current variation on carbon black to synthesize MWCNTs using pulsed arc discharge method. Materials Today: Proceedings, 4(9), 9394–9398.

Arunkumar, T., Karthikeyan, R., Subramani, R. R., Viswanathan, K., & Anish, M. (2020). Synthesis and characterisation of multi-walled carbon nanotubes (MWCNTs). International Journal of Ambient Energy, 41(4), 452–456.

ASTM D7136 / D7136M-20. (2020). Standard Test Method for Measuring the Damage Resistance of a Fiber-Reinforced Polymer Matrix Composite to a Drop-Weight Impact Event, ASTM International, West Conshohocken, PA.

ASTM D7905 / D7905M-19e1. (2019). Standard Test Method for Determination of the Mode II Interlaminar Fracture Toughness of Unidirectional Fiber-Reinforced Polymer Matrix Composites, ASTM International, West Conshohocken, PA.

ASTM D7137 / D7137M-17. (2017). Standard Test Method for Compressive Residual Strength Properties of Damaged Polymer Matrix Composite Plates, ASTM International, West Conshohocken, PA.

ASTM D5528-13. (2013). Standard Test Method for Mode I Interlaminar Fracture Toughness of Unidirectional Fiber-Reinforced Polymer Matrix Composites, ASTM International, West Conshohocken, PA.

Ashrafi, B., Guan, J., Mirjalili, V., Zhang, Y., Chun, L., Hubert, P., Simard, B., Kingston, C. T., Bourne, O. & Johnston, A. (2011). Enhancement of mechanical performance of epoxy/carbon fiber laminate composites using single-walled carbon nanotubes. Composites science and technology, 71, 1569-1578.

Baddour, C. E., & Briens, C. (2005). Carbon Nanotube Synthesis: A Review. International Journal of Chemical Reactor Engineering, 3(1).

Baibarac, M., Baltog, I., Godon, C., Lefrant, S., & Chauvet, O. (2004). Covalent functionalization of single-walled carbon nanotubes by aniline electrochemical polymerization. Carbon, 42(15), 3143–3152.

Bao, H.-D., Guo, Z.-X., & Yu, J. (2008). Effect of electrically inert particulate filler on electrical resistivity of polymer/multi-walled carbon nanotube composites. Polymer, 49(17), 3826–3831.

Bellayer, S., Gilman, J. W., Eidelman, N., Bourbigot, S., Flambard, X., Fox, D. M., De Long, H. C., & Trulove, P. C. (2005). Preparation of Homogeneously Dispersed Multiwalled Carbon Nanotube/Polystyrene Nanocomposites via Melt Extrusion Using Trialkyl Imidazolium Compatibilizer. Advanced Functional Materials, 15(6), 910–916.

Bellucci, S., Balasubramanian, C., Micciulla, F., & Rinaldi, G. (2007). CNT composites for aerospace applications. Journal of Experimental Nanoscience, 2(3), 193–206.

Beyer, G. (2002). Short communication: Carbon nanotubes as flame retardants for polymers. Fire and Materials, 26(6), 291–293.

Bhattacharyya, A. R., Pötschke, P., Häußler, L., & Fischer, D. (2005). Reactive Compatibilization of Melt Mixed PA6/SWNT Composites: Mechanical Properties and Morphology. Macromolecular Chemistry and Physics, 206(20), 2084–2095.

Biagiotti, J., Puglia, D., & Kenny, J. M. (2004). A review on natural fibre-based composites-part I: Structure, processing and properties of vegetable fibres. Journal of Natural Fibers, 1(2), 37–68.

Bisht, A., Dasgupta, K., & Lahiri, D. (2020). Evaluating the effect of addition of nanodiamond on the synergistic effect of graphene-carbon nanotube hybrid on the mechanical properties of epoxy based composites. Polymer Testing, 81, 106274.

Boland, C. S., De Kleine, R., Keoleian, G. A., Lee, E. C., Kim, H. C., & Wallington, T. J. (2016). Life Cycle Impacts of Natural Fiber Composites for Automotive Applications: Effects of Renewable Energy Content and Lightweighting. Journal of Industrial Ecology, 20(1), 179–189.

Boroujeni, A. Y., & Al-Haik, M. (2019). Carbon nanotube – Carbon fiber reinforced polymer composites with extended fatigue life. Composites Part B: Engineering, 164, 537–545.

Bose, S., Khare, R. A., & Moldenaers, P. (2010). Assessing the strengths and weaknesses of various types of pre-treatments of carbon nanotubes on the properties of polymer/carbon nanotubes composites: A critical review. Polymer, 51(5), 975–993.

Breuer, O., & Sundararaj, U. (2004). Big returns from small fibers: A review of polymer/carbon nanotube composites. Polymer Composites, 25(6), 630–645.

Brukh, R., & Mitra, S. (2006). Mechanism of carbon nanotube growth by CVD. Chemical Physics Letters, 424(1), 126–132.

Caradonna, A.; Badini, C.; Padovano, E.; Pietroluongo, M. Electrical and Thermal Conductivity of Epoxy-Carbon Filler Composites Processed by Calendaring. Materials 2019, 12, 1522

Cha, J., Jin, S., Shim, J. H., Park, C. S., Ryu, H. J., & Hong, S. H. (2016). Functionalization of carbon nanotubes for fabrication of CNT/epoxy nanocomposites. Materials & Design, 95, 1-8.

Chen, W., Auad, M. L., Williams, R. J. J., & Nutt, S. R. (2006). Improving the dispersion and flexural strength of multiwalled carbon nanotubes–stiff epoxy composites through β-hydroxyester surface functionalization coupled with the anionic homopolymerization of the epoxy matrix. European Polymer Journal, 42(10), 2765–2772.

Chen, W., Tao, X., & Liu, Y. (2006). Carbon nanotube-reinforced polyurethane composite fibers. Composites Science and Technology, 66(15), 3029–3034.

Chen, Y. L., Liu, B., He, X. Q., Huang, Y., & Hwang, K. C. (2010). Failure analysis and the optimal toughness design of carbon nanotube-reinforced composites. Composites Science and Technology, 70(9), 1360–1367.

Cheng, Y., Deng, S., Chen, P., & Ruan, R. (2009). Polylactic acid (PLA) synthesis and modifications: A review. Frontiers of Chemistry in China, 4(3), 259–264.

Cheung, H., Ho, M., Lau, K., Cardona, F., & Hui, D. (2009). Natural fibre-reinforced composites for bioengineering and environmental engineering applications. Composites Part B: Engineering, 40(7), 655–663.

Choi, I. H., Park, M., Lee, S.-S., & Hong, S. C. (2008). Pyrene-containing polystyrene segmented copolymer from nitroxide mediated polymerization and its application for the noncovalent functionalization of as-prepared multiwalled carbon nanotubes. European Polymer Journal, 44(10), 3087–3095.

Chou, T.-W., Gao, L., Thostenson, E. T., Zhang, Z., & Byun, J.-H. (2010). An assessment of the science and technology of carbon nanotube-based fibers and composites. Composites Science and Technology, 70(1), 1–19.

Chowdhury, S. C., & Okabe, T. (2007). Computer simulation of carbon nanotube pull-out from polymer by the molecular dynamics method. Composites Part A: Applied Science and Manufacturing, 38(3), 747–754.

Chung, D. D. L. (2010). Composite Materials: Science and Applications. Springer Science & Business Media.

Ciecierska, E., Boczkowska, A., Kurzydlowski, K. J., Rosca, I. D. & Van Hoa, S. (2013). The effect of carbon nanotubes on epoxy matrix nanocomposites. Journal of thermal analysis and calorimetry, 111, 1019-1024.

Coleman, J. N., Khan, U., Blau, W. J., & Gun'ko, Y. K. (2006). Small but strong: A review of the mechanical properties of carbon nanotube–polymer composites. Carbon, 44(9), 1624–1652.

Compston, P., Jar, P.-Y. & Davies, P. (1998). Matrix effect on the static and dynamic interlaminar fracture toughness of glass-fibre marine composites. Composites Part B: Engineering, 29, 505-516.

Courty, S., Mine, J., Tajbakhsh, A. R., & Terentjev, E. M. (2003). Nematic elastomers with aligned carbon nanotubes: New electromechanical actuators. EPL (Europhysics Letters), 64(5), 654.

Damian, C. M., Garea, S. A., Vasile, E., & Iovu, H. (2012). Covalent and non-covalent functionalized MWCNTs for improved thermo-mechanical properties of epoxy composites. Composites Part B: Engineering, 43(8), 3507–3515.

Das, R., Shahnavaz, Z., Ali, Md. E., Islam, M. M., & Abd Hamid, S. B. (2016). Can We Optimize Arc Discharge and Laser Ablation for Well-Controlled Carbon Nanotube Synthesis? Nanoscale Research Letters, 11(1), 510.

Davies, G. A. O., Hitchings, D., & Ankersen, J. (2006). Predicting delamination and debonding in modern aerospace composite structures. Composites Science and Technology, 66(6), 846–854.

De Menezes, B. R. C., Rodrigues, K. F., da Silva Fonseca, B. C., Ribas, R. G., do Amaral Montanheiro, T. L., & Thim, G. P. (2019). Recent advances in the use of carbon nanotubes as smart biomaterials. Journal of Materials Chemistry B, 7(9), 1343–1360.

De Volder, M. F., Tawfick, S. H., Baughman, R. H., & Hart, A. J. (2013). Carbon nanotubes: Present and future commercial applications. Science, 339(6119), 535–539.

Dillon, A. C., Parilla, P. A., Alleman, J. L., Gennett, T., Jones, K. M., & Heben, M. J. (2005). Systematic inclusion of defects in pure carbon single-wall nanotubes and their effect on the Raman D-band. Chemical Physics Letters, 401(4), 522–528.

Endo, M., Hayashi, T., Kim, Y. A., & Muramatsu, H. (2006). Development and Application of Carbon Nanotubes. Japanese Journal of Applied Physics, 45(6R), 4883.

Erdogan, G. and K. Bilisik. (2018) Compression after low-velocity impact (CAI) properties of multistitched composites. Mechanics of Advanced Materials and Structures, 25(8), 623-636

Estellé, P.; Halelfadl, S.; Thierry, M. Thermal conductivity of CNT water based nanofluids: Experimental trends and models overview. J. Therm. Eng. 2015, 1, 381–390.

F.H. Gojny, M.H.G. Wichmann, B. Fiedler, I.A. Kinloch, W. Bauhofer, A.H. Windle, 541 and K. Schulte. Evaluation and identification of electrical and thermal conduction 542 mechanisms in carbon nanotube/epoxy composites. Polymer, Volume 47, Issue 6, 543 2006, Pages 2036-2045

Falzon, B. G., Hawkins, S. C., Huynh, C. P., Radjef, R., & Brown, C. (2013). An investigation of Mode I and Mode II fracture toughness enhancement using aligned carbon nanotubes forests at the crack interface. Composite Structures, 106, 65–73.

Fan, Y., Goldsmith, B. R., & Collins, P. G. (2005). Identifying and counting point defects in carbon nanotubes. Nature Materials, 4(12), 906–911.

Farghali, A. A., Abdel Tawab, H. A., Abdel Moaty, S. A., & Khaled, R. (2017). Functionalization of acidified multi-walled carbon nanotubes for removal of heavy metals in aqueous solutions. Journal of Nanostructure in Chemistry, 7(2), 101–111.

Faruk, O., Bledzki, A. K., Fink, H.-P., & Sain, M. (2012). Biocomposites reinforced with natural fibers: 2000–2010. Progress in Polymer Science, 37(11), 1552–1596.

Feng, Q.-P., Yang, J.-P., Fu, S.-Y., & Mai, Y.-W. (2010). Synthesis of carbon nanotube/epoxy composite films with a high nanotube loading by a mixed-curing-

agent assisted layer-by-layer method and their electrical conductivity. Carbon, 48(7), 2057–2062.

Fernández-Toribio, J. C., Alemán, B., Ridruejo, Á., & Vilatela, J. J. (2018). Tensile properties of carbon nanotube fibres described by the fibrillar crystallite model. Carbon, 133, 44–52.

Fiedler, B., Gojny, F. H., Wichmann, M. H. G., Nolte, M. C. M., & Schulte, K. (2006). Fundamental aspects of nano-reinforced composites. Composites Science and Technology, 66(16), 3115–3125.

Fiedler B, Gojny FH, Wichmann MHG, Nolte MCM, Schulte K. Fundamental aspects of nano-reinforced composites. Compos Sci Technol 2006;66(16):3115–25

Fornes, T. D., Baur, J. W., Sabba, Y., & Thomas, E. L. (2006). Morphology and properties of melt-spun polycarbonate fibers containing single- and multi-wall carbon nanotubes. Polymer, 47(5), 1704–1714.

Francis, A. P., & Devasena, T. (2018). Toxicity of carbon nanotubes: A review. Toxicology and Industrial Health, 34(3), 200–210.

Galkov, M. S., Stepina, N. P., Predtechenskiy, M. R., Bezrodny, A. E., Kirienko, V. V., & Dvurechenskii, A. V. (2019). Preparation and transport properties of oriented buckypapers with single walled carbon nanotubes. Materials of Electronics Engineering, 22, 104–111.

Gao, X., Huang, Z., & Fang, D. (2017). Curvature-dependent interfacial energy and its effects on the elastic properties of nanomaterials. International Journal of Solids and Structures, 113, 100–107.

Ge, J. J., Hou, H., Li, Q., Graham, M. J., Greiner, A., Reneker, D. H., Harris, F. W., & Cheng, S. Z. D. (2004). Assembly of Well-Aligned Multiwalled Carbon Nanotubes in Confined Polyacrylonitrile Environments: Electrospun Composite Nanofiber Sheets. Journal of the American Chemical Society, 126(48), 15754–15761.

Goel, M., Harsha, S. P., Singh, S., & Sahani, A. K. (2020). Analysis of temperature, helicity and size effect on the mechanical properties of carbon nanotubes using molecular dynamics simulation. Materials today: proceedings, 26, 897-904.

Gojny, F. H., Wichmann, M. H. G., Köpke, U., Fiedler, B., & Schulte, K. (2004). Carbon nanotube-reinforced epoxy-composites: Enhanced stiffness and fracture toughness at low nanotube content. Composites Science and Technology, 64(15), 2363–2371.

Gojny F.H., Wichmann, M.H.G., Fiedler, B., & Schulte, K. (2005). Influence of different carbon nanotubes on the mechanical properties of epoxy matrix composites – a comparative study. Compos Sci Technol 2005;65(15–16):2300–13

Gou, J., Minaie, B., Wang, B., Liang, Z., & Zhang, C. (2004). Computational and experimental study of interfacial bonding of single-walled nanotube reinforced composites. Computational Materials Science, 31(3–4), 225–236.

Guo, J.; Saha, P.; Liang, J.; Saha, M.; Grady, B.P. Multi-walled carbon nanotubes coated by multi-layer silica for improving thermal conductivity of polymer composites. J. Therm. Anal. Calorim. 2013, 113, 467–474.

Gupta, G., Kumar, A., Tyagi, R., & Kumar, S. (2016). Application and future of composite materials: A review. Journal of Innovative Research in Science, Engineering and Technology, 5(5), 6907–6911.

Gurunathan, T., Mohanty, S., & Nayak, S. K. (2015). A review of the recent developments in biocomposites based on natural fibres and their application perspectives. Composites Part A: Applied Science and Manufacturing, 77, 1–25.

Guadagno L, Vertuccio L, Sorrentino A, Raimondo M, Naddeo C, Vittoria V, et al. Mechanical and barrier properties of epoxy resin filled with multi-walled carbon nanotubes. Carbon 2009;47(10):2419–30

Ha, J.-H.; Lee, S.-E.; Park, S.-H. Effect of Dispersion by Three-Roll Milling on Electrical Properties and Filler Length of Carbon Nanotube Composites. Materials 2019, 12, 3823

Habisreutinger, S. N., Nicholas, R. J., & Snaith, H. J. (2017). Carbon nanotubes in perovskite solar cells. Advanced Energy Materials, 7(10), 1601839.

Hirsch, A., & Vostrowsky, O. (2005). Functionalization of Carbon Nanotubes. In A. D. Schlüter (Ed.), Functional Molecular Nanostructures: -/- (pp. 193–237). Springer.

Hine, P., Brew, B., Duckett, R. & Ward, I. (1989). Failure mechanisms in continuous carbon-fibre reinforced PEEK composites. Composites Science and technology, 35, 31-51.

Hosur, M. V., Chowdhury, F. & Jeelani, S. (2007). Low-velocity impact response and ultrasonic NDE of woven carbon/epoxy—Nanoclay nanocomposites. Journal of composite materials, 41, 2195-2212.

Hollaway, L. C. (2010). A review of the present and future utilisation of FRP composites in the civil infrastructure with reference to their important in-service properties. Construction and Building Materials, 24(12), 2419–2445.

Hu, N. (2012). Composites and their applications. BoD–Books on Demand.

Huang, Y. Y., & Terentjev, E. M. (2012). Dispersion of Carbon Nanotubes: Mixing, Sonication, Stabilization, and Composite Properties. Polymers, 4(1), 275–295.

Huda, M. S., Drzal, L. T., Ray, D., Mohanty, A. K., & Mishra, M. (2008). Natural-fiber composites in the automotive sector. In Properties and performance of natural-fibre composites (pp. 221–268). Elsevier.

Hutchison, J. L., Kiselev, N. A., Krinichnaya, E. P., Krestinin, A. V., Loutfy, R. O., Morawsky, A. P., Muradyan, V. E., Obraztsova, E. D., Sloan, J., Terekhov, S. V., & Zakharov, D. N. (2001). Double-walled carbon nanotubes fabricated by a hydrogen arc discharge method. Carbon, 39(5), 761–770.

Ibrahim, K. S. (2013). Carbon nanotubes-properties and applications: A review. Carbon Letters, 14(3), 131–144.

Iijima, S. (1991). Helical microtubules of graphitic carbon. Nature, 354(6348), 56–58.

Iijima, S., & Ichihashi, T. (1993). Single-shell carbon nanotubes of 1-nm diameter. Nature, 363(6430), 603–605.

Inam, F., Wong, D. W., Kuwata, M., & Peijs, T. (2010). Multiscale hybrid micro-nanocomposites based on carbon nanotubes and carbon fibers. Journal of Nanomaterials, 2010.

Ismail, K., Sultan, M., Shah, A., Jawaid, M. & Safri, S. (2019). Low velocity impact and compression after impact properties of hybrid bio-composites modified with multi-walled carbon nanotubes. Composites Part B: Engineering, 163, 455-463.

Islam, M. E., Mahdi, T. H., Hosur, M. V., & Jeelani, S. (2015). Characterization of carbon fiber reinforced epoxy composites modified with nanoclay and carbon nanotubes. Procedia Engineering, 105, 821–828.

Icten, B. M. (2015). Low temperature effect on single and repeated impact behavior of woven glass-epoxy composite plates. Journal of Composite Materials, 49, 1171-1178.

Iqbal, K., Khan, S.-U., Munir, A. & Kim, J.-K. (2009). Impact damage resistance of CFRP with nanoclay-filled epoxy matrix. Composites Science and Technology, 69, 1949-1957.

Jang, I., Sinnott, S. B., Danailov, D., & Keblinski, P. (2004). Molecular dynamics simulation study of carbon nanotube welding under electron beam irradiation. Nano Letters, 4(1), 109–114.

Jawaid, M., & Abdul Khalil, H. P. S. (2011). Cellulosic/synthetic fibre reinforced polymer hybrid composites: A review. Carbohydrate Polymers, 86(1), 1–18.

Jeong, J.-Y., Lee, H.-J., Kang, S.-W., Tan, L.-S., & Baek, J.-B. (2008). Nylon 610/functionalized multiwalled carbon nanotube composite prepared from in-situ interfacial polymerization. Journal of Polymer Science Part A: Polymer Chemistry, 46(18), 6041–6050.

Jiao, J., & Seraphin, S. (2000). Single-walled tubes and encapsulated nanoparticles: Comparison of structural properties of carbon nanoclusters prepared by three different methods. Journal of Physics and Chemistry of Solids, 61(7), 1055–1067.

Jogi, B. F., Sawant, M., Kulkarni, M., & Brahmankar, P. K. (2012). Dispersion and performance properties of carbon nanotubes (CNTs) based polymer composites: A review.

Joshi, S. C., & Dikshit, V. (2012). Enhancing interlaminar fracture characteristics of woven CFRP prepreg composites through CNT dispersion. Journal of Composite Materials, 46(6), 665-675.

Journet, C., Maser, W. K., Bernier, P., Loiseau, A., de La Chapelle, M. L., Lefrant, dl S., Deniard, P., Lee, R., & Fischer, J. E. (1997). Large-scale production of single-walled carbon nanotubes by the electric-arc technique. Nature, 388(6644), 756–758.

Karapappas, P., Vavouliotis, A., Tsotra, P., Kostopoulos, V., & Paipetis, A. (2009). Enhanced fracture properties of carbon reinforced composites by the addition of multi-wall carbon nanotubes. Journal of Composite Materials, 43(9), 977–985.

Karbhari, V. M. (2007). 1 - Introduction: The use of composites in civil structural applications. In Vistasp M. Karbhari (Ed.), Durability of Composites for Civil Structural Applications (pp. 1–10). Woodhead Publishing.

Kashiwagi, T., Du, F., Douglas, J. F., Winey, K. I., Harris, R. H., & Shields, J. R. (2005). Nanoparticle networks reduce the flammability of polymer nanocomposites. Nature Materials, 4(12), 928–933.

Kashyap, K. T., & Patil, R. G. (2008). On Young's modulus of multi-walled carbon nanotubes. Bulletin of Materials Science, 31(2), 185–187.

Kataura, H., Kumazawa, Y., Maniwa, Y., Ohtsuka, Y., Sen, R., Suzuki, S., & Achiba, Y. (2000). Diameter control of single-walled carbon nanotubes. Carbon, 38(11), 1691–1697.

Katerelos, D. T. G., Kashtalyan, M., Soutis, C., & Galiotis, C. (2008). Matrix cracking in polymeric composites laminates: Modelling and experiments. Composites Science and Technology, 68(12), 2310–2317.

Ke, K., Wang, Y., Liu, X.-Q., Cao, J., Luo, Y., Yang, W., Xie, B.-H., & Yang, M.-B. (2012). A comparison of melt and solution mixing on the dispersion of carbon nanotubes in a poly (vinylidene fluoride) matrix. Composites Part B: Engineering, 43(3), 1425–1432.

Keshavarz, T., & Roy, I. (2010). Polyhydroxyalkanoates: Bioplastics with a green agenda. Current Opinion in Microbiology, 13(3), 321–326.

Khabashesku, V. N., Zhu, J., Peng, H., Barrera, E. V., & Margrave, J. L. (2009). Fabrication of carbon nanotube reinforced epoxy polymer composites using functionalized carbon nanotubes (United States Patent No. US7601421B2).

Khan, S. U., & Kim, J. K. (2011a). Interlaminar shear properties of CFRP composites with CNF-bucky paper interleaves. The 18th International Conference on Composite Materials.

Khan, S. U., & Kim, J.-K. (2011b). Impact and Delamination Failure of Multiscale Carbon Nanotube-Fiber Reinforced Polymer Composites: A Review. International Journal of Aeronautical and Space Sciences, 12(2), 115–133.

Khare, R., & Bose, S. (2005). Carbon Nanotube Based Composites- A Review. Journal of Minerals and Materials Characterization and Engineering, 04(01), 31.

Kharissova, O. V., & Kharisov, B. I. (2014). Variations of interlayer spacing in carbon nanotubes. RSC Advances, 4(58), 30807–30815.

Kim, K. H., & Jo, W. H. (2008). Improvement of tensile properties of poly(methyl methacrylate) by dispersing multi-walled carbon nanotubes functionalized with poly(3-hexylthiophene)-graft-poly(methyl methacrylate). Composites Science and Technology, 68(9), 2120–2124.

Kim, W.-J., Kang, S.-O., Ah, C.-S., Lee, Y.-W., Ha, D.-H., Chol, I.-S. S. & Yun, W.-S. (2004). Functionalization of shortened SWMWCNTs using esterification. Bulletin of the Korean Chemical Society, 25, 1301-1302.

Kim, Y. J., Shin, T. S., Choi, H. D., Kwon, J. H., Chung, Y.-C., & Yoon, H. G. (2005). Electrical conductivity of chemically modified multiwalled carbon nanotube/epoxy composites. Carbon, 43(1), 23–30.

Kishi, N., Sugai, T., & Shinohara, H. (2009). Synthesis of Single- and Double-Wall Carbon Nanotubes by Gas Flow-Modified Catalyst-Supported Chemical Vapor Deposition. IEICE TRANSACTIONS on Electronics, E92-C(12), 1483–1486.

Kmetty, Á., Bárány, T., & Karger-Kocsis, J. (2010). Self-reinforced polymeric materials: A review. Progress in Polymer Science, 35(10), 1288–1310.

Kostopoulos, V., Baltopoulos, A., Karapappas, P., Vavouliotis, A. & Paipetis, A. (2010). Impact and after-impact properties of carbon fibre reinforced composites enhanced with multi-wall carbon nanotubes. Composites Science and Technology, 70, 553-563.

Koerner, H., Price, G., Pearce, N. A., Alexander, M., & Vaia, R. A. (2004). Remotely actuated polymer nanocomposites—Stress-recovery of carbon-nanotube-filled thermoplastic elastomers. Nature Materials, 3(2), 115–120.

Krause, B., Pötschke, P., & Häußler, L. (2009). Influence of small scale melt mixing conditions on electrical resistivity of carbon nanotube-polyamide composites. Composites Science and Technology, 69(10), 1505–1515.

Kroto, H. W., Heath, J. R., O'Brien, S. C., Curl, R. F., & Smalley, R. E. (1985). C 60: Buckminsterfullerene. Nature, 318(6042), 162–163.

Ku, H., Wang, H., Pattarachaiyakoop, N., & Trada, M. (2011). A review on the tensile properties of natural fiber reinforced polymer composites. Composites Part B: Engineering, 42(4), 856–873.

Kumar, M., & Ando, Y. (2010). Chemical Vapor Deposition of Carbon Nanotubes: A Review on Growth Mechanism and Mass Production. Journal of Nanoscience and Nanotechnology, 10(6), 3739–3758.

Kumar Sardiwal, Md. Abdul Sami, B.V.Sai Anoop, Gudipudi Susmita,Lahari Vooturi Syed Arsha, S. (2014). Advanced Composite Materials in Typical Aerospace Applications. *Global Journal Of Research In Engineering,* . Retrieved from https://engineeringresearch.org/index.php/GJRE/article/view/1071

L. Zhang, H. Deng, and Q. Fu. Recent progress on thermal conductive and electrical 548 insulating polymer composites. Composites Communications, Volume 8, 2018, Pages 549 74-82

Lednev, V. N., Pershin, S. M., Obraztsova, E. D., Kudryashov, S. I., & Bunkin, A. F. (2013). Single-shot and single-spot measurement of laser ablation threshold for carbon nanotubes. Journal of Physics D: Applied Physics, 46(5), 052002.

Lee, H. S., Yun, C. H., Kim, H. M., & Lee, C. J. (2007). Persistence Length of Multiwalled Carbon Nanotubes with Static Bending. The Journal of Physical Chemistry C, 111(51), 18882–18887.

Lehman, J. H., Terrones, M., Mansfield, E., Hurst, K. E., & Meunier, V. (2011). Evaluating the characteristics of multiwall carbon nanotubes. Carbon, 49(8), 2581–2602

Leone, C., Di Siena, M., Genna, S., & Martone, A. (2022). Effect of graphite nanoplatelets percentage on the in plane thermal diffusivity of ultra-thin graphene based (nanostructured) composite. Optics & Laser Technology, 146, 107552.

Liu, H., Zhang, Y., Li, R., Sun, X. & Abou-Rachid, H. (2012). Thermal and chemical durability of nitrogen-doped carbon nanotubes. Journal of Nanoparticle Research, 14, 1016-1021.

Li, C., & Chou, T.-W. (2008). Modeling of damage sensing in fiber composites using carbon nanotube networks. Composites Science and Technology, 68(15–16), 3373–3379.

Li, C., Thostenson, E. T., & Chou, T.-W. (2008). Sensors and actuators based on carbon nanotubes and their composites: A review. Composites Science and Technology, 68(6), 1227–1249.

Li, H.-X.; Zare, Y.; Rhee, K.Y. The percolation threshold for tensile strength of polymer/CNT nanocomposites assuming filler network and interphase regions. Mater. Chem. Phys. 2018, 207, 76–83.

Li, F., Cheng, H. M., Bai, S., Su, G., & Dresselhaus, M. S. (2000). Tensile strength of single-walled carbon nanotubes directly measured from their macroscopic ropes. Applied Physics Letters, 77(20), 3161–3163.

Li, H., Zhao, N., He, C., Shi, C., Du, X., & Li, J. (2008). Thermogravimetric analysis and TEM characterization of the oxidation and defect sites of carbon nanotubes synthesized by CVD of methane. Materials Science and Engineering: A, 473(1), 355–359.

Li, J., Wang, Q., Deng, L., Kou, X., Tang, Q., & Hu, Y. (2020). Fabrication and characterization of carbon nanotubes-based porous composite forward osmosis membrane: Flux performance, separation mechanism, and potential application. Journal of Membrane Science, 604, 118050.

Li, Y., Hori, N., Arai, M., Hu, N., Liu, Y., & Fukunaga, H. (2009). Improvement of interlaminar mechanical properties of CFRP laminates using VGCF. Composites Part A: Applied Science and Manufacturing, 40(12), 2004–2012.

Li, Y., Wang, S., Wang, Q., & Xing, M. (2018). Enhancement of fracture properties of polymer composites reinforced by carbon nanotubes: A molecular dynamics study. *Carbon*, *129*, 504-509. https://doi.org/10.1016/j.carbon.2017.12.029

Liew, K. M., Wong, C. H., & Tan, M. J. (2006). Tensile and compressive properties of carbon nanotube bundles. Acta Materialia, 54(1), 225–231.

Liu, L., & Grunlan, J. C. (2007). Clay Assisted Dispersion of Carbon Nanotubes in Conductive Epoxy Nanocomposites. Advanced Functional Materials, 17(14), 2343–2348.

Li, X., Wong, S. Y., Tjiu, W. C., Lyons, B. P., & Oh, S. A. (2008). Non-covalent functionalization of multi walled carbon nanotubes and their application for conductive composites. Carbon (New York, NY), 46(5), 829-831.

Loos, M. R., Coelho, L. A. F., Pezzin, S. H. & Amico, S. C. (2008). Effect of carbon nanotubes addition on the mechanical and thermal properties of epoxy matrices. Material Research, 11, 347–352.

Luhyna, N., & Inam, F. (2012). Carbon nanotubes for epoxy nanocomposites: A review on recent developments. Advanced Composite Materials and Technologies for Aerospace Applications, 80.

Luo, Y., Gong, Z., He, M., Wang, X., Tang, Z., & Chen, H. (2012). Fabrication of high-quality carbon nanotube fibers for optoelectronic applications. Solar Energy Materials and Solar Cells, 97, 78–82.

Mahajan, A., Kingon, A., Kukovecz, Á., Konya, Z. & Vilarinho, P. M. (2013a). Studies on the thermal decomposition of multiwall carbon nanotubes under different atmospheres. Materials Letter, 90, 165–168.

Mahdi, T. H., Islam, M. E., Hosur, M. V. & Jeelani, S. (2013b). Low velocity impact characterization of carbon fiber reinforced epoxy composites modified with multi-walled carbon nanotubes, nanoclay and hybrid nanoparticles.

Mansfield, E., Kar, A. & Hooker, S. A. (2010). Applications of TGA in quality control of SWMWCNTs. Analytical and Bioanalytical Chemistry, 396, 1071–1077.

Maljaee, H., Ghiassi, B. & Lourenço, P. B. (2017). Effect of synergistic environmental conditions on thermal properties of a cold curing epoxy resin. Composites Part B: Engineering, 113, 152-163

Malikan, M., Nguyen, V. B., Dimitri, R., & Tornabene, F. (2019). Dynamic modeling of non-cylindrical curved viscoelastic single-walled carbon nanotubes based on the second gradient theory. Materials Research Express, 6(7), 075041.

Mallick, P. K. (2007). Fiber-reinforced composites: materials, manufacturing, and design. CRC press.

Martin, C. A., Sandler, J. K. W., Windle, A. H., Schwarz, M.-K., Bauhofer, W., Schulte, K., & Shaffer, M. S. P. (2005). Electric field-induced aligned multi-wall carbon nanotube networks in epoxy composites. Polymer, 46(3), 877–886.

Martínez, M. T., Callejas, M. A., Benito, A. M., Cochet, M., Seeger, T., Ansón, A., Schreiber, J., Gordon, C., Marhic, C., Chauvet, O., Fierro, J. L. G., & Maser, W. K. (2003). Sensitivity of single wall carbon nanotubes to oxidative processing: Structural modification, intercalation and functionalisation. Carbon, 41(12), 2247–2256.

Meng, L., Fu, C., & Lu, Q. (2009). Advanced technology for functionalization of carbon nanotubes. Progress in Natural Science, 19(7), 801–810.

M. S. Dresselhaus, G. Dresselhaus, and A. Jorio, "Unusual properties and structure of carbon nanotubes," Annual Review of Materials Research, vol. 34, pp. 247–278, 2004

M. Terrones, "SScience and technology of the twenty-first century: synthesis, properties, and applications of carbon nanotubes," Annual Review of Materials Research, vol. 33, pp. 419–501, 2003.

M. Zhang and J. Li, "Carbon nanotube in different shapes," Materials Today, vol. 12, no. 6, pp. 12–18, 2009.

Michels, J., Widmann, R., Czaderski, C., Allahvirdizadeh, R. & Motavalli, M. (2015). Glass transition evaluation of commercially available epoxy resins used for civil engineering applications. Composites Part B: Engineering, 77, 484–493.

Mohanty, A. K., Misra, M., & Drzal, L. T. (2002). Sustainable bio-composites from renewable resources: Opportunities and challenges in the green materials world. Journal of Polymers and the Environment, 10(1), 19–26.

Nurazzi, M. N., Khalina, A., Sapuan, S. M., Dayang Laila, A., Rahmah, M., & Hanafee, Z. (2017). A Review: Fibres, Polymer Matrices and Composites. Pertanika Journal of Science & Technology, 25(4).

Montazeri, A., & Chitsazzadeh, M. (2014). Effect of sonication parameters on the mechanical properties of multi-walled carbon nanotube/epoxy composites. Materials & Design (1980-2015), 56, 500–508.

Moradi, O., Yari, M., Zare, K., Mirza, B., & Najafi, F. (2012). Carbon Nanotubes: A Review of Chemistry Principles and Reactions. Fullerenes, Nanotubes and Carbon Nanostructures, 20(2), 138–151.

Mubarak, N. M., Abdullah, E. C., Jayakumar, N. S., & Sahu, J. N. (2014). An overview on methods for the production of carbon nanotubes. Journal of Industrial and Engineering Chemistry, 20(4), 1186–1197.

Muhammad, A., Rahman, Md. R., Baini, R., & Bin Bakri, M. K. (2021). 8—Applications of sustainable polymer composites in automobile and aerospace industry. In Md.

R. Rahman (Ed.), Advances in Sustainable Polymer Composites (pp. 185–207). Woodhead Publishing.

Mylvaganam, K., & Zhang, L. C. (2007). Fabrication and Application of Polymer Composites Comprising Carbon Nanotubes. Recent Patents on Nanotechnology, 1(1), 59–65.

Nam, T. H., Goto, K., Yamaguchi, Y., Premalal, E. V. A., Shimamura, Y., Inoue, Y., Naito, K., & Ogihara, S. (2015). Effects of CNT diameter on mechanical properties of aligned CNT sheets and composites. Composites Part A: Applied Science and Manufacturing, 76, 289–298.

Narlikar, A. V., & Fu, Y. Y. (2010). Oxford Handbook of Nanoscience and Technology: Volume 2: Materials: Structures, Properties and Characterization Techniques. Oxford University Press.

Nasuha, N., Azmi, A. I., & Tan, C. L. (2017). A review on mode-I interlaminar fracture toughness of fibre reinforced composites. Journal of Physics: Conference Series, 908(1), 012024.

Natsuki, T., Tantrakarn, K., & Endo, M. (2004). Effects of carbon nanotube structures on mechanical properties. Applied Physics A, 79(1), 117–124.

Naz, A., Kausar, A., Siddiq, M., & Choudhary, M. A. (2016). Comparative Review on Structure, Properties, Fabrication Techniques, and Relevance of Polymer Nanocomposites Reinforced with Carbon Nanotube and Graphite Fillers. Polymer-Plastics Technology and Engineering, 55(2), 171–198.

Nikfar, B., & Njuguna, J. (2014, August). Compression-after-impact (CAI) performance of epoxycarbon fibre-reinforced nanocomposites using nanosilica and rubber particle enhancement. In IOP conference series: materials science and engineering, 64(1), 012009.

Noël, D., Hechler, J.-J., Cole. K. C., Chouliotis, A. & Overbury, K. C. (1988). Quantitative thermal characterization of carbon-epoxy composites using differential scanning calorimetry and thermogravimetric analysis. Thermochima Acta, 125, 191-208.

O'Connor, I., De, S., Coleman, J. N., & Gun'ko, Y. K. (2009). Development of transparent, conducting composites by surface infiltration of nanotubes into commercial polymer films. Carbon, 47(8), 1983–1988.

O'Connor, I., Hayden, H., Coleman, J. N., & Gun'ko, Y. K. (2009). High-Strength, High-Toughness Composite Fibers by Swelling Kevlar in Nanotube Suspensions. Small, 5(4), 466–469.

Ogawa, D., Morimune-Moriya, S., & Nakamura, K. (2022). Effective polymerization technique for plasma-treated multiwalled carbon nanotubes to maximize wear resistance of composite polyurethane. Journal of Vacuum Science & Technology B, Nanotechnology and Microelectronics: Materials, Processing, Measurement, and Phenomena, 40(2), 022803.

Ohnishi, M., Shiga, T., & Shiomi, J. (2017). Effects of defects on thermoelectric properties of carbon nanotubes. Physical Review B, 95(15), 155405.

Opelt, C. V., Cândido, G. M., & Rezende, M. C. (2018). Fractographic study of damage mechanisms in fiber reinforced polymer composites submitted to uniaxial compression. Engineering Failure Analysis, 92, 520–527.

Owens, F. J. (2005). Properties of composites of fluorinated single walled carbon nanotubes and polyacrylonitrile. Materials Letters, 59(28), 3720–3723.

Özden-Yenigün, E., Menceloğlu, Y. Z., & Papila, M. (2012). MWCNTs/P (St-co-GMA) composite nanofibers of engineered interface chemistry for epoxy matrix nanocomposites. ACS Applied Materials & Interfaces, 4(2), 777–784.

Ozkan, D., Gok, M. S., & Karaoglanli, A. C. (2020). Carbon fiber reinforced polymer (CFRP) composite materials, their characteristic properties, industrial application areas and their machinability. In *Engineering Design Applications III* (pp. 235-253). Springer, Cham.

Panchagnula, K. K., & Palaniyandi, K. (2018). Drilling on fiber reinforced polymer/nanopolymer composite laminates: A review. Journal of Materials Research and Technology, 7(2), 180–189.

Pantano, A., M. Parks, D., & Boyce, M. C. (2004). Mechanics of deformation of single- and multi-wall carbon nanotubes. Journal of the Mechanics and Physics of Solids, 52(4), 789–821.

Park, B., An, Y.-K., & Sohn, H. (2014). Visualization of hidden delamination and debonding in composites through noncontact laser ultrasonic scanning. Composites Science and Technology, 100, 10–18.

Park, S.-B., Lih, E., Park, K.-S., Joung, Y. K., & Han, D. K. (2017). Biopolymer-based functional composites for medical applications. Progress in Polymer Science, 68, 77–105.

Park, D.W.; Shim, S.E. A review on thermal conductivity of polymer composites using carbon-based fillers: Carbon nanotubes and carbon fibers. Carbon Lett. 2010, 11, 347–356.

Pickering, K. L., Efendy, M. A., & Le, T. M. (2016). A review of recent developments in natural fibre composites and their mechanical performance. Composites Part A: Applied Science and Manufacturing, 83, 98–112.

Ponnamma, D., Sung, S. H., Hong, J. S., Ahn, K. H., Varughese, K. T., & Thomas, S. (2014). Influence of non-covalent functionalization of carbon nanotubes on the rheological behavior of natural rubber latex nanocomposites. European Polymer Journal, 53, 147–159.

Prasek, J., Drbohlavova, J., Chomoucka, J., Hubalek, J., Jasek, O., Adam, V., & Kizek, R. (2011). Methods for carbon nanotubes synthesis—Review. Journal of Materials Chemistry, 21(40), 15872–15884.

Prashanth, S., Subbaya, K. M., Nithin, K., & Sachhidananda, S. (2017). Fiber reinforced composites-a review. J. Mater. Sci. Eng, 6(03), 2–6.

Punetha, V. D., Rana, S., Yoo, H. J., Chaurasia, A., McLeskey, J. T., Ramasamy, M. S., Sahoo, N. G., & Cho, J. W. (2017). Functionalization of carbon nanomaterials for advanced polymer nanocomposites: A comparison study between CNT and graphene. Progress in Polymer Science, 67, 1–47.

Qian D, Dickey EC. In situ transmission electron microscopy studies of polymer–carbon nanotube composite deformation. J Microsc 2001;204(1):39–45

Quan, D., Urdániz, J. L., & Ivanković, A. (2018). Enhancing mode-I and mode-II fracture toughness of epoxy and carbon fibre reinforced epoxy composites using multi-walled carbon nanotubes. Materials & Design, 143, 81–92.

Queipo, P., Nasibulin, A. G., Shandakov, S. D., Jiang, H., Gonzalez, D., & Kauppinen, E. I. (2009). CVD synthesis and radial deformations of large diameter single-walled CNTs. Current Applied Physics, 9(2), 301–305.

Rahman, M., Hosur, M., Zaiuddin, S., Vaidya, U., Tauhid, A., Kumar, A., Trovillion, J. & Jeelani, S. (2013). Effects of amino-functionalized MWMWCNTs on ballistic impact performance of E-glass/epoxy composites using a spherical projectile. International Journal of Impact Engineering, 57, 108-118.

Rahman, M., Zaiuddin, S., Hosur, M., Malone, J., Salam, M., Kumar, A. & Jeelani, S. (2012). Improvements in mechanical and thermo-mechanical properties of e-glass/epoxy composites using amino functionalized MWMWCNTs. Composite Structures, 94, 2397-2406.

Radushkevich, L. V., & Lukyanovich, V. M. (1952). The carbon structure formed by thermal decomposition of carbon monoxide on an iron contact. J. Phys. Chem, 26, 88–95.

Rafiee, R., & Sharaei, M. (2020). Investigating the influence of bonded and non-bonded interactions on the interfacial bonding between carbon nanotube and polymer. Composite Structures, 238, 111996.

Rafique, M. M. A., & Iqbal, J. (2011). Production of carbon nanotubes by different routes-a review. Journal of Encapsulation and Adsorption Sciences, 1(02), 29.

Raju, A., & Shanmugaraja, M. (2020). Recent researches in fiber reinforced composite materials: A review. Materials Today: Proceedings.

Rana, S., & Fangueiro, R. (2016). 1—Advanced composites in aerospace engineering. In Sohel Rana & R. Fangueiro (Eds.), Advanced Composite Materials for Aerospace Engineering (pp. 1–15). Woodhead Publishing.

Rathore, D. K., Prusty, R. K., Kumar, D. S., & Ray, B. C. (2016). Mechanical performance of CNT-filled glass fiber/epoxy composite in in-situ elevated temperature environments emphasizing the role of CNT content. Composites Part A: Applied Science and Manufacturing, 84, 364–376.

Ravishankar, B., Nayak, S. K., & Kader, M. A. (2019). Hybrid composites for automotive applications – A review. Journal of Reinforced Plastics and Composites, 38(18), 835–845.

Ribeiro, B., Botelhoet, E. C., Costa, M. L., & Bandeiraal, C.F. (2017). Carbon nanotube buckypaper reinforced polymer composites: a review. Polímeros, 27(3), 247-255.

Rinaldi, M., Puglia, D., Dominici, F., Cherubini, V., Torre, L., & Nanni, F. (2017). Melt processing and mechanical property characterization of high-performance poly(ether ether ketone)–carbon nanotube composite. Polymer International, 66(12), 1731–1736.

Roch, A., Jost, O., Schultrich, B., & Beyer, E. (2007). High-yield synthesis of single-walled carbon nanotubes with a pulsed arc-discharge technique. Physica Status Solidi (b), 244(11), 3907–3910.

Rowell, R. M., Han, J. S., & Rowell, J. S. (2000). Characterization and factors effecting fiber properties. Natural Polymers and Agrofibers Bases Composites. Embrapa Instrumentacao Agropecuaria, P. O. Box 741, Sao Carlos, 13560-970 SP, Brazil, 2000., 115–134.

Ruoff, R. S., Qian, D., & Liu, W. K. (2003). Mechanical properties of carbon nanotubes: Theoretical predictions and experimental measurements. Comptes Rendus Physique, 4(9), 993–1008.

Sacchetti, F., Grouve, W. J., Warnet, L. L. & Villegas, I. F. (2018). Interlaminar fracture toughness of 5HS carbon/PEEK laminates. A comparison between DCB, ELS and mandrel peel tests. Polymer testing, 66, 13-23.

Salam, M., Hosur, M., Zaiuddin, S. & Jeelani, S. (2013). Improvement in mechanical and thermo-mechanical properties of epoxy composite using two different functionalized multi-walled carbon nanotubes.

Sanchez-Saez, S., Barbero, E., Zaera, R. & Navarro, C. (2005). Compression after impact of thin composite laminates. Composites Science and Technology, 65, 1911-1919.

Saba, N., Jawaid, M., Alothman, O. Y., Paridah, M., & Hassan, A. (2016). Recent advances in epoxy resin, natural fiber-reinforced epoxy composites and their applications. Journal of Reinforced Plastics and Composites, 35(6), 447–470.

Saboori, B., & Ayatollahi, M. R. (2017). Experimental fracture study of MWCNT/epoxy nanocomposites under the combined out-of-plane shear and tensile loading. Polymer Testing, 59, 193–202.

Saito, T., Matsushige, K., & Tanaka, K. (2002). Chemical treatment and modification of multi-walled carbon nanotubes. Physica B: Condensed Matter, 323(1), 280–283.

Salvetat-Delmotte, J.-P., & Rubio, A. (2002). Mechanical properties of carbon nanotubes: A fiber digest for beginners. Carbon, 40(10), 1729–1734.

Sammalkorpi, M., Krasheninnikov, A., Kuronen, A., Nordlund, K., & Kaski, K. (2004). Mechanical properties of carbon nanotubes with vacancies and related defects. Physical Review B, 70(24), 245416.

Sastry, N.V.; Bhunia, A.; Sundararajan, T.; Das, S.K. Predicting the effective thermal conductivity of carbon nanotube based nanofluids. Nanotechnology 2008, 19, 055704

Sathishkumar, T. P., Satheeshkumar, S., & Naveen, J. (2014). Glass fiber-reinforced polymer composites–a review. Journal of Reinforced Plastics and Composites, 33(13), 1258–1275.

Satyanarayana, K. G., Arizaga, G. G., & Wypych, F. (2009). Biodegradable composites based on lignocellulosic fibers—An overview. Progress in Polymer Science, 34(9), 982–1021.

Saether, E., Frankland, S. J. V., & Pipes, R. B. (2003). Transverse mechanical properties of single-walled carbon nanotube crystals. Part I: Determination of elastic moduli. Composites Science and Technology, 63(11), 1543–1550.

Seyhan, A. T., Tanoglu, M. & Sshulte, K. (2008). Mode I and mode II fracture toughness of E-glass non-crimp fabric/carbon nanotube (CNT) modified polymer based composites. Engineering Fracture Mechanics, 75, 5151-5162.

Seligra, P. G., Nuevo, F., Lamanna, M., & Famá, L. (2013). Covalent grafting of carbon nanotubes to PLA in order to improve compatibility. Composites Part B: Engineering, 46, 61–68.

Sepasdar, R., & Shakiba, M. (2022). Micromechanical study of multiple transverse cracking in cross-ply fiber-reinforced composite laminates. Composite Structures, 281, 114986. https://doi.org/10.1016/j.compstruct.2021.114986

Shyr, T.-W. & Pan, Y.-H. (2003). Impact resistance and damage characteristics of composite laminates. Composite structures, 62, 193-203.

Shah, K. A., & Tali, B. A. (2016). Synthesis of carbon nanotubes by catalytic chemical vapour deposition: A review on carbon sources, catalysts and substrates. Materials Science in Semiconductor Processing, 41, 67–82.

Sharma, S. P., & Lakkad, S. C. (2011). Effect of CNTs growth on carbon fibers on the tensile strength of CNTs grown carbon fiber-reinforced polymer matrix composites. Composites Part A: Applied Science and Manufacturing, 42(1), 8–15.

Shim, B. S., Podsiadlo, P., Lilly, D. G., Agarwal, A., Lee, J., Tang, Z., Ho, S., Ingle, P., Paterson, D., Lu, W., & Kotov, N. A. (2007). Nanostructured Thin Films Made by Dewetting Method of Layer-By-Layer Assembly. Nano Letters, 7(11), 3266–3273.

Shokrieh, M. M., & Rafiee, R. (2010). A review of the mechanical properties of isolated carbon nanotubes and carbon nanotube composites. Mechanics of Composite Materials, 46(2), 155–172.

Shtein, M., Nadiv, R., Lachman, N., Daniel Wagner, H., & Regev, O. (2013). Fracture behavior of nanotube–polymer composites: Insights on surface roughness and failure mechanism. Composites Science and Technology, 87, 157–163.

Shukla, M. J., Kumar, D. S., Rathore, D. K., Prusty, R. K., & Ray, B. C. (2016). An assessment of flexural performance of liquid nitrogen conditioned glass/epoxy composites with multiwalled carbon nanotube. Journal of Composite Materials, 50(22), 3077-3088.

Siegfried, M., Tola, C., Claes, M., Lomov, S. V., Verpost, I. & Gorbatikh, L. (2014). Impact and residual after impact properties of carbon fiber/epoxy composites modified with carbon nanotubes. Composite Structures, 111, 488-496.

Somanathan, T., & Pandurangan, A. (2010). Helical multiwalled carbon nanotubes (h-MWCNTs) synthesized by catalytic chemical vapor deposition. New Carbon Materials, 25(3), 175–180.

Soni, S. K., Thomas, B., & Kar, V. R. (2020). A Comprehensive Review on CNTs and CNT-Reinforced Composites: Syntheses, Characteristics and Applications. Materials Today Communications, 101546.

Soutis, C. (2005). Fibre reinforced composites in aircraft construction. Progress in Aerospace Sciences, 41(2), 143–151.

Spitalsky, Z., Tasis, D., Papagelis, K., & Galiotis, C. (2010). Carbon nanotube–polymer composites: Chemistry, processing, mechanical and electrical properties. Progress in Polymer Science, 35(3), 357–401.

Sridharan, S. (Ed.). (2008). Delamination behaviour of composites. Elsevier.

Srivastava, S., & Kotov, N. A. (2008). Composite Layer-by-Layer (LBL) Assembly with Inorganic Nanoparticles and Nanowires. Accounts of Chemical Research, 41(12), 1831–1841.

Startsev, O. V., Vapirov, Y. M., Lebedev, M. P. & Kychkin, A. K. (2020). Comparison of glass-transition temperatures for epoxy polymers obtained by methods of thermal analysis. Mechanics of Composite Materials, 56, 227-240.

Stéphan, C., Nguyen, T. P., Lahr, B., Blau, W., Lefrant, S., & Chauvet, O. (2002). Raman spectroscopy and conductivity measurements on polymer-multiwalled carbon nanotubes composites. Journal of Materials Research, 17(2), 396–400.

Sternberg, M., Curtiss, L. A., Gruen, D. M., Kedziora, G., Horner, D. A., Redfern, P. C., & Zapol, P. (2006). Carbon Ad-Dimer Defects in Carbon Nanotubes. Physical Review Letters, 96(7), 075506.

St-Pierre, L., Martorell, N. J., & Pinho, S. T. (2017). Stress redistribution around clusters of broken fibres in a composite. Composite Structures, 168, 226–233.

Su, D. H. (2014). Application of Fiber Reinforced Composites for Sports Instruments. Applied Mechanics and Materials, 687–691, 4256–4259.

Subadra, S. P., Yousef, S., Griskevicius, P., & Makarevicius, V. (2020). High-performance fiberglass/epoxy reinforced by functionalized CNTs for vehicle applications with less fuel consumption and greenhouse gas emissions. Polymer Testing, 86, 106480.

Sun, L., Warren, G. L., O'Reilly, J. Y., Everett, W. N., Lee, S. M., Davis, D., Lagoudas, D., & Sue, H.-J. (2008). Mechanical properties of surface-functionalized SWCNT/epoxy composites. Carbon, 46(2), 320–328.

Tan, K. T., Yoshimura, A., Watanbe, N., Iwahori, Y. & Ishikawa, T. (2013). Effect of stitch density and stitch thread thickness on damage progression and failure characteristics of stitched composites under out-of-plane loading. Composites science and technology, 74, 194-204.

Tang L-C, Zhang H, Wu X-P, Zhang Z. A novel failure analysis of multi-walled carbon nanotubes in epoxy matrix. Polymer 2011;52(9):2070–4

Tarfaoui, M., El Moumen, A., Lafdi, K., Hassoon, O. H., & Nachtane, M. (2018). Inter laminar failure behavior in laminate carbon nanotubes-based polymer composites. Journal of Composite Materials, 52(26), 3655–3667.

Tebeta, R. T., Fattahi, A. M., & Ahmed, N. A. (2020). Experimental and numerical study on HDPE/SWCNT nanocomposite elastic properties considering the processing techniques effect. *Microsystem Technologies*, *26*(8), 2423-2441.

Tessonnier, J.-P., & Su, D. S. (2011). Recent Progress on the Growth Mechanism of Carbon Nanotubes: A Review. ChemSusChem, 4(7), 824–847.

Thostenson, E. T., & Chou, T.-W. (2002). Aligned multi-walled carbon nanotube-reinforced composites: Processing and mechanical characterization. Journal of Physics D: Applied Physics, 35(16), L77.

Thostenson, E. T., Ren, Z., & Chou, T.-W. (2001). Advances in the science and technology of carbon nanotubes and their composites: A review. Composites Science and Technology, 61(13), 1899–1912.

Toozandehjani, M., Kamarudin, N., Dashtizadeh, Z., Lim, E., Gomes, A., & Gomes, C. (2018). Conventional and Advanced Composites in Aerospace Industry: Technologies Revisited. *American Journal Of Aerospace Engineering*, *5*(1), 9. https://doi.org/10.11648/j.ajae.20180501.12

Treacy, M. J., Ebbesen, T. W., & Gibson, J. M. (1996). Exceptionally high Young's modulus observed for individual carbon nanotubes. Nature, 381(6584), 678–680.

Trojanowicz, M. (2006). Analytical applications of carbon nanotubes: A review. TrAC Trends in Analytical Chemistry, 25(5), 480–489.

Tsai, Y. Y., Su, J. S., Su, C. Y., & He, W. H. (2009). Production of carbon nanotubes by single-pulse discharge in air. Journal of Materials Processing Technology, 209(9), 4413–4416.

Tserpes, K. I., & Papanikos, P. (2005). Finite element modeling of single-walled carbon nanotubes. Composites Part B: Engineering, 36(5), 468–477.

Ulus, H., Üstun, T., Şahon, Ö. S., KAarabulut, S. E., Eskizeyber, V. & Ava, A. (2016). Low-velocity impact behavior of carbon fiber/epoxy multiscale hybrid nanocomposites reinforced with multiwalled carbon nanotubes and boron nitride nanoplates. Journal of Composite Materials, 50, 761-770.

Vaidya, U. K. (2011). Impact response of laminated and sandwich composites. Impact engineering of composite structures. Springer.

Vaisman, L., Marom, G., & Wagner, H. D. (2006). Dispersions of surface-modified carbon nanotubes in water-soluble and water-insoluble polymers. Advanced Functional Materials, 16(3), 357–363.

Vaisman, L., Wagner, H. D., & Marom, G. (2006). The role of surfactants in dispersion of carbon nanotubes. Advances in Colloid and Interface Science, 128, 37–46.

Veedu, V. P., Cao, A., Li, X., Ma, K., Soldano, C., Kar, S., Ajayan, P. M., & Ghasemi-Nejhad, M. N. (2006). Multifunctional composites using reinforced laminae with carbon-nanotube forests. Nature Materials, 5(6), 457–462.

Vijay Kumar, V., Balaganesan, G., Lee, J. K. Y., Neisiany, R. E., Surendran, S., & Ramakrishna, S. (2019). A review of recent advances in nanoengineered polymer composites. Polymers, 11(4), 644.

Vijayan, R., Ghazinezami, A., Taklimi, S. R., Khan, M. Y., & Askari, D. (2019). The geometrical advantages of helical carbon nanotubes for high-performance multifunctional polymeric nanocomposites. Composites Part B: Engineering, 156, 28–42.

Wang, D., Song, P., Liu, C., Wu, W., & Fan, S. (2008). Highly oriented carbon nanotube papers made of aligned carbon nanotubes. Nanotechnology, 19(7), 075609.

Wang, J., Fang, Z., Gu, A., Xu, L., & Liu, F. (2006). Effect of amino-functionalization of multi-walled carbon nanotubes on the dispersion with epoxy resin matrix. Journal of Applied Polymer Science, 100(1), 97–104.

Wang, K., Li, N., Sun, L., Zhang, J., & Liu, X. (2020). Free-Standing N-Doped Carbon Nanotube Films with Tunable Defects as a High Capacity Anode for Potassium-Ion Batteries. ACS Applied Materials & Interfaces, 12(33), 37506–37514.

Wei, H.-F., Hsiue, G.-H., & Liu, C.-Y. (2007). Surface modification of multi-walled carbon nanotubes by a sol–gel reaction to increase their compatibility with PMMA resin. Composites Science and Technology, 67(6), 1018–1026.

Wolfrum, J., Eibl. S. & Lietch, L. (2009). Rapid evaluation of long-term thermal degradation of carbon fibre epoxy composites. Compos Science and Technology, 69, 523–530.

Wu, C.-C., Su, C.-C., & Yang, C.-F. (2015). Preparation, structure and properties of carbon nanotube reinforced polymer nanocomposites. Synthetic Metals, 205, 98–105.

Wu, D.; Wu, L.; Zhou, W.; Sun, Y.; Zhang, M. Relations between the aspect ratio of carbon nanotubes and the formation of percolation networks in biodegradable polylactide/carbon nanotube composites. J. Polym. Sci. Part B Polym. Phys. 2010, 48, 479–489.

Wu, D., Wu, L., Zhang, M., & Zhao, Y. (2008). Viscoelasticity and thermal stability of polylactide composites with various functionalized carbon nanotubes. Polymer Degradation and Stability, 93(8), 1577–1584.

Wu, C. S., Liu, Y. L., Chiu, Y. C. & Chiu, Y.S. (2002). Thermal stability of epoxy resins containing flame retardant components: an evaluation with thermogravimetric analysis. Polymer Degradation and Stability,78, 41-48.

Xiong, S., Zhao, Y., Wang, Y., Song, J., Zhao, X., & Li, S. (2021). Enhanced interfacial properties of carbon fiber/epoxy composites by coating carbon nanotubes onto carbon fiber surface by one-step dipping method. Applied Surface Science, 546, 149135.

Xiao, J. R., Gama, B. A., & Gillespie Jr, J. W. (2005). An analytical molecular structural mechanics model for the mechanical properties of carbon nanotubes. International Journal of Solids and Structures, 42(11–12), 3075–3092.

Xiao, W.; Luo, X.; Ma, P.; Zhai, X.; Fan, T.; Li, X. Structure factors of carbon nanotubes on the thermal conductivity of carbon nanotube/epoxy composites. AIP Adv. 2018, 8, 035107.

Xie, X.-L., Mai, Y.-W., & Zhou, X.-P. (2005a). Dispersion and alignment of carbon nanotubes in polymer matrix: A review. Materials Science and Engineering: R: Reports, 49(4), 89–112.

Xie, X.-L., Mai, Y.-W., & Zhou, X.-P. (2005b). Dispersion and alignment of carbon nanotubes in polymer matrix: A review. Materials Science and Engineering: R: Reports, 49(4), 89–112.

Xu, S., Chan, Y. C., Zhu, X., Lu, H., & Bailey, C. (2014). Effective method to disperse and incorporate Carbon nanotubes in electroless Ni-P deposits. 2014 IEEE 64th Electronic Components and Technology Conference (ECTC), 1342–1347.

Xu, X., Zhou, Z., Hei, Y., Zhang, B., Bao, J., & Chen, X. (2014). Improving compression-after-impact performance of carbon–fiber composites by CNTs/thermoplastic hybrid film interlayer. Composites science and technology, 95, 75-81.

Xue, Q. Z. (2005). Model for thermal conductivity of carbon nanotube-based composites. Physica B: Condensed Matter, 368(1), 302–307.

Yadav, R., Tirumali, M., Wang, X., Naebe, M., & Kandasubramanian, B. (2020). Polymer composite for antistatic application in aerospace. Defence Technology, 16(1), 107–118.

Yan, L., Kasal, B., & Huang, L. (2016). A review of recent research on the use of cellulosic fibres, their fibre fabric reinforced cementitious, geo-polymer and polymer composites in civil engineering. Composites. Part B, Engineering, 92, 94–132.

Yang, Bing-Xing, Shi, J.-H., Pramoda, K. P., & Goh, S. H. (2007). Enhancement of stiffness, strength, ductility and toughness of poly(ethylene oxide) using phenoxy-grafted multiwalled carbon nanotubes. Nanotechnology, 18(12), 125606.

Yang, B.-X., Pramoda, K. P., Xu, G. Q., & Goh, S. H. (2007). Mechanical Reinforcement of Polyethylene Using Polyethylene-Grafted Multiwalled Carbon Nanotubes. Advanced Functional Materials, 17(13), 2062–2069.

Yang, K., He, J., Puneet, P., Su, Z., Skove, M. J., Gaillard, J., Tritt, T. M., & Rao, A. M. (2010). Tuning electrical and thermal connectivity in multiwalled carbon nanotube buckypaper. Journal of Physics: Condensed Matter, 22(33), 334215.

Yang, Y. H., & Li, W. Z. (2011). Radial elasticity of single-walled carbon nanotube measured by atomic force microscopy. Applied Physics Letters, 98(4), 041901.

Yao, Q., Chen, L., Zhang, W., Liufu, S., & Chen, X. (2010). Enhanced Thermoelectric Performance of Single-Walled Carbon Nanotubes/Polyaniline Hybrid Nanocomposites. ACS Nano, 4(4), 2445–2451.

Yasa, E., & Ersoy, K. (2018). Additive manufacturing of polymer matrix composites. Aircraft Technology; InTech: Rijeka, Croatia, 7, 147–169.

Yee, M. J., Mubarak, N. M., Khalid, M., Abdullah, E. C., & Jagadish, P. (2018). Synthesis of polyvinyl alcohol (PVA) infiltrated MWCNTs buckypaper for strain sensing application. Scientific Reports, 8(1), 17295.

Yokozeki, T., Iwahori, Y., & Ishiwata, S. (2007). Matrix cracking behaviors in carbon fiber/epoxy laminates filled with cup-stacked carbon nanotubes (CSCNTs). Composites Part A: Applied Science and Manufacturing, 38(3), 917–924.

Yokozeki, T., Iwahori, Y., Ishiwata, S., & Enomoto, K. (2007). Mechanical properties of CFRP laminates manufactured from unidirectional prepregs using CSCNT-dispersed epoxy. Composites Part A: Applied Science and Manufacturing, 38(10), 2121–2130.

Yoshida, H., & Takeda, S. (2014). Elucidation of the origin of grown-in defects in carbon nanotubes. Carbon, 70, 266–272.

Yuen, S.-M., Ma, C.-C. M., Lin, Y.-Y., & Kuan, H.-C. (2007). Preparation, morphology and properties of acid and amine modified multiwalled carbon nanotube/polyimide composite. Composites Science and Technology, 67(11), 2564–2573.

Zhou, G., Mikinka, E., Golding, J., Bao, X., Sun, W. & Ashby, A. (2020). Investigation of thermal degradation and decomposition of both pristine and damaged

carbon/epoxy samples with thermal history. Composites Part B: Engineering, 201, 1083-1082.

Zhou, Y., Pervin, F., Lewis, L. & Jeelani, S. (2007). Experimental study on the thermal and mechanical properties of multi-walled carbon nanotube-reinforced epoxy. Material Science and Engineering A, 452–453, 657–664.

Zohar E, Baruch S, Shneider M, Dodiuk H, Kenig S, Tenne R, et al. The effect of WS2 nanotubes on the properties of epoxy-based nanocomposites. J Adhes Sci Technol 2011;25(13):1603–17

.

.